University of Massachusetts Amherst
ScholarWorks@UMass Amherst

Doctoral Dissertations 1896 - February 2014

1-1-1987

Visualization of the evolution of a continuous crystalline phase in uniaxially drawn polyethylene :: decrystallization and strain-induced (re)crystallization/

Jean Marie Brady
University of Massachusetts Amherst

Follow this and additional works at: https://scholarworks.umass.edu/dissertations_1

Recommended Citation
Brady, Jean Marie, "Visualization of the evolution of a continuous crystalline phase in uniaxially drawn polyethylene :: decrystallization and strain-induced (re)crystallization/" (1987). *Doctoral Dissertations 1896 - February 2014*. 726.
https://scholarworks.umass.edu/dissertations_1/726

This Open Access Dissertation is brought to you for free and open access by ScholarWorks@UMass Amherst. It has been accepted for inclusion in Doctoral Dissertations 1896 - February 2014 by an authorized administrator of ScholarWorks@UMass Amherst. For more information, please contact scholarworks@library.umass.edu.

UMASS/AMHERST
3120660076914 74

VISUALIZATION OF THE EVOLUTION OF A CONTINUOUS CRYSTALLINE PHASE IN UNIAXIALLY DRAWN POLYETHYLENE: DECRYSTALLIZATION AND STRAIN-INDUCED (RE)CRYSTALLIZATION

A Dissertation Presented

by

JEAN MARIE BRADY

Submitted to the Graduate School of the
University of Massachusetts in partial fulfillment
of the requirements for the degree of

DOCTOR OF PHILOSOPHY

September 1987

Polymer Science and Engineering

Copyright by

© Jean Marie Brady 1987

All Rights Reserved

VISUALIZATION OF THE EVOLUTION OF A CONTINUOUS CRYSTALLINE PHASE IN UNIAXIALLY DRAWN POLYETHYLENE: DECRYSTALLIZATION AND STRAIN-INDUCED (RE)CRYSTALLIZATION

A Dissertation Presented

by

JEAN MARIE BRADY

Approved as to style and content by:

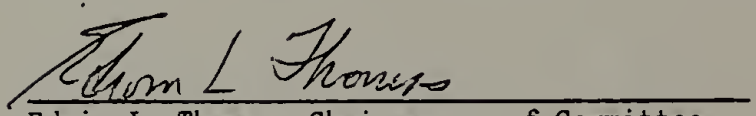

Edwin L. Thomas, Chairperson of Committee

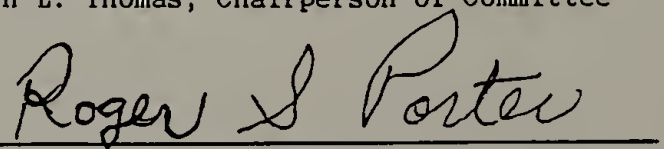

Roger S. Porter, Member

James A. Donovan, Member

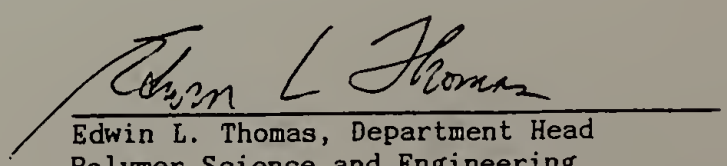

Edwin L. Thomas, Department Head
Polymer Science and Engineering

DEDICATION

To my parents, John J. and Mary F. Brady,

and to my husband, Nilesh, whose encouragement,

support, and love will be always treasured.

ACKNOWLEDGEMENTS

I would like to thank Professor Edwin L. Thomas for his guidance of my research. I would also like to thank Professors Roger S. Porter and James A. Donovan for serving as committee members. In addition, I thank the National Science Foundation for funding this research.

I thank Dr. Tetsuo Kanamoto for providing me with solid state extruded/post-drawn samples of polyethylene and Dr. Lewis J. Fetters for synthesizing and characterizing model linear low density polyethylene samples. Thanks also go to Dr. Chris Henkee, who not only supplied me with linear low density materials, but with hours of conversation as well. I thank Mike Connolly for operating the DMTA for me, Lou Raboin for keeping the electron microscopy lab running smoothly, and Dave Martin for providing me with a phase contrast transfer function plot. In addition, I thank Dave Gobran, who set up the computer used to write this thesis, who patiently taught me the techniques of small angle x-ray scattering and who, with the likes of Dr. Randal Richards, teased me enough to make life interesting. Most of all, I thank everyone in the group for their friendship.

Special thanks go to my husband and best friend, Nilesh, who has endured (and survived!) weekend commuting from Pennsylvania to Amherst for two years.

ABSTRACT

VISUALIZATION OF THE EVOLUTION OF A CONTINUOUS CRYSTALLINE PHASE IN UNIAXIALLY DRAWN POLYETHYLENE: DECRYSTALLIZATION AND STRAIN-INDUCED (RE)CRYSTALLIZATION

SEPTEMBER 1987

JEAN MARIE BRADY

B.Sc., MCGILL UNIVERSITY

M.S., UNIVERSITY OF WASHINGTON

Ph.D., UNIVERSITY OF MASSACHUSETTS

Directed by: Professor Edwin L. Thomas

The morphology and deformation behavior of polyethylene as a function of deformation temperature and branching characteristics was studied by transmission electron microscopy (TEM). In the latter case, the crystallization behavior and the morphology of as-drawn and uniaxially deformed, thin, oriented films of branched polyethylene was studied. Branch content (up to 2.36 mole % short branches) affected deformation behavior by interrupting the crystallization process, reducing the average crystal size, perfection, and crystallinity. This would then influence the modulus and crystalline phase ductility.

The effect of temperature on the deformation behavior of linear polyethylene was studied using both bulk solid state extruded/post-drawn (SSE/PD) ultrahigh modulus and strength (> 175 GPa and 3 GPa, respectively) polyethylene (draw ratios varying from 6 to 250) and thin, oriented, gel-drawn films. The thin films were uniaxially elongated

along the chain direction at temperatures ranging from 25 to 129 °C and observed by TEM. When deformed below the alpha transition (73 °C at 1 hz for isotropic polyethylene) the films fibrillated into bundles of shish-kebabs which elongated. Materials deformed above the alpha transition crazed and formed protofibrils in crazed regions. Protofibrils were continuously crystalline for hundreds of nanometers and were less than 10 nm wide. They formed in both ultradrawn thin films and SSE/PD bulk.

Protofibrils formed from chain-folded crystals by decrystallization and strain-induced (re)crystallization. Darkfield mode TEM revealed the details of decrystallization, which occurred at 25 as well as 129 °C. It involved <001> crystal shear (and accompanying chain slip), as well as defect generation within crystals. Significant strain-induced crystallization was observed only in material deformed above the alpha transition.

It was concluded that the ultrahigh modulus materials were composed of a continuous crystalline phase with a protofibril substructure. This was based on the observations that protofibrils laterally coalesced, forming crystalline regions at least as long as 3 microns (darkfield TEM yielding only a lower bound of crystal size). Moreover, a sample-spanning crystalline phase could arise from laterally interconnected protofibrils even if individual protofibrils were not sample-spanning.

TABLE OF CONTENTS

LIST OF TABLES

Table

LIST OF FIGURES

CHAPTER I

INTRODUCTION

The purpose of this research was to extend the understanding of structure-property relationships in semicrystalline polymers. Major goals were to determine the effect of short branches on microstructure and deformation behavior, and to determine those factors giving rise to high modulus and strength. Particular emphasis was placed on ellucidating the formation and structure of a continuous crystalline phase in ultradrawn polyethylene, and to detail those deformation mechanisms and conditions which brought about its formation. Indeed, the formation of a continuous crystalline phase in ultradrawn polyethylene has been given much indirect support (by crystallinity measurements, mechanical properties, wide angle and small angle x-ray scattering measurements, etc.). Moreover, darkfield microscopy measurements have indicated that long (80 nm) crystals do indeed form upon drawing. However, detailed (direct) information on the formation and structure of a continuous crystalline phase has been lacking up to this point. Furthermore, the morphological models of a continuous crystalline phase which exist in the literature are generally based on averaged structural data, which can be interpretted using more than one model. A major objective of the present study was to view in detail the microstructure of a continuous crystalline phase.

Here, polyethylene was chosen to represent the class of semi-crystalline polymers since it is both a chemically and structurally simple molecule. Moreover, the high moduli and strengths which have recently been realized in ultradrawn polyethylene have resulted in a renewal of interest in polyethylene and have drawn attention to the processing techniques used to achieve ultimate mechanical properties. As polyethylene is composed solely of hydrogen and carbon, it does not experience the additional forces between chains which are found in polymers which hydrogen bond, are polar, or which have reactive pendant groups. The crystallinity of polyethylene varies with branching and processing, and has been reported to be as high as ca. 90%. The conformation of chains in the crystalline phase is planar zigzag (2_1 helix) while chains in noncrystalline regions acquire more of a Gaussian conformation.

Polyethylene crystallizes into various morphological forms, depending on crystallization conditions. Single crystals, for example, can be grown from dilute solution, while fibrous structures arise from flowing solution, and sperulites grow from the quiescent melt. Spherulites are comprised of lamellae radiating from a central nucleus, with the chain direction being tangentially oriented. Fibrous structures grow in the form of shish-kebabs, which consist of an inner chain-extended core (shish) and an overgrowth of chain-folded crystals (kebab). Both single crystals and spherulites are comprised of folded chains.

The exact way in which polymer chains fold has been a topic of great controversy and to this day remains unresolved (See Royal Society of Chemistry, London, Faraday Discussions #68, 1979). In fact, the concept of chain folding was initially criticized as being highly improbable. The fringed micellar model, in which small regions of chains align and crystallize without folding, provided an alternative. However, it has since been well established that the chains must return back to the lattice of origin so that the flux of chains emanating from the crystalline phase and continuing into the (less dense and isotropic) noncrystalline phase is reduced (Flory and Yoon, 1978; Flory et al., 1984).

Currently, the main debate concerning chain folding centers around the way in which chains reenter the lattice from which they originated. Flory's model (the "switchboard model") offers one extreme case in which chains reenter the crystal lattice in an entirely random fashion. The other extreme case is given in the "adjacent reentry" model in which chains fold back upon themselves. Neutron scattering studies have revealed that the amount of adjacent reentry in melt-crystallized material is less than that in solution-crystallized material (Sadler and Keller, 1979). Other studies have indicated that little chain reorganization occurs during crystallization from the melt (Schelten et al., 1976), suggesting that the switchboard model is more appropriate for melt-crystallized- rather than solution-grown- crystals.

Polyethylene is in all likelihood the most highly studied polymer in existance. Even so, numerous questions remain unanswered concerning,

among other things, its deformation behavior. The general effect of drawing is to increase density, crystallinity, stiffness (tensile modulus), and strength (stress at fracture). Macroscopic mechanical testing and x-ray scattering techniques have been extensively used to study the structural and mechanical changes incurred by deformation. As alluded to previously, these techniques yield an average measurement for the entire sample and can at best be used to devise nonunique structural models. It is therefore desirable to study deformation by a method which yields much more detailed information. The structural elements which are of interest in deformation studies (lamellae, mosaic blocks, shish-kebabs, protofibrils, etc.) are in the size range of 10 nm. Electron microscopy can be used to study this size scale, enabling the details of deformation to be probed.

Although a great deal of the research done so far has centered on isotropic PE, it is imperative that the deformation behavior of drawn PE be studied as well. Chain orientation is imparted to polyethylene when it is crystallized under the influence of strain. This occurs when PE is processed by such techniques as fiber spinning, film blowing or extrusion, hot rolling or even when filling molds with molten material. The resultant orientation can significantly affect both mechanical and transport properties (Peterlin, 1976). The degree and type of orientation imparted to a product depends on the thermal and flow gradients present during crystallization. In blown films, for example, it was noted that the b-axis preferentially orients in the film plane while the a- and c- axes form 45 ° angles with the film plane (Maddams

and Preedy, 1978). Microstructural studies of injection molded PE, on the other hand, revealed a skin/core effect in which the outer surface of the molded product was highly oriented and fibrillar while the interior of the part was isotropic and spherulitic (Katti and Schultz, 1982). These findings underscore the need to study the mechanical behavior of both isotropic and highly oriented material.

Before discussing the microscopic aspects of deformation, the mechanical behavior observed by macroscopic mechanical methods will be briefly outlined. A typical stress/strain curve of a semicrystalline polymer is given in Fig. 1.1. In general terms, this curve exhibits three regions of deformation during the transformation of isotropic, spherulitic material into fibrous material. At very low strains (in region I), the polymer behaves elastically, the relationship between stress and strain being close to linear. As strain increases, the material eventually yields (region II). The onset of yielding is associated with the appearance of a maximum in the stress/strain curve, the stress at this peak being defined as the yield stress. Here, the material deforms irreversibly by chain slip through entanglements or by chain scission (Kausch and Devries, 1975; Porter and Casale, 1985), as well as by crystal twinning, crystal shear via dislocation motion, and for polyethylene, by martensitic transformation (via simple shear) from an orthorhombic to metastable monoclinic unit cell (Bowden and Young, 1974; Bevis and Crellin, 1971).

Upon yielding, the material often forms a sudden contraction known as a neck. The neck propagates through the sample at a constant stress

Figure 1.1

Typical stress as a function of strain curve of a semicrystalline polymer displaying elastic deformation (I), yielding and necking (II), and strain hardening (III).

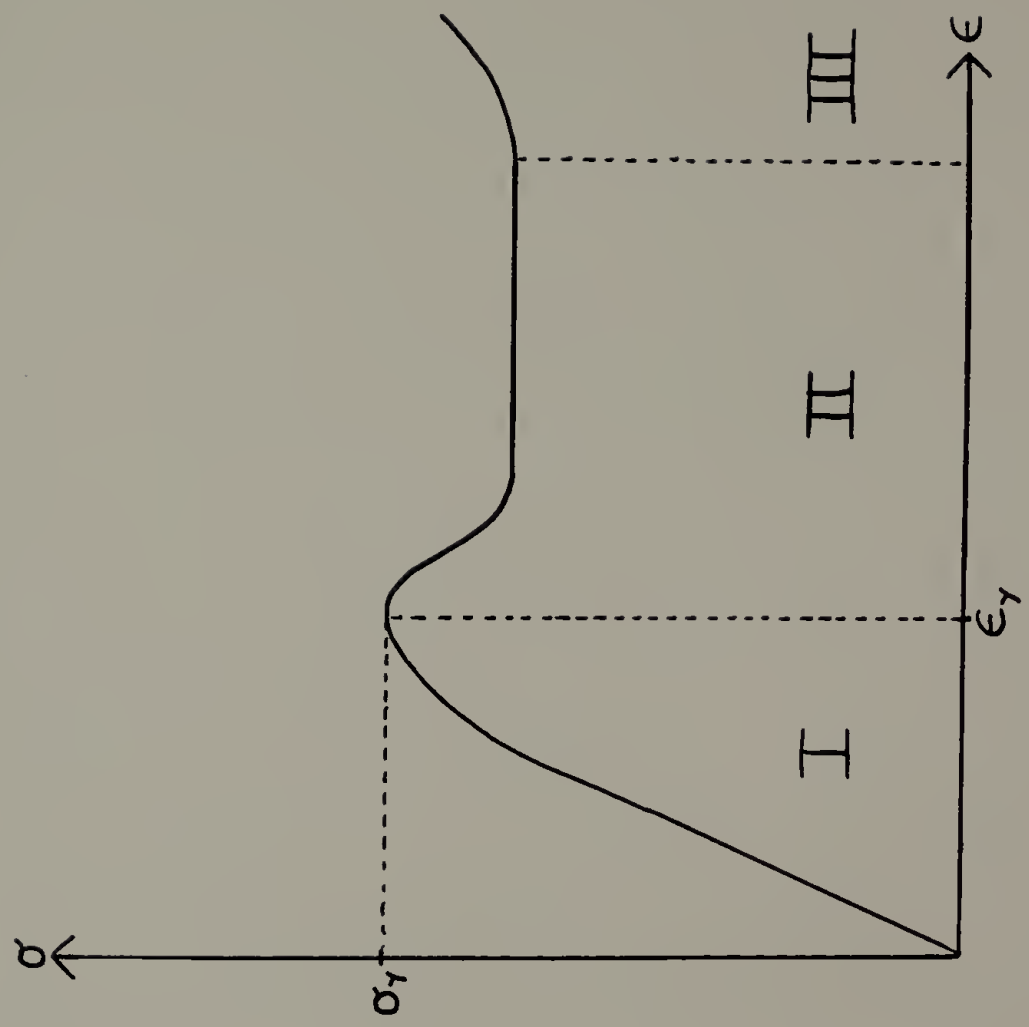
σ
σ1
ε1
ε
I
II
III

level. The material in the neck is drawn to the "natural draw ratio". At room temperature, the natural draw ratio for low density polyethylene is typically equal to about five while for high density polyethylene it is about eleven (Bunn, 1960). These values vary with crystallinity, strain rate, and draw temperature. Once the neck has propagated through the entire sample, additional straining results in a stress rise. This constitutes the third region (III) of the stress/strain curve. The convex shape of the stress/strain curve in this region indicates that the material is "strain hardening". Strain hardening apparently occurs when chains in the neck are highly extended and therefore can no longer relieve stress by conformational changes, rotations, and reorientation. In fact, some of the noncrystalline chains may even crystallize at these high strains. The formation of a neck, and the strain hardening phenomenon can be suppressed by deforming near the melting point, since at high temperature the material can flow more easily (due to crystalline phase ductility) to relieve stress. In fact, "strain softening", characterized by a concave stress/strain curve at high strains, has been known to replace strain hardening.

Unfortunately, macroscopic mechanical testing offers little insight into the microstructural mechanisms by which the above phenomena occur. To reach a greater level of understanding of the microstructural changes which accompany the various regions of the stress/strain curve, it is imperative that the microstructural evolution during deformation be studied. Electron microscopy offers a way by which the transormation of structural elements with draw can be studied.

The mechanical behavior and structure/property relationships of PE have been extensively reviewed elsewhere (Ward, 1983; Ciferri and Ward, 1979; Popli and Mandelkern, 1987; Perkins and Porter, 1977; Zachariades et al., 1980, and references therein). Many aspects of the mechanical behavior are, however, relevant to the present investigation and therefore will be mentioned here. For instance, the tensile modulus of PE has been reported to increase with an increase in crystallinity, average crystal thickness, and draw ratio. It is known in fact that drawing (under appropriate conditions) results in an increase in crystallinity and average crystal thickness by the process of strain-induced crystallization, whereby chains in the amorphous phase orient, extend, align, become closely packed, and crystallize. Moreover, such drawing results in an increase in the number of taut tie molecules interconnecting crystallites. In the present set of experiments, the relationship between modulus and crystallinity as well as crystal thickness was further explored.

Here, attention was focused on ultradrawn PE, in which extensive crystallization as well as a transformation of the crystalline phase morphology during drawing resulted in what was speculated to be a continuous crystalline phase. Using darkfield TEM, the detailed morphology of bulk solid state extruded/post-drawn (SSE/PD) PE was analyzed as a function of draw ratio. The morphology of the most highly drawn sample, known to exhibit an ultrahigh tensile modulus, served as a basis of comparison for accompanying thin film studies which were designed to understand the drawing process as a function of temperature.

The transformation of the crystalline phase morphology with draw in thin films was compared with the morphological evolution seen in SSE/PD bulk material. The main intention was to characterize the processes involved in the formation of a continuous crystalline phase and to analyze the resultant structure. The experimental conditions favoring the formation of such a phase were then discussed in terms of the destruction of the original crystalline phase microstructure, chain reorganization, and strain-induced (re)crystallization. In particular, the reduction of yield stress and the increase in chain mobility with increasing temperature was addressed.

Additional experiments were concerned with the effect of short branches on deformation behavior. The yield stress of PE increases with increasing crystallinity and crystal thickness, while the modulus and yield stress of PE decrease with increasing branch content. Samples of differing branch content and branch length were characterized and subsequently deformed and analyzed to determine how branching affected deformation mechanisms and microstructure.

It should be mentioned that the studies done here concentrated on the crystalline rather than amorphous phase. In fact, the state of the amorphous phase was mainly discussed in the context of a precursor state for strain-induced crystallization. Let this not cloud the reader's perception of the deformation process. Both phases are transformed during deformation. Numerous articles have discussed the role of entanglements and molecular topology in the drawing process (Capaccio et al., 1976; Smith et al., 1981a; Irvine and Smith, 1986). For instance,

such a quantity as draw ratio at break is known to decrease with an increase in molecular weight, and as such, an increase in entanglement density. The entanglement network comprises an important element in the deformation microstructure, and is in fact responsible for much of the crystalline phase reorganization which was viewed.

Organization of Thesis

This thesis is divided into nine self-contained chapters. Relevant literature surveys appear throughout the text as required. A historical overview of the synthesis, properties and uses of polyethylene is given in Chapter 2 so that the reader may acquire a perspective on polyethylene research and development. Chapter 3 outlines the experimental procedures and precautions used for the study of polymers by TEM. Chapter 4 concerns the process of gel-drawing and its relevance to the preparation of the thin films used here, which until now were considered to be melt-drawn. The as-drawn morphology and crystallization behavior of these films is then addressed, giving a basis for understanding the deformation behavior, as elucidated in subsequent chapters. Chapter 5 constitutes the first major deformation study. Here, HDPE films are deformed at room temperature both parallel and perpendicular to the chain axis. The way in which the crystalline phase deforms at near isothermal conditions is discussed. The microstructure of ultrahigh molecular weight solid state extruded/post-drawn polyethylene is elucidated in Chapter 6. Specific attention is

given to the mode by which single crystal mats of polyethylene are transformed into a highly crystalline and fibrous structure. By comparing the microstructure of material deformed to draw ratios of 6, 42, 97, and 250, the evolution of structure with draw is clarified. In Chapter 7, discussion centers on the effect of deformation temperature on the resultant microstructure. HDPE films are deformed at 56, 93, and 129 °C. The subsequent changes in microstructure, especially at 129 °C, offer an unprecedented detailed ultrastructural view into the deformation process. In particular, the destruction of the crystalline phase is clearly imaged in darkfield mode. In addition, long crystalline "protofibrils", much like those shown in the ultrahigh modulus solid state extruded/post-drawn samples, form. The conditions under which, and mechanisms by which protofibrils form are summarized and related to the observations of Chapter 6. Chapter 8 follows the effect of branching on deformation behavior. Specifically, the effect of branching on crystallization behavior, and the resultant enhancement of crystalline phase ductility and reduction of tensile modulus is discussed. The salient features of this research are summarized in Chapter 9.

C H A P T E R II

HISTORICAL OVERVIEW

As the present study deals solely with polyethylene, a brief survey of its synthesis and properties follows. For a more complete review refer to Nowlin (1985), Ehrlich and Mortimer (1970), Furumiya et al. (1985), Wunderlich (1973), Mandelkern (1964 and 1976), Fava (1971), Renfrew and Morgan (1960), Seymour and Cheng (1986), Geil (1963), and Keller (1968).

Polyethylene was first synthesized in 1933 when researchers at Imperial Chemical Industries, Ltd. were studying the effects of high pressure on chemical reactivity (Fawcett and Gibson, 1934). In one particular reaction, E.W. Fawcett and R.O. Gibson reacted ethylene with benzaldehyde in the presence of trace amounts of oxygen at 170 °C, 1400 atm. Under these conditions, ethylene is above its critical pressure and behaves as a solvent for polyethylene, while oxygen radicals initiate the polymerization (Ehrlich and Mortimer, 1970). This resulted in a thin waxy film being deposited onto the reaction vessel walls. This product was highly branched with both long and short branches and turned out to be the polymer we now call low density polyethylene (LDPE). Between the years of 1935 - 1939, the polymerization process of LDPE was developed and "scaled up" for manufacturing purposes. The first LDPE plant was opened in 1939. At that time, LDPE was valuable for wartime applications in the United Kingdom and United States. For

instance, LDPE served as insulation in under water telephone cables as well as radar equipment. Later, blown LDPE film was used for rifle covers because of its barrier properties to moisture and favorable mechanical properties.

After World War II, new and widespread uses for LDPE became apparent, and production boomed. Due to its low permeability to moisture, it served as an ideal packaging material for foods and other goods and could also be used for bottles and paper or metal coating. As injection molding techniques developed, so did the complexity of LDPE articles available to the consumer. The uses of polyethylene, however, became much more diversified when a new synthesis technique resulted in the production of a stiffer and stronger, unbranched material.

In 1955, Karl Ziegler discovered that unbranched polyethylene could be made at low temperature and pressure (50 - 70 °C, 3 - 4 atm) by using a catalyst of $Al(C_2H_5)_3$ and $TiCl_4$, suspended in an inert liquid hydrocarbon solvent (Ziegler et al., 1955). Ethylene gas was dissolved into the catalyst slurry and a heterogeneously-catalyzed reaction followed in which polymer formed on the surface of the (insoluble) titanium compound (Natta, 1956).

Not only ethylene, but also other alpha-olefins could be polymerized in this way. Catalyzed reactions were thus not only energetically more economical (due to the moderate reaction conditions employed), but they also gave great control over branching characteristics and stereoregularity. For instance, i-polypropylene as well as linear low density polyethylene (LLDPE) could be made for the

first time using Ziegler catalysts. LLDPE was formed by copolymerizing ethylene with alpha-olefins. Each alpha-olefin molecule which added onto the chain backbone gave rise to a short branch. The resultant control over branching meant better control over physical and mechanical properties; a major step forward in the history in polyethylene. Structurally as well as mechanically, LLDPE was a "compromise" between HDPE and LDPE.

Industrial scientists had already perceived the possible use of catalysts for polymerization. At Phillips Petroleum Company, a solution polymerization process was developed which used a catalyst consisting of chromium oxides on silica/alumina (Hogan and Banks, 1958). At Standard Oil Co. of Indiana, one catalyst system consisted of Ni or Co on activated charcoal while a still more promising one consisted of molybdenum oxide on alumina (promoted by the presence of alkalai or alkalai earth compounds) (D'Ouville, 1960). It was later found that several different transition metals could be substituted for molybdenum while still retaining catalytic activity. The solution polymerization processes of both Standard Oil and Phillips Petroleum required significantly higher temperatures and pressures (250 °C, 40 atm; and 150 °C, 30 atm, respectively) than the Ziegler-Natta process.

By 1960, DuPont joined the list of chemical companies competing in the solution polymerized LLDPE market. By 1977, Union Carbide had developed and commercialized the Unipol process, a gas phase process which utilizes a fluidized bed reactor for the synthesis of LLDPE. Today this process is widely used by numerous companies. The production

of HDPE and LLDPE relies essentially on Ziegler-Natta and Phillips catalysts. In fact, Phillips catalysts are used for ca. 60% of the HDPE produced in the world. Chromium oxide catalysts, however, cannot be used for the production of stereospecific polymers (e.g. i-polypropylene). Instead, refined versions of Ziegler-Natta catalysts (which include magnesium compounds in the catalyst system) are used. These catalysts show improved efficiency over first generation Ziegler-Natta catalysts and yield a product with a narrower molecular weight distribution.

In addition to the above techniques, LLDPE can be synthesized by the hydrogenation of polydienes (Rachapudy et al., 1979) which are synthesized anionically from diene monomer (Morton and Fetters, 1975). This method offers the advantage of having greater control over branch sequencing since the amount of 1,2 versus 1,4 addition to double bonds can be varied by changing the solvent polarity. Provided the vinyl content is not too high (solvent not too polar), this technique results in an essentially Bernoullian distribution of vinyl groups along the chain (Krigas et al., 1985) as well as a narrow molecular weight distribution.

More recent developments have dealt with the production of unbranched ultra-high molecular weight polyethylene (UHMWPE, $M_v > 10^6$). These polymers have proven very useful in the specialty applications market. For instance, the Fiber Division of Allied Corp. has recently developed and marketed a line of gel-spun UHMWPE fibers (Spectra 1000 Series) which are so stiff they are competing with some of the specialty

polyaramid fiber markets. Specifically, this material is used for rope and cording, sailcloth, helmets, and for making helicopter seats bullet-proof. The high strength and light weight of this fiber makes it particularly attractive for low temperature ($\leq$ 100 °C) reinforcement applications.

The achievement of ultimate mechanical properties relies heavily on the processing conditions employed. For example, UHMWPE crystallized (quiescently) from the melt forms smaller crystals and has lower crystallinity than lower molecular weight material, due to poor chain mobility during crystallization. However when gel-drawn, the degree of chain mobility and extension becomes quite high, leading to high crystallinity, chain axis orientation, and possibly crystalline phase continuity. Gel spinning is but one of the techniques used to achieve high chain axis orientation (Keller, 1979). Typically, polyethylene is cold-drawn, solid state extruded (Perkins and Porter, 1977; Zachariades et al., 1980), solution spun or solution cast and drawn (Smith and Lemstra, 1980), or grown in the form of fibers from flowing solution (Barham, 1982; Zwijnenburg and Pennings, 1976; Pennings, 1977; Pennings and Meihuizen, 1979). All of these methods are believed to have underlying similarities, since in all cases the stiffness, strength, and melting points of these materials increase with draw in the same way (Smith and Lemstra, 1980).

C H A P T E R III

TRANSMISSION ELECTRON MICROSCOPY

The principal technique employed in this study was transmission electron microscopy (TEM). It is therefore appropriate to briefly survey the contrast mechanisms and beam damage considerations associated with this technique. For further details, the reader is referred to Reimer (1984), Glauert (1972 - 1981), Thomas (1986), Grubb and Keller (1972), Grubb et al. (1972), Grubb (1982), Bassett (1981), and Heidenreich (1964). The contrast mechanisms of electron microscopy can be divided into two major categories: those which derive mainly from the modulation of the amplitude (mass thickness contrast and diffraction contrast), and that which depends mainly on the modulation of the phase of an electron wave (phase contrast). In the case of polyethylene, both phase and diffraction contrast are available. These mechanisms provided sufficient contrast in the present studies.

TEM contrast arises generally from elastically scattered electrons. When a beam of accelerated electrons interacts with the electropotential field of an atom, the electrons scatter at various angles from the incident beam, such that the scattered intensity gradually falls off with increasing angle. The rate at which the intensity decreases with increasing scattering angle varies with the particular atom in question. The distribution of scattered intensity with angle for an isolated atom is given by the atomic scattering

factor. For instance, heavy atoms such as osmium or gold have large scattering cross sections, and therefore the scattered intensity diminishes slowly with increasing scattering angle. Carbon, on the other hand, has a relatively small scattering cross section and therefore the intensity decreases rapidly with angle. If the sample is noncrystalline, the scattered intensity can be approximated as due to incoherent scattering from its constituent atoms. For large scattering angles electrons are scattered outside of the objective aperture acceptance angle, and therefore do not contribute to the projected image. This gives rise to so called "mass thickness" contrast.

Mass thickness contrast can often be enhanced by the use of proper preparation techniques (Glauert, 1980, vol. 8; Watt, 1985; and Patel, 1980). In materials with poor contrast between phases, it is common to preferentially stain a reactive phase of the material with a heavy metal salt. For instance when stretched, cis-polyisoprene undergoes strain-induced crystallization. However, the mass thickness contrast between the noncrystalline and crystalline phases is quite poor. Due to the higher permeability of the noncrystalline phase to osmium tetroxide, however, the double bonds in the noncrystalline phase can be preferentially oxidized and stained. Staining with osmium tetroxide greatly enhances the contrast between the two phases (Andrews, 1964). Such a treatment has also been used for example, in phase-separated polystyrene/polybutadiene copolymers and their blends, since only the double bonds of the rubber are oxidized. However, care must be used

when quantifying phase size, as dimensions can be changed by staining (Berney et al., 1982).

As implied above, staining with a heavy metal salt generally requires that the permeability or reactivity of a given phase be greater than the unstained phase. However, it is also possible to "pre-treat" a material to make it receptive to a heavy metal stain. This is what is commonly done in the case of bulk polyethylene. Here, the amorphous phase is infiltrated with chlorosulfonic acid, which is subsequently reacted with uranyl acetate (Kanig, 1973 and 1975). This not only increases mass thickness in the amorphous phase, but also stabilizes the material against plastic deformation during cryo-microtomy. In the present set of experiments, this technique was not used as staining and microtomy procedures are prone to the generation of artifacts and therefore should be avoided or used in conjunction with other contrast mechanisms.

It should be noted that mass thickness contrast relies on the projected scattering cross-section. Therefore, thickness variations in a sample also contribute to this contrast mechanism. Since very thin samples ($\leq$ 100 nm thick, for 100 kV accelerating voltage) must be employed for TEM, significant thickness variations are often encountered. If a sample is too thick, multiple scattering and energy loss of electrons due to inelastic scattering occurs to a significant extent. This gives rise to chromatic aberration in the image, since the electrons exiting from the sample have a broad distribution of wavelengths. Since the focal length of a given lens varies with the

wavelength of incident radiation, chromatic aberration reduces the resolution of the resultant image.

Diffraction contrast constitutes another type of amplitude contrast. Due to the periodic arrangement of atoms in a crystal, electrons scatter coherently. These scattered electrons constructively interfere in well defined regions of scattering space, giving rise to diffraction spots which correspond to a given set of spacial frequencies. Diffraction contrast in brightfield mode relies on the exclusion of these spacial frequencies from the image. In this way, unscattered electrons and electrons which scattered an angles as high as the chosen objective aperture angle contribute to the image. Crystallites which diffract at angles exceeding the objective aperture acceptance angle appear dark in the resultant image, since these scattered electrons do not contribute to the image.

Darkfield imaging constitutes another mode of diffraction contrast. Here, the image is formed by electrons which contribute to a specified Bragg diffraction reflection(s). In the present case, multiple darkfield images of polyethylene were obtained by using the closely spaced (110), (200), (210), and (020) equatorial reflections. This was accomplished by exciting a set of electromagnetic coils in the illumination system which, in turn, modified the magnetic field through which the electron beam travels. The magnetic field tilted the incident electron beam off of the optic axis and the desired Bragg reflections onto the optic axis. Alternatively, the objective aperture can simply be moved such that only the desired diffraction reflections pass

through. This latter technique, however, gives poorer resolution since the image-forming electrons are far from the optic axis and therefore suffer significant spherical aberration. Moreover, the orientation of the electron beam with respect to the sample may differ considerably between these two techniques, depending on the Bragg angle of the reflection(s) used. The sensitivity of darkfield imaging to beam orientation is outlined below.

Diffraction contrast is very dependent on the orientation of crystalline regions with respect to the incident electron beam. Contrast arises from the variation of the diffraction intensity with misorientation from the Bragg angle. Such misorientation typically arises from for instance, the elastic bending of crystals or from defects within the lattice. The diffracted intensity is given by

$$I(s) \approx F(hkl)^2 \frac{\sin^2 \pi st}{\sin^2 \pi s}$$

where s is a measure of misorientation with respect to the Bragg angle (where s = 0), and t is the crystal thickness. F(hkl) is the structure factor for the (hkl) reflection, a measure of diffracted intensity from each crystal phase unit cell in the Bragg condition. Within a couple degrees of misorientation, the diffracted intensity decreases to zero (Thomas, 1986). Specifically, the intensity of the (110) reflection vanishes at a misorientation angle of 1.95 degrees for a single 12 nm thick polyethylene crystal at 100 kV electron accelerating voltage. In

the context of the present studies, this means that crystal sizes measured by the darkfield mode constitute lower bounds to the actual crystal sizes. This fact is particularly important when discussing the formation of a continuous crystalline phase, as such a phase would most likely not be simultaneously in the Bragg diffraction condition throughout the specimen.

Phase contrast is the final mechanism to be discussed. Unlike amplitude contrast, phase contrast does not arise from the exclusion of a particular set of electrons from the image. Rather, it arises from the interference of the scattered and unscattered electron waves. Upon scattering, an electron experiences a phase shift of 90°. Additional phase shift occurs depending on the scattering cross-section (and therefore distribution of intensity with scattering angle) of the sample. This arises from the fact that the imaging optics of the TEM induce phase changes as a complex function of scattering angle (i.e. spacial frequency), spherical aberration, and objective lens defocus. This phase modification of scattered signal by the TEM optics has been extensively analyzed in what is known as transfer theory. In fact, the phase shifts incurred by changing defocus cause the scattered amplitude to be modulated in both magnitude and sign. Specifically, the image amplitude is directly related to sin g(k), which is the phase contrast component of the microscope transfer function. Here, g(k) gives the phase shift as a function of wave vector (k). In addition, g(k) is a function of spherical aberration and defocus. The variation of sin g(k) with k is shown in Fig. 3.1. Note in particular the change in the sign

Figure 3.1

Variation of the phase contrast component of the microscope transfer function with wave vector (k), where g(k) is the phase shift which is a function of defocus and spherical aberration. The resultant image amplitude is directly related to sine g(k). Here a defocus (Df) of -150 nm, a spherical aberration (Cs) of 2.3 mm, and an accelerating voltage of 200 kV (electron wavelength of 0.0251 Å) were used.

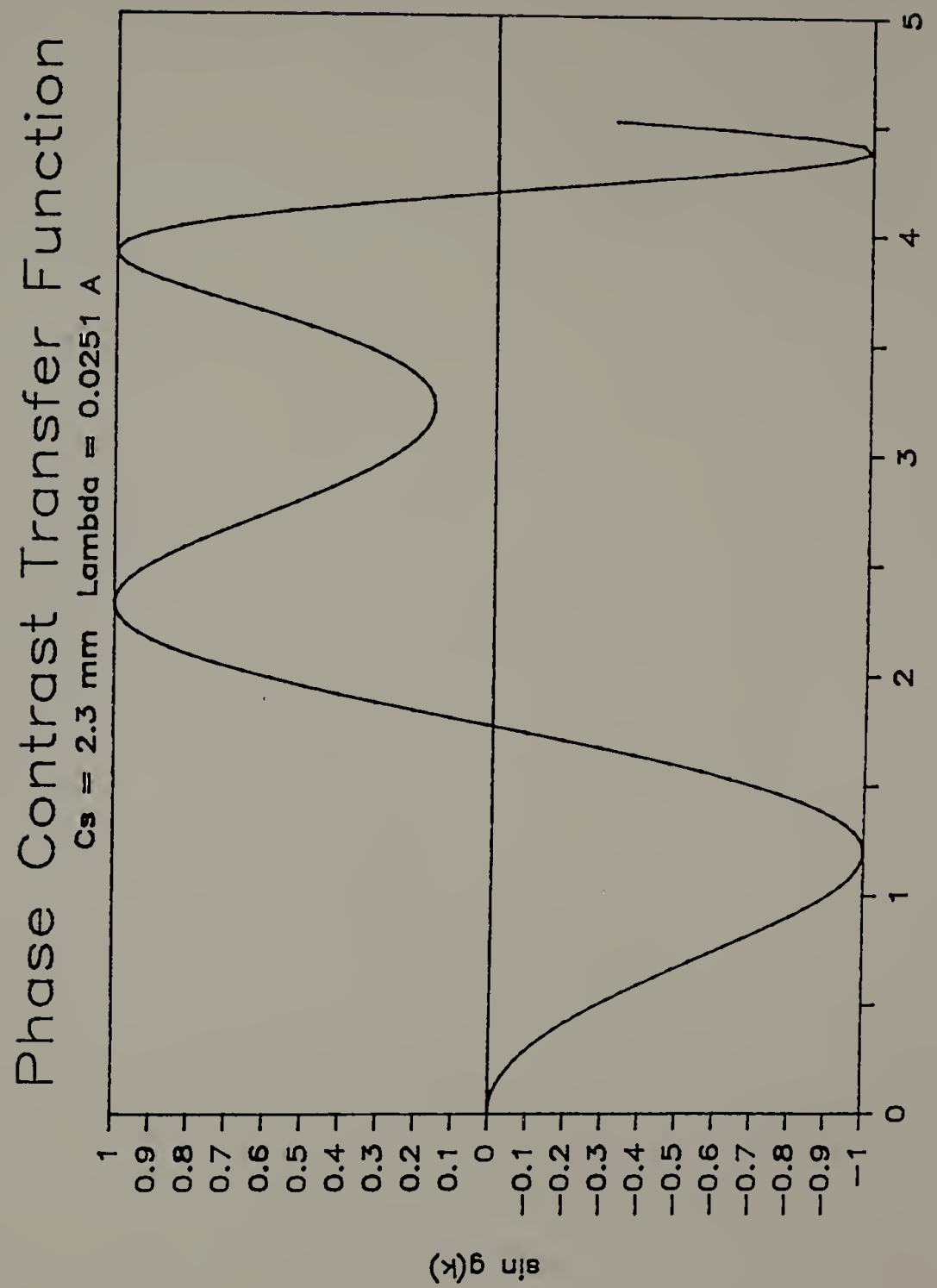
Phase Contrast Transfer Function
Cs = 2.3 mm Lambda = 0.0251 A
sin g(k)
1
0.9
0.8
0.7
0.6
0.5
0.4
0.3
0.2
0.1
0
−0.1
−0.2
−0.3
−0.4
−0.5
−0.6
−0.7
−0.8
−0.9
−1
0
1
2
3
4
5
k (nm−1)
Df = −150 nm

of sin g(k) with wave vector. This sign change is responsible, for example, for the alternation of light and dark fringes (Fresnel fringes) which are seen around holes in films which are viewed under defocus conditions.

This oscillatory modulation of spacial frequencies results in the enhancement of some frequencies and the total exclusion of others in the resultant image. This is used advantageously in the technique of lattice imaging. Here, a given set of lattice planes of a crystal are imaged under defocus conditions which optimize the amplitude at the frequency corresponding to the lattice spacing of interest and therefore increase the image contrast over other frequencies. The lattice planes are clearly imaged while structural information corresponding to other frequencies is removed or supressed. This technique was recently used on ultradrawn polyethylene gels to show the transition from orthorhombic to triclinic crystallite unit cells across a grain boundary (Chanzy et al., 1987).

The preceeding techniques are commonly used when a material is directly viewed by TEM. However, polymeric materials are generally not stable in the electron beam. For instance, exposure of polyethylene to the electron beam leads to bond scission and the generation of radicals. Specifically, C-H as well as C-C bonds are broken, and form hydrogen and carbon radicals, C-H bond scission being the most prevalent (Patridge, 1970). These chain scission reactions lead to mass loss as well as cross-linking reactions, mass loss generally occurring when C-C bonds undergo scission near chain or branch ends (Grubb, 1974; Keller, 1982;

Petermann and Gleiter, 1973a; and Isaacson, 1977). The introduction of cross-links on crystal fold surfaces reduces crystal perfection as well as content. The electron diffraction patterns shown in Fig. 3.2 portray the dentrimental effect of 100 kV electron irradiation on the crystalline phase. Note that the (110) and (200) reflections broaden along the equator and merge with increasing electron dose. Eventually, the crystals lose their periodicity altogether. The amount of beam damage depicted in Fig. 3.2 would occur in ca. 20 seconds at room temperature, 100 kV, using the typical dose rate employed for brightfield imaging.

The damage which accompanies irradiation causes brightfield and darkfield images to become an electron-dose-averaged representation of structure, rather than an image of the unirradiated material. In the present experiments, precautions were taken to minimize beam damage whenever possible, so that even if some beam damage occurred, the resultant image still retained features characteristic of the undamaged material. For instance, focusing was routinely performed on an area adjacent to the area to be examined, and brightfield micrographs were taken at a magnification of 4800 X while darkfield micrographs were taken at 3200 X. In all cases, samples were exposed to the minimum possible electron dosage when searching for deformed areas of the film. The degree to which polyethylene film was beam damaged was qualitatively monitored by the presence (or absence) of diffracting crystallites in brightfield and darkfield images. Figure 3.3 shows how irradiation changed the appearance of oriented, lamellar HDPE. Note that not only

Figure 3.2

Electron diffraction patterns illustrating the effect of electron irradiation on order in polyethylene crystals. The radiation dose increases from A to C. Each diffraction pattern is shown at two different exposures. Chain axis vertical.


A
B
C

Figure 3.3

Effect of electron irradiation on brightfield image of polyethylene. Very dark areas are diffracting crystallites. A) slightly damaged, B) highly damaged.

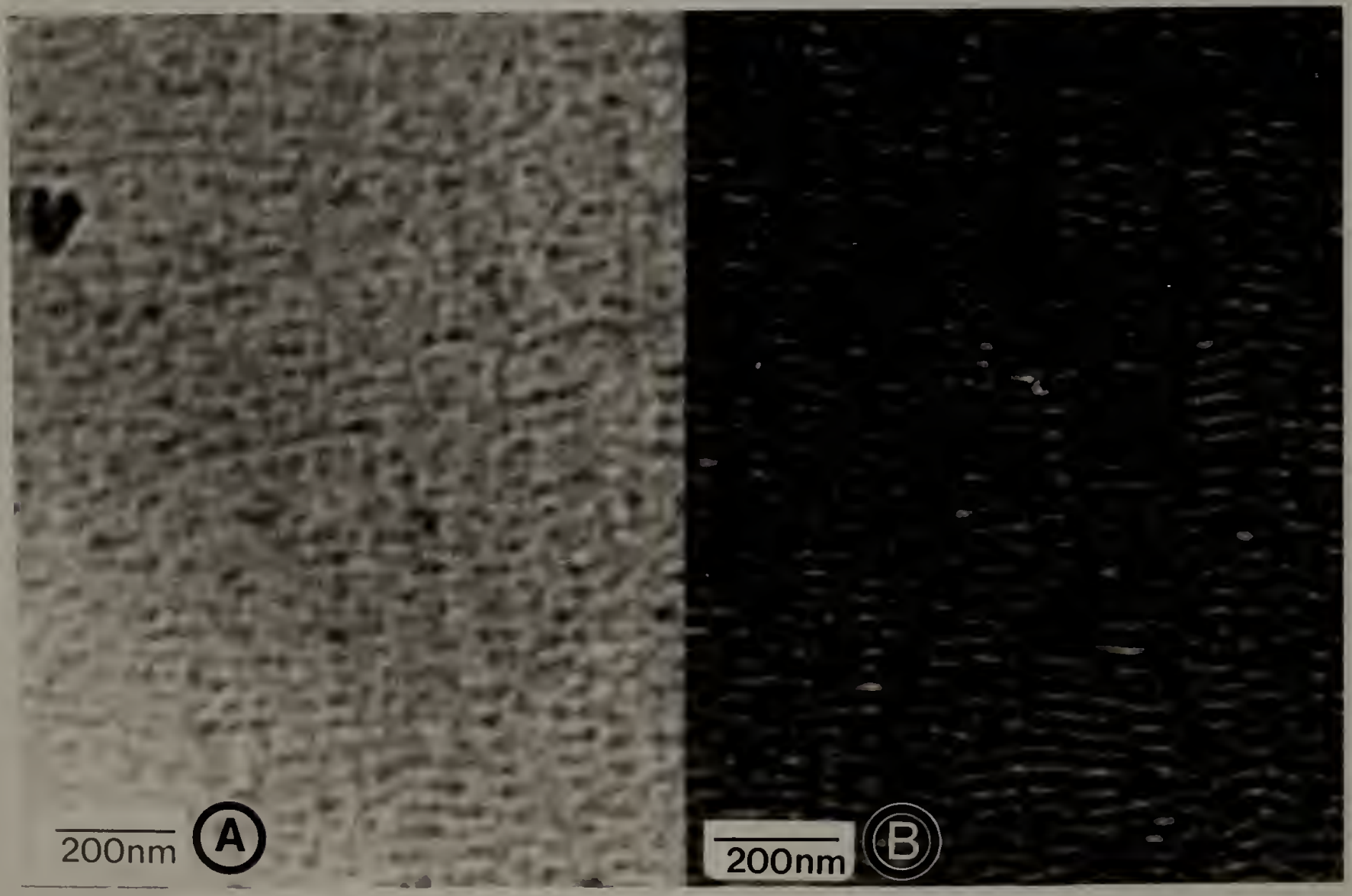
200nm
A
200nm
B

are fewer crystallites diffracting in the more highly damaged image, but also the contrast between amorphous and crystalline layers increased with electron dose.

In addition to bond breakage, inelastic collisions of the electron beam with the sample also result in a rise in temperature. This, however, can be minimized by making sure the sample is in good thermal contact with the specimen grid, and by carbon coating samples, thereby adding a thermally conductive layer. Under these conditions, temperature rise in thin films is considered to be a relatively minor consideration (Grubb, 1974).

Other forms of beam damage include electrical charging and contamination. In the former case, the interaction of primary electrons (which pass through thin films) with a material results in the emission of (low energy $\leq$ 50 eV) secondary electrons, resulting in positive charge buildup. This of course modifies the electropotential field of the specimen. Charging, however, is not considered as important in TEM as in scanning electron microscopy, where absorption of the primary beam in the much thicker sample brings about a negatively charged material.

Sample contamination results when residual contaminants in the microscope column (e.g. volatilized hydrocarbons) deposit onto the sample and undergo a beam-induced cross-linking reaction, resulting in mass buildup. Such a buildup was particularly evident when using annular darkfield scanning transmission electron microscopy (STEM). In STEM, an electron beam of ca. 6 - 10 nm diameter is rastered across the sample, and the transmitted beam intensity is simultaneously recorded on

a cathode ray tube, pixel by pixel. In the annular darkfield technique, a darkfield image is obtained by centering the HDPE diffraction pattern inside an objective aperture, and by blocking out the unscattered beam and unwanted reflections with the beam stop. This is easily done, since the effective sample to detector distance can be modified by adjusting the manual lens controls. An example of sample contamination can be seen in Fig. 3.4. Here, the square region was heavily beam damaged during focusing. Contamination and the subsequent increase in mass thickness in this beam-damaged noncrystalline region resulted in the incoherent scattering of electrons. These "amorphous halo" scattered electrons, as well as electrons from diffracting crystallites outside of the beam-damaged region, contributed to the darkfield image.

One technique commonly used to circumvent the problems endemic to beam-damageable materials is to view inert surface replicas of the samples under study. This process generally involves transcribing the topography of a low temperature fractured and/or etched sample. In the former case, samples are fractured well below their glass transition temperatures to limit alteration by plastic deformation of the original structure. In the latter technique, free or fractured surfaces are acid etched. For example, polyolefins are typically etched with nitric acid (Hay and Keller, 1966; Palmer and Cobbold, 1964; Holdsworth and Keller, 1969), or with a solution of $KMnO_4$ and sulfuric acid (Olley et al., 1979; Freedman et al., 1986). The etchant preferentially attacks and removes the noncrystalline phase. Under extreme conditions, the crystalline phase may also be etched somewhat. In particular, defective

Figure 3.4

Scanning transmission electron micrograph of drawn polyethylene viewed in annular darkfield mode. Bright square region was heavily irradiated and has become contaminated.


200nm

regions of crystallites are prone to attack (Freedman et al., 1986). Replicas are then made by shadowing the sample with Pt/C followed by carbon coating at 90 ° to the film plane. The Pt/C replica can then be separated from the sample and viewed by microscopy. Still another replication technique, known as a "detachment replication", involves the detachment of very thin pieces of the material from the bulk sample, enabling electron diffraction and micrographs to be taken of the actual specimen. The specific details of this technique will be discussed in Chapter 6, where it was used in the study of bulk SSE and SSE/PD polyethylene.

C H A P T E R IV

PREPARATION AND MORPHOLOGY OF GEL-DRAWN FILMS OF HIGH AND LOW DENSITY POLYETHYLENE

Abstract

Thin, single crystal-like textured, shish-kebab morphology films of drawn polyethylene were prepared. The precursor state of these films was found to be a gel. As-drawn films were characterized by differential scanning calorimetry (DSC), dynamic mechanical thermal analysis (DMTA), transmission electron microscopy (TEM), and electron diffraction. The polymers studied were high density polyethylene (HDPE) and randomly branched linear low density polyethylene (LLDPE) of varying branch length (ethyl- to hexyl-) and content (up to 2.4 mole percent). Thermal analysis indicated that branch length had little effect on the crystallization process, and that crystallinity and crystal size decreased as branch content increased. In fact, the peak melting temperature could be predicted based solely on branch content (assuming randomly branched material) and the provision that branches be excluded from the crystalline lattice. Moreover, the range of crystal sizes present increased as branch content increased. It was further noted that randomly branched materials of approximately equal average branch content contained very different distributions of crystal sizes, implying fractionation took place during crystallization. Such

fractionation emphasized the need of a branching polydispersity index to characterize the variation of branch content from chain to chain.

DMTA data revealed a decrease in the α loss peak temperature as branch content increased, indicating a reduction in the mechanical stability of the crystalline phase with increasing branch content. In fact, at high enough branch content the α and β peaks apparently merged into a single peak at 3 °C, 1 hz. The α transition occurred at 73 °C, 1 hz for isotropic HDPE, cooled from 180 °C at room temperature. At lower branch contents the β relaxation was identified with a distinct peak. In the case of HDPE, no β peak was detected at all.

Microscopy studies verified the reduction of crystal size with increased branching. In addition, highly branched material did not form periodically alternating noncrystalline and crystalline layers. Indeed, the lamellar character of highly branched polyethylene film was poorly defined with respect to that seen in HDPE film. In all cases, the gel-drawing process resulted in a shish-kebab morphology, indicating that strain-induced crystallization occurred even in branched material.

Introduction

The influence of processing, morphology, and molecular topology on mechanical properties has long been recognized (Samuels, 1985; Kanamoto et al., 1983a; Peterlin, 1977 and 1979; Capaccio et al., 1976; Ward, 1984; Smith et al., 1981b). A broad range of properties can in fact be obtained by simply varying branching characteristics. It is important

to understand the means by which this occurs (Wunderlich, 1973a; Sequela and Rietsch, 1986a and b; Alamo et al., 1984; Mandelkern, 1985; Krigas et al., 1985; Martuscelli, 1975; Cady, 1987; Furumiya et al., 1985). In particular, how do branch content, length, and the distribution of branches both along a single chain and among chains affect the crystallization behavior and microstructure of polyethylene?

Here, HDPE and LLDPE were studied in both the bulk isotropic form, and in the form of oriented thin films. Thin films were used to permit microstructural examination by TEM. The films were made using a processing technique which up to this point has not been adequately understood. To better understand this process, the gelation behavior of HDPE solution was determined, and the probability of gelation during film production (at temperatures just below the melting point) ascertained.

Previous quiescent gelation studies (Domszy et al., 1986) have indicated that a polymer with a weight average molecular weight of 2×10^5 would gel in the temperature range of 120 - 125 °C for concentrations equal to or exceeding the critical concentration of ca. 3 - 4.5 % (w/v). However, at temperatures near the crystalline melting point, gelation usually is quite slow, taking several days to reach completion at or near the critical concentration. In the present case, it is conceivable that the crystallization rate and thus gelation would be accelerated by the attainment of concentrations far exceeding the critical gelation concentration due to solvent loss during film

preparation. In addition, once gelation commenced, the application of strain would further accelerate the crystallization process.

As-drawn films were characterized by both TEM and DSC. Moreover, isotropic samples of LLDPE and HDPE were characterized by DMTA as well as DSC. These techniques enabled the crystallization process to be better understood, and in particular allowed the comparative stability of crystals to be determined. Using DSC data, the effect of branching on crystal size, perfection, and content was determined by melting endotherm width and the enthalpy of fusion. The alpha transition temperature was determined using DMTA data, giving insight into the mobility of chains in the crystalline phase at low stress levels.

The alpha loss has been well studied and documented by others (Hoffman et al., 1966; Kajiyama et al., 1973; Takayanagi and Kajiyama, 1973; Tanaka et al., 1973; Stein, 1973; Gibson et al., 1978; Cembrola and Stein, 1980) and has been associated with a drop in the crystalline phase shear modulus (Gibson et al., 1978). This mechanical loss transition can be resolved into two peaks for annealed polyethylene. The low temperature part (α_1) is thought to be associated with grain boundary motion and possibly chain fold motion on crystal surfaces, while the high temperature part (α_2) is suggested to correspond to intracrystalline motion. In unannealed single crystals, only the latter component (α_2) is present and is found to depend on crystal thickness, perfection, and thermal history. The former (α_1) transition on the other hand, is greatly affected by crystalline phase morphology, lamellar orientation, and possibly the nature of the interface between

mosaic blocks (Mandelkern, 1985). The temperatures at which the α_1 and α_2 processes occur vary with deformation rate, the loss peak temperature increasing with increasing strain rate (Kajiyama et al., 1973). Typical values of the α_1 and α_2 transition temperatures at 11 Hz for HDPE, quenched in an ice bath from 175 °C, are 60 and 72 °C, respectively (Ueda et al., 1986).

Two additional peaks are often present in polyethylene. These peaks have been designated the β and γ peaks. The γ peak is what is customarily cited as the glass transition peak, and is associated with both crystalline and noncrystalline phase components (Hoffman et al., 1966). The β peak, on the other hand, is believed to arise from the noncrystalline phase. It too has been related to with the glass transition (Hoffman et al., 1966). More specifically, the beta relaxation has been associated with interlamellar motion in which the fold surfaces of two adjacent lamellae move past one another (Takayanagi and Kajiyama, 1973). Beta peaks are only found in materials with appreciable interfacial content (branched or ultrahigh molecular weight polyethylene), the transition temperature depending on copolymer type (Mandelkern, 1985).

Experimental

Materials

The materials used are given in Table 4.1. All LLDPE samples were essentially randomly branched. Those prefaced by RC- or PBD- were made by Dr. L. Fetters of Exxon Corp. by hydrogenating polybutadiene. All other branched material is commercially available and was made by the copolymerization of the desired alpha-olefin with ethylene (Nowlin, 1985). The materials prefaced by NTX- or MJX- were obtained from Mobil Chemical Co., while Marlex was obtained from Phillips Petroleum Co., Hifax from Hercules, and Dowlex from Dow Chemical. The hydrogenated polybutadiene samples were of low molecular weight polydispersity, in contrast to the broad molecular weight distribution in commercially available materials, and were believed to be more uniformly branched than their commercial counterparts. These differences will be addressed in a later section when discussing fractionation during crystallization.

All as-received LLDPE specimens except Dowlex 61500.40 and the hydrogenated polybutadienes had been characterized by ^{13}C NMR to determine branch content and branch distribution along the chain (Randall, 1977; Hsieh and Randall, 1982 a and b). For the Dowlex sample, the methyl group content, which had been determined by infrared spectroscopy, was converted to branch content. The ethyl branch content of hydrogenated polybutadienes had been calculated by determining the

Table 4.1

Polyethylene characterization

Material	Branch Type	M_w ($\times 10^5$)	M_w/M_n	Mole % Branches	% Crystallinity (Enthalpic)
Hifax 1900	---	20.	7.6	ca. 0	49
Marlex 6003	--	1.95	7-13	ca. 0	76
PBD-A1	ethyl	0.48	1.04	4.14	22
PBD-A2	ethyl	0.43	1.04	5.68	14
RC-2	ethyl	4.0	1.09	2.08	26
RC-4	ethyl	1.45	1.07	2.36	30
MJX-501	ethyl	1.04	5.2	2.05	38
NTX-017	butyl	0.97	5.4	1.23	46
NTX-018	butyl	1.05	5.5	2.29	39
Dowlex 61500.40	hexyl	0.84	4.7	0.3	58

vinyl group content of parent polybutadienes, as measured by ^{1}H NMR (Santee et al., 1973a). Branching distributions in hydrogenated polybutadienes have been shown to be essentially Bernoullian at low vinyl concentrations (Santee et al., 1973b).

Film Production

As-drawn films of LLDPE and HDPE were prepared according to the technique of Petermann and Gohil (1979). Ortho-xylene solutions of 0.5% (w/w) concentration were employed. Using this technique, a hot solution was placed on a preheated glass plate. Processing temperatures are indicated in Table 4.2. Once the solution reached a critical concentration, crystallization commenced. Though the solvent and crystalline content of the material at any given time was unknown, it is believed that a network of crystallites interconnected by noncrystalline regions developed. This made the film sufficiently rigid and coherent to be drawn from the glass surface.

Very high elongations were achieved during drawing and subsequent crystallization, producing thin films which could be directly viewed by TEM. The entanglement density in these films was assumed to be low (regardless of branching), since the initial solutions were dilute, and solvent loss as well as crystallization occurred very quickly. As-drawn films were annealed on the surface of glycerol for two hours in an air oven to enhance crystal perfection (temperatures indicated in Table 4.2). This increased the sharpness of boundaries between crystalline

Table 4.2

Processing of films for microscopy

Material	Branch Type	T (°C) draw	T (°C) anneal	T_m (°C) onset
Marlex 6003	--	120-125	130	125
RC-4	ethyl	85-95	89	83
NTX-017	butyl	100-104	110	117
NTX-018	butyl	101-104	105	119
Dowlex 61500.40	hexyl	108-111	106	114

and amorphous layers, and the lateral extent of lamellae. The films were then washed with water, floated from a water surface onto copper grids, and dried in a vacuum oven at room temperature.

To study the effect of solution concentration on gelation rates, o-xylene solutions of Marlex 6003 at concentrations ranging from 2.6 to 14.5 % (w/w) were prepared in capped pressure vials. These solutions were heated overnight in a Tamson oil bath set at 120 °C to assure homogeneity. The oil bath and solutions were then allowed to cool to 23 °C. Cohesive gels formed in all cases. The temperature of the oil bath was then slowly increased and the temperatures at which the gels dissolved (as discerned visually by the onset of flow) were recorded. Attempts were not made to reach equilibrium conditions, as nonequilibrium conditions better mimicked the film processing conditions under study.

Thermal and Mechanical Analysis

The quiescent crystallization behavior of the materials listed in Table 4.1 was characterized using DSC. These results were then compared with those obtained for corresponding as-drawn films. A Perkin-Elmer DSC-II, interfaced with standard Thermal Analysis Data Station software was employed. To mitigate processing history effects, undrawn samples were heated to 177 °C and maintained at that temperature (under nitrogen) for at least thirty minutes. These samples were then cooled at a rate of 5 °C/min, to 27 °C. Subsequent heating was conducted at a

rate of 20 °C/min over a temperature range of 30 - 167 °C, and melting endotherms were recorded. Temperatures and enthalpies of fusion were calibrated with indium and naphthalene standards. Crystallinities were calculated from enthalpies of fusion, taking the enthalpy of fusion for a perfect polyethylene single crystal to be 69 cal/gm (Wunderlich, 1973b). The results of the above experiments were compared with data obtained for rapidly crystallized copolymers (Alamo et al., 1984).

Samples for DMTA characterization were prepared by melting them on a hot (180 °C) press for 5 minutes and subsequently applying a pressure of 150 psi for 3 minutes. The samples were then removed and cooled at 25 °C. Note that the crystallization conditions used to make DMTA samples were far from equilibrium, so as to better represent the crystallization conditions present during film preparation. Even so, the DMTA specimens were isotropic while the as-drawn films were highly oriented. This means that the DMTA data should only be used as rough quidelines for the analogous transitions in as-drawn films. These isotropic films were typically 0.3 mm thick, 6.0 mm long, and 2 mm wide. A DMTA from Polymer Labs, Amherst, Mass. was used. Testing was done under nitrogen, using the dual cantilever mode at a frequency of 1 hz, and a scan rate of 5 °/min over a temperature range of -120 °C to near melting.

Microscopy

TEM analysis was done on thin, oriented, as-drawn films of all of the samples listed in Table 4.2. The films were carbon coated to increase thermal conductivity and mechanical stability, and then directly viewed without further treatment. Under no circumstances were replicas or heavy metal stains used.

Results

Gelation studies and Thermal Analysis

The gel dissolution temperature increased linearly with concentration (Fig. 4.1). For reference, the dissolution temperature for single crystals crystallized under equilibrium conditions is 110.4 °C (Wunderlich, 1973c).

DSC results on both quiescently crystallized and drawn samples are shown in Figures 4.2 and 4.3, respectively. Crystalline content decreased as branch content increased, and was not sensitive to branch length (Fig. 4.4). The invariance of crystal thermal stability with branch length supported the conclusions of others (Alamo et al., 1984; Vile et al., 1984; Burfield and Kashiwa, 1985; Perez et al., 1987; Mandelkern, 1985) which state that branch points are mostly if not entirely excluded from the crystalline phase when crystallization occurs at or near equilibrium conditions. The more slowly the LLDPE is

Figure 4.1

HDPE gel dissolution temperature as a function of solution concentration.

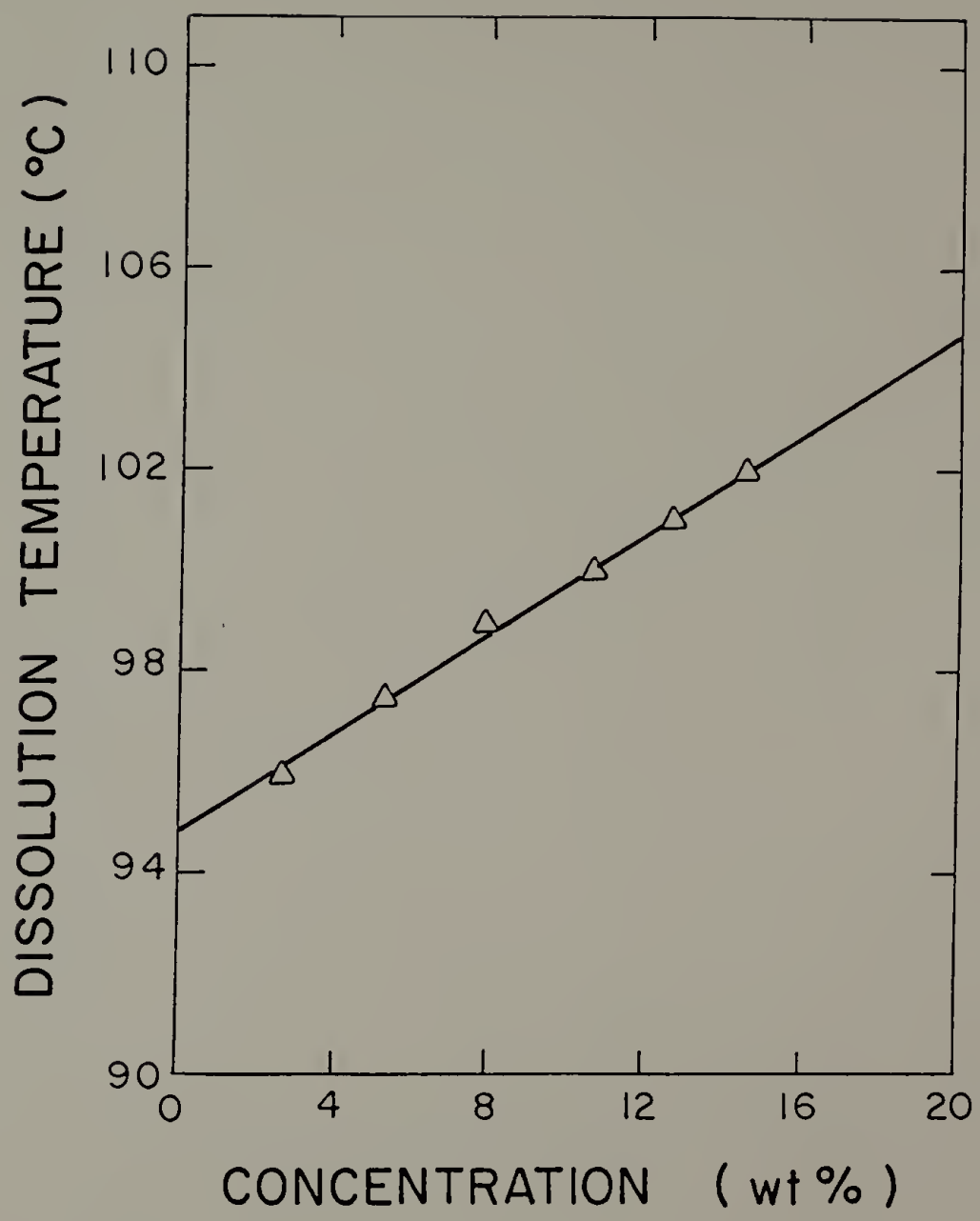
DISSOLUTION TEMPERATURE (°C)
110
106
102
98
94
90
0
4
8
12
16
20
CONCENTRATION (wt %)

Figure 4.2

Normalized (by weight) melting endotherms of polyethylene cooled from the melt and then scanned at a rate of 20 °C/min. Solid lines correspond to linear low density polyethylene (branched) while broken lines correspond to high density polyethylene (essentially unbranched). The high density polyethylenes are designated as follows:

dashed line - Hifax 1900

dash-dot-dash line - Marlex 6003

The branched polymers are designated as follows:

A - PBD-A2	D - RC-2	G - NTX-017
B - PBD-A1	E - MJX-501	H - Dowlex 61500.40
C - RC-4	F - NTX-018	

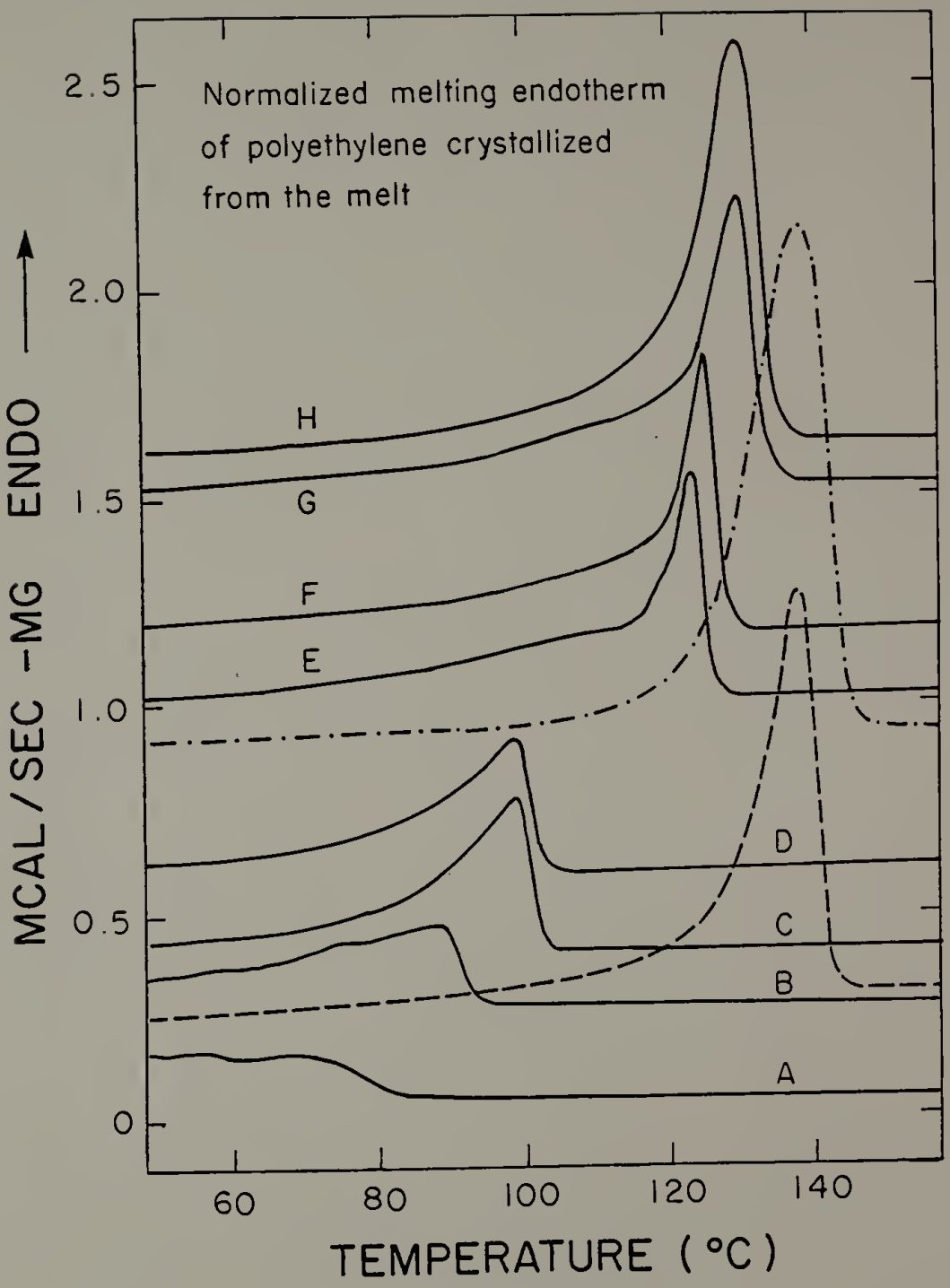
Normalized melting endotherm
of polyethylene crystallized
from the melt
MCAL / SEC -MG ENDO
2.5
2.0
1.5
1.0
0.5
0
H
G
F
E
D
C
B
A
60
80
100
120
140
TEMPERATURE (°C)

Figure 4.3

Normalized (by weight) melting endotherms of as-drawn polyethylene, scanned at 20 °C/min. Solid lines correspond to linear low density polyethylene (branched) while broken lines correspond to high density polyethylene (essentially unbranched). The high density polyethylenes are designated as follows:

dash - Hifax 1900

dash-dot-dash - Marlex 6003.

The branched polymers are designated as follows:

A - PBD-A2	D - RC-2	G - NTX-017
B - PBD-A1	E - MJX-501	H - Dowlex 61500.40
C - RC-4	F - NTX-018	

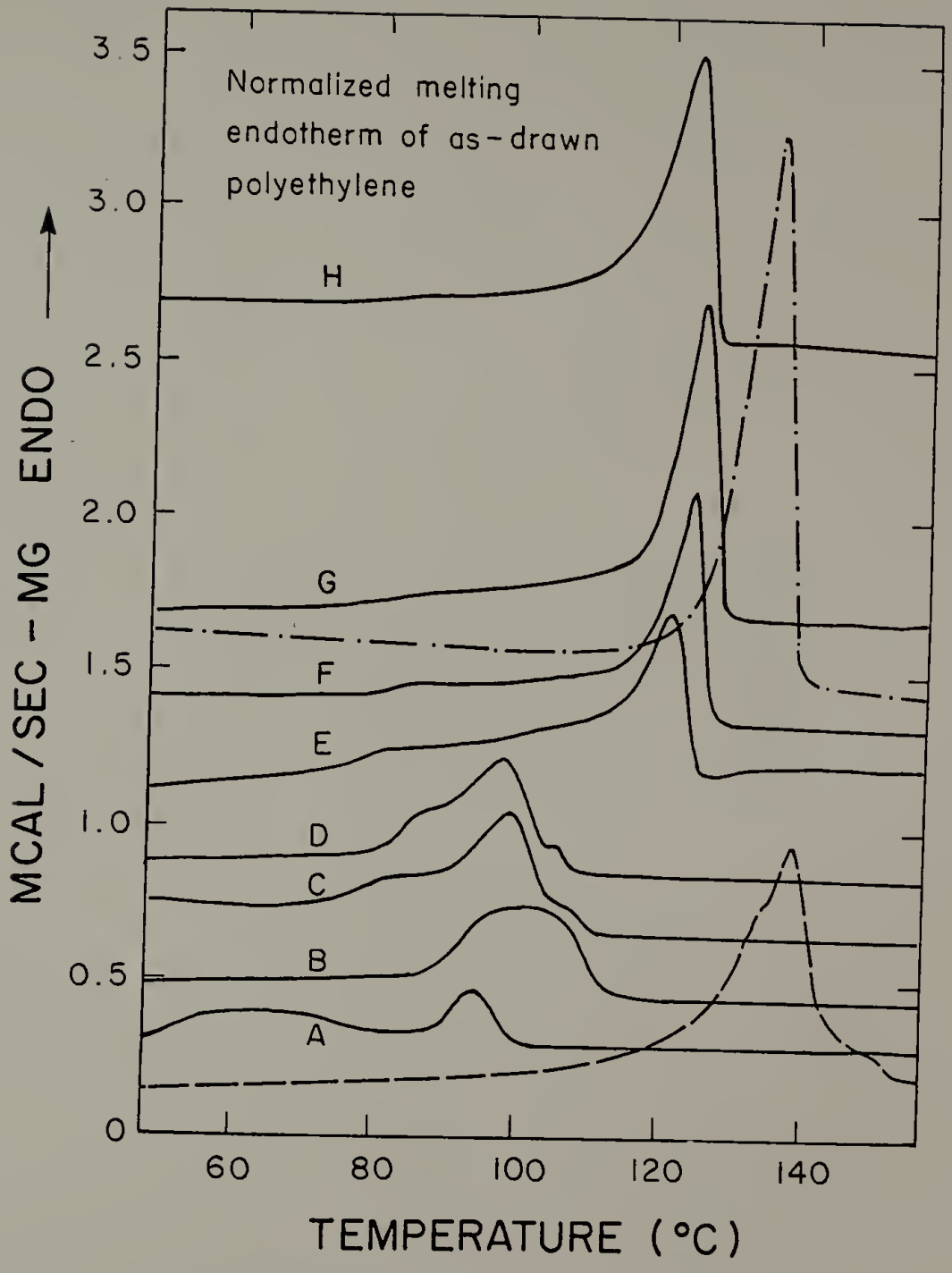
Normalized melting
endotherm of as-drawn
polyethylene
MCAL/SEC-MG ENDO
3.5
3.0
2.5
2.0
1.5
1.0
0.5
0
H
G
F
E
D
C
B
A
60
80
100
120
140
TEMPERATURE (°C)

Figure 4.4

Enthalpic crystallinity as a function of branch content in polyethylene for both drawn (oriented) and undrawn (isotropic) samples. Data of Alamo et al., (1984) was plotted for comparison.

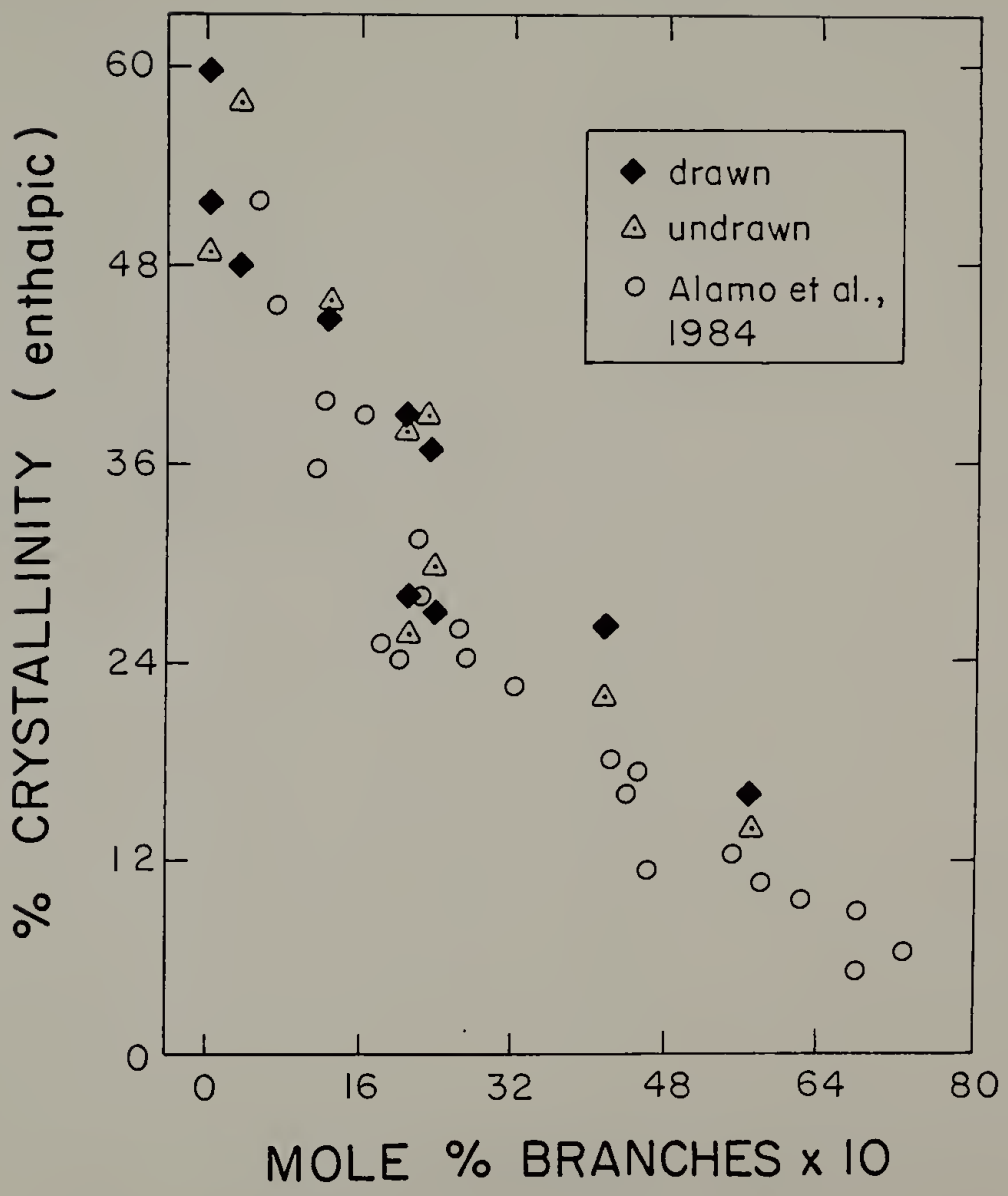
% CRYSTALLINITY (enthalpic)
60
48
36
24
12
0
0
16
32
48
64
80
MOLE % BRANCHES x 10
drawn
undrawn
Alamo et al., 1984

crystallized, the fewer branches are incorporated in the crystalline phase (Sanchez Cuesta et al., 1987). One exception involves methyl branches, which are sufficiently small to be incorporated into the crystal phase.

The reduction in crystal size brought on by branching results in melting point depression, since the ratio of crystal surface area to volume, and therefore crystallization free energy, increases as crystal size decreases. Branch content can be related to melting point depression by the following equation where the heat of mixing of branch points into the melt is ignored (Flory, 1949):

$$1/T_m - 1/T_m^{\bullet} = - (R/\Delta H_u)\ln(1 - x)$$

Here ΔH_u is the enthalpy per repeat unit, x is the mole percent branch points along the backbone, and $T_m^{\bullet}$ is the melting point of an infinitely long unbranched chain. This equation was derived for the case of equilibrium crystallization. The melting point is thus related to the probability that a randomly chosen crystallizable unit in the backbone is followed by another such unit. A plot of $1/T_m$ versus $-\ln(1 - x)$ showed approximately linear behavior and gave a $T_m^{\bullet}$ value of 135 $^{\bullet}$C (Fig. 4.5). This value equalled the melting point of unbranched material (Fig. 4.6), but was lower than the published equilibrium value of 141.4 $^{\bullet}$C (Wunderlich, 1973c) due to nonequilibrium conditions and possibly defects within crystals. The successful application of Flory's equation to experimental data suggests that the reduction in crystallite

Figure 4.5

Plot of Flory (1949) equation depicting dependence of melting point of LLDPE crystals on the mole fraction of crystallizable units.

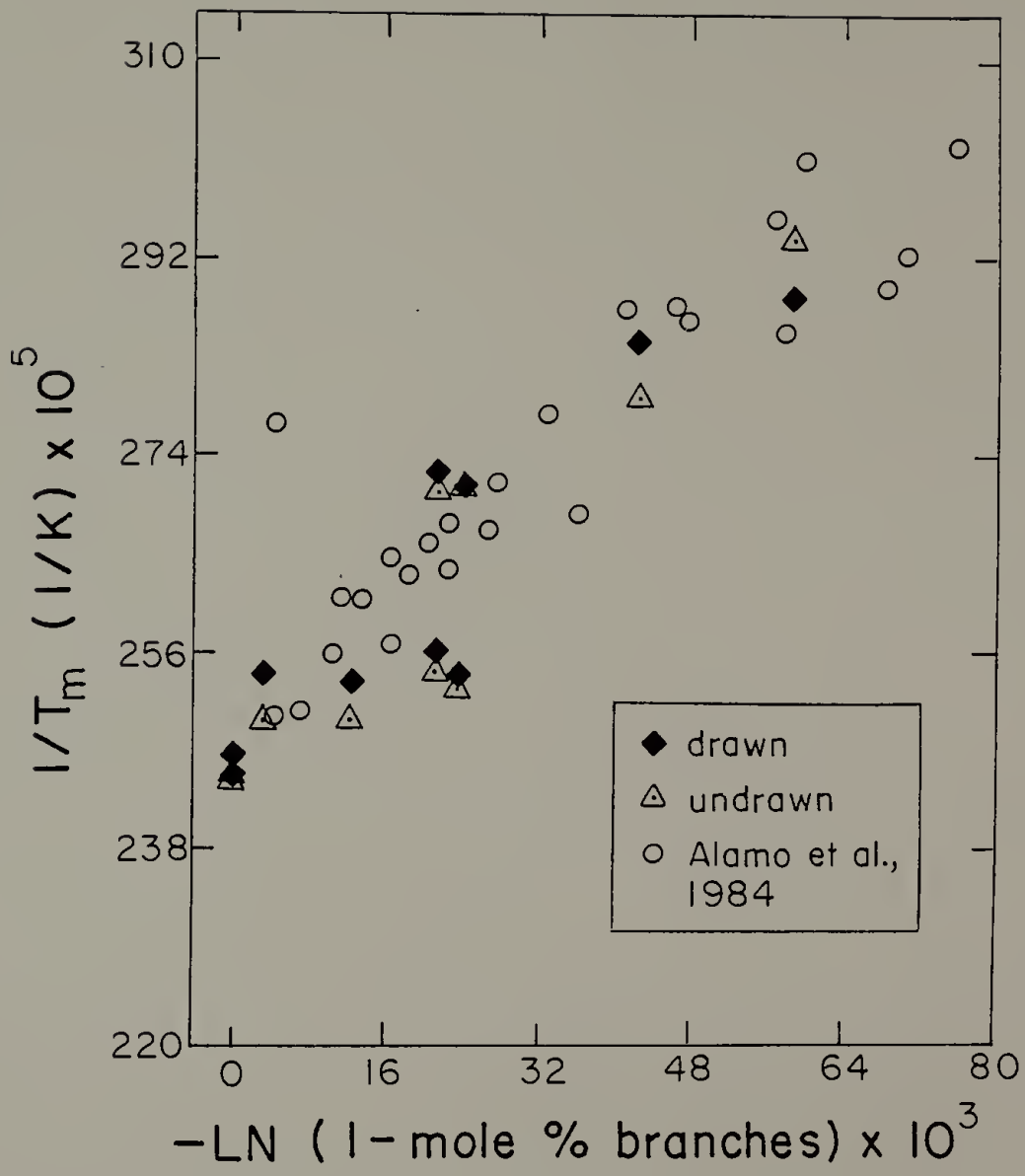
310
292
274
256
238
220
0
16
32
48
64
80
$1/T_m$ (1/K) x 10^5
−LN (1−mole % branches) x 10^3
drawn
undrawn
Alamo et al., 1984

Figure 4.6

Peak melting temperature as a function of branch content in LLDPE for both drawn (oriented) and undrawn (unoriented) samples. Data of Alamo et al., (1984) was plotted for comparison.

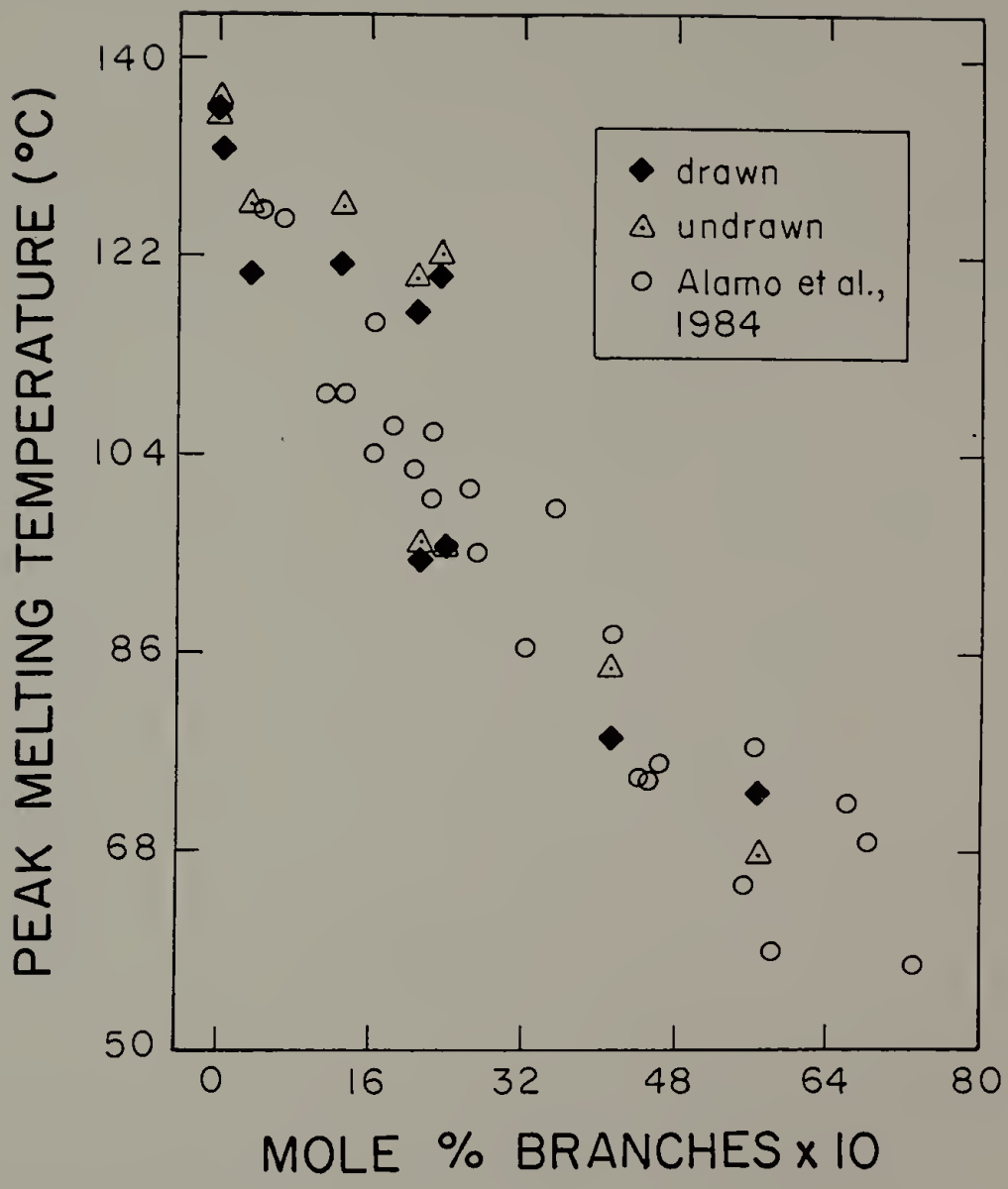
PEAK MELTING TEMPERATURE (°C)
140
122
104
86
68
50
0
16
32
48
64
80
MOLE % BRANCHES x 10
drawn
undrawn
Alamo et al., 1984

size with increased branch content can be explained solely in terms of the exclusion of branch points from the crystalline phase. This indicated that not only are most branches excluded from the crystalline phase, but that the effect of branching on the diffusion of chains to crystallization sites played a negligible role during crystallization.

The disruption of the crystallization process by branching is also evidenced in Fig. 4.4, where crystallinity decreased approximately exponentially with branch content. It appears that either the drawing process did not substantially affect crystallinity, or annealing and chain reorganization during thermal analysis obscured any differences which were originally present. Visual extrapolation of the data suggests that the material would be entirely noncrystalline at a branch content of about 14 - 16 mole percent. The dependence of crystal size on molecular weight was minor, as evidenced by the comparable melting points of the two HDPE samples.

The number of melting peaks observed by DSC varied significantly between the undrawn and drawn materials (Figures 4.2 and 4.3, respectively), the drawn samples usually exhibiting a greater number of peaks and/or shoulders. For instance, undrawn HDPE samples (Marlex and Hifax) showed a single melting endotherm whereas drawn Hifax yielded three peaks and drawn Marlex displayed a main peak with a shoulder. In addition, DSC scans of drawn HDPE and LLDPE (Hifax, RC-2, and RC-4), each displayed a satellite peak at temperatures exceeding that of the main (most intense) peak.

Melting peak breadth and therefore the distribution of crystal sizes (and defects within crystals) was found to increase as branch content increased. For example, the main melting peaks of RC samples were much broader than those of MJX-501 and NTX-017. Even NTX-018 samples had a much narrower peak than RC-4, although they had essentially the same branch content. This implied that another variable, such as the polydispersity of branch content between chains had affected crystallization behavior.

Mechanical Analysis

In these experiments, the storage modulus, loss modulus, and tangent phase lag angle (tan δ) were recorded as a function of temperature for unbranched polyethylene (Marlex 6003) as well as commercially available LLDPE (NTX-series) and hydrogenated polybutadiene (RC-4) (Figures 4.7 - 4.10). The results indicated that the storage modulus at 25 °C decreased from about 1.5 GPa for unbranched material to about 0.11 GPa for the hydrogenated polybutadiene. The α, β, and γ loss peaks were determined by averaging tan δ and loss modulus peak temperatures. The α loss peaks were located at 73 °C, 70 °C, and 50 °C for Marlex 6003, NTX-017, and NTX-018, respectively; indicating that the α peak occurred at lower temperatures as branch content increased. This is consistent with previously cited observations that the transition temperature decreases as crystal thickness decreases. In addition to the α peak, a β peak was found for the NTX- polymers at -15 °C, while no

Figure 4.7

Smoothed dynamic mechanical thermal analysis curves of compression molded (isotropic) Marlex 6003 bulk film using the dual cantilever mode at a frequency of 1 hz and a scan rate of 5 °C/min. Solid lines correspond to the storage (E') and loss (E'') tensile moduli as indicated. The broken line corresponds to the tangent phase lag angle between the storage and loss moduli. Note that all ordinates are plotted on a logarithmic scale.

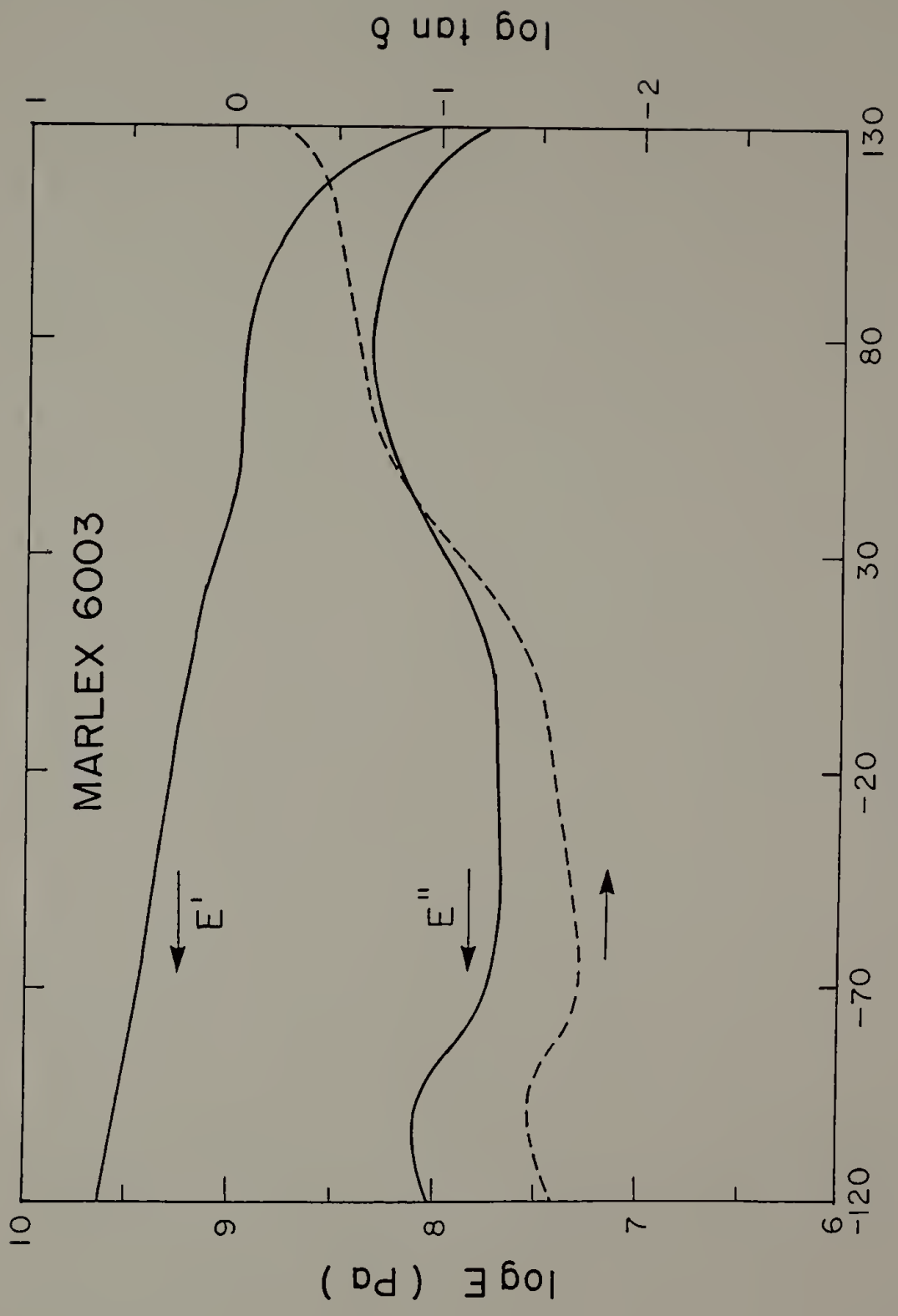
MARLEX 6003
E'
E''
log E (Pa)
log tan δ
TEMPERATURE (°C)
10
9
8
7
6
1
0
-1
-2
-120
-70
-20
30
80
130

Figure 4.8

Smoothed dynamic mechanical thermal analysis curves of compression molded (isotropic) NTX-017 bulk film using the dual cantilever mode at a frequency of 1 hz and a scan rate of 5 °C/min. Solid lines correspond to the storage (E') and loss (E'') tensile moduli as indicated. The broken line corresponds to the tangent phase lag angle between the storage and loss moduli. Note that all ordinates are plotted on a logarithmic scale.

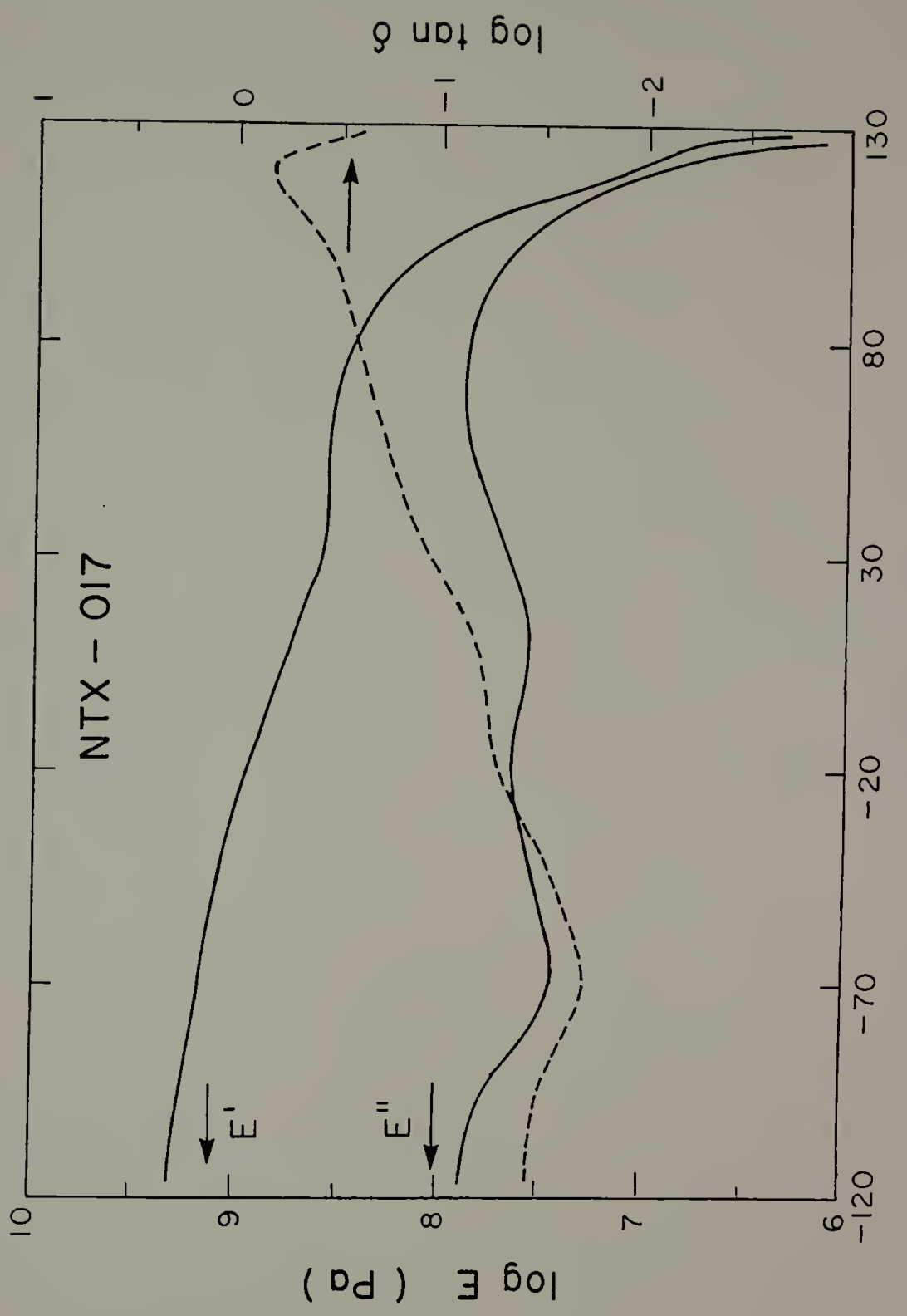
log tan δ
1
0
-1
-2
log E (Pa)
10
9
8
7
6
NTX - 017
E'
E''
-120
-70
-20
30
80
130
TEMPERATURE (°C)

Figure 4.9

Smoothed dynamic mechanical thermal analysis curves of compression molded (isotropic) NTX-018 bulk film using the dual cantilever mode at a frequency of 1 hz and a scan rate of 5 °C/min. Solid lines correspond to the storage (E') and loss (E'') tensile moduli as indicated. The broken line corresponds to the tangent phase lag angle between the storage and loss moduli. Note that all ordinates are plotted on a logarithmic scale.

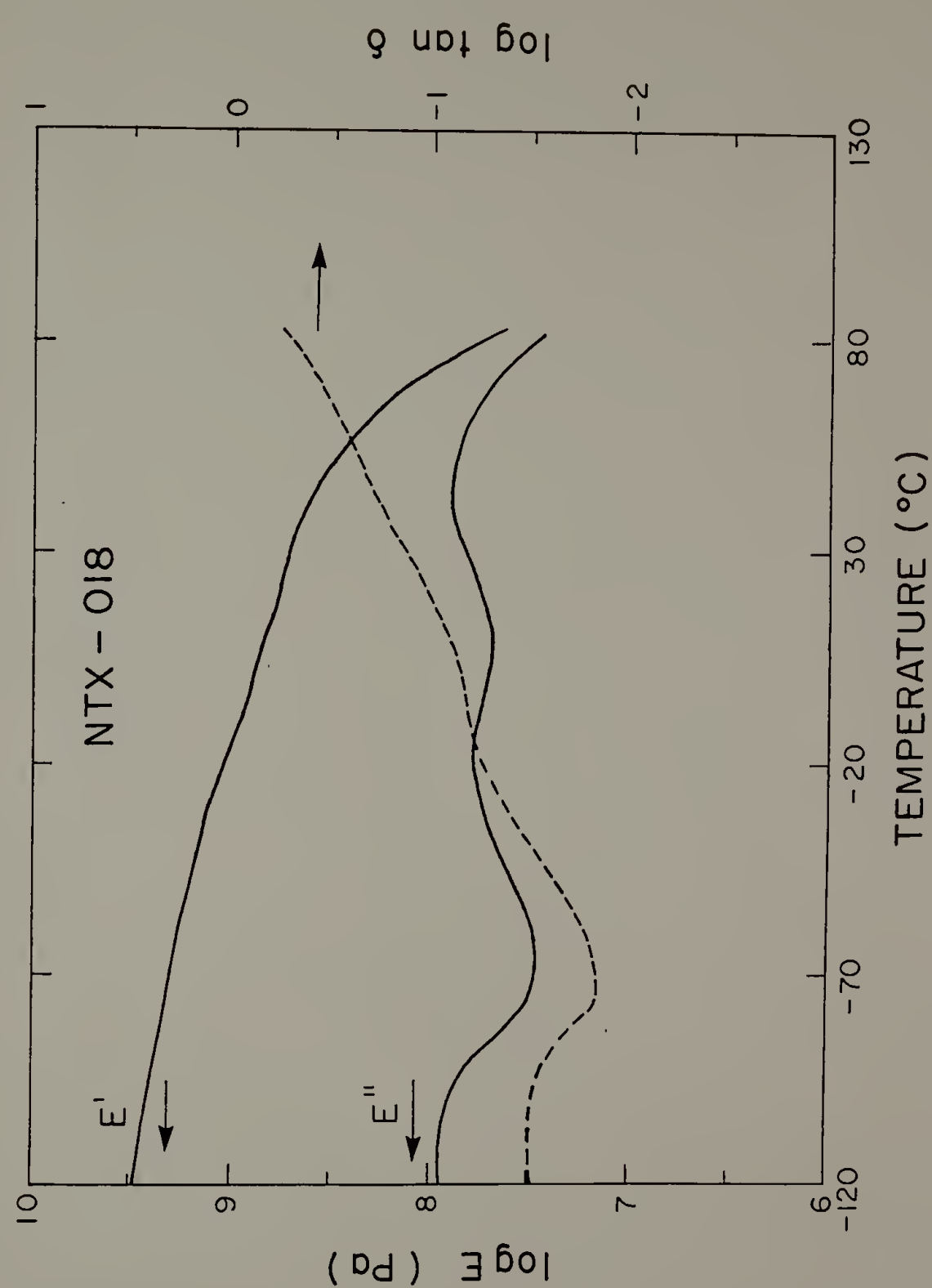
log E (Pa)
log tan δ
TEMPERATURE (°C)
NTX-018
E'
E''
10
9
8
7
6
1
0
-1
-2
-120
-70
-20
30
80
130

Figure 4.10

Smoothed dynamic mechanical thermal analysis curves of compression molded (isotropic) RC-4 bulk film using the dual cantilever mode at a frequency of 1 hz and a scan rate of 5 °C/min. Solid lines correspond to the storage (E') and loss (E'') tensile moduli as indicated. The broken line corresponds to the tangent phase lag angle between the storage and loss moduli. Note that all ordinates are plotted on a logarithmic scale.

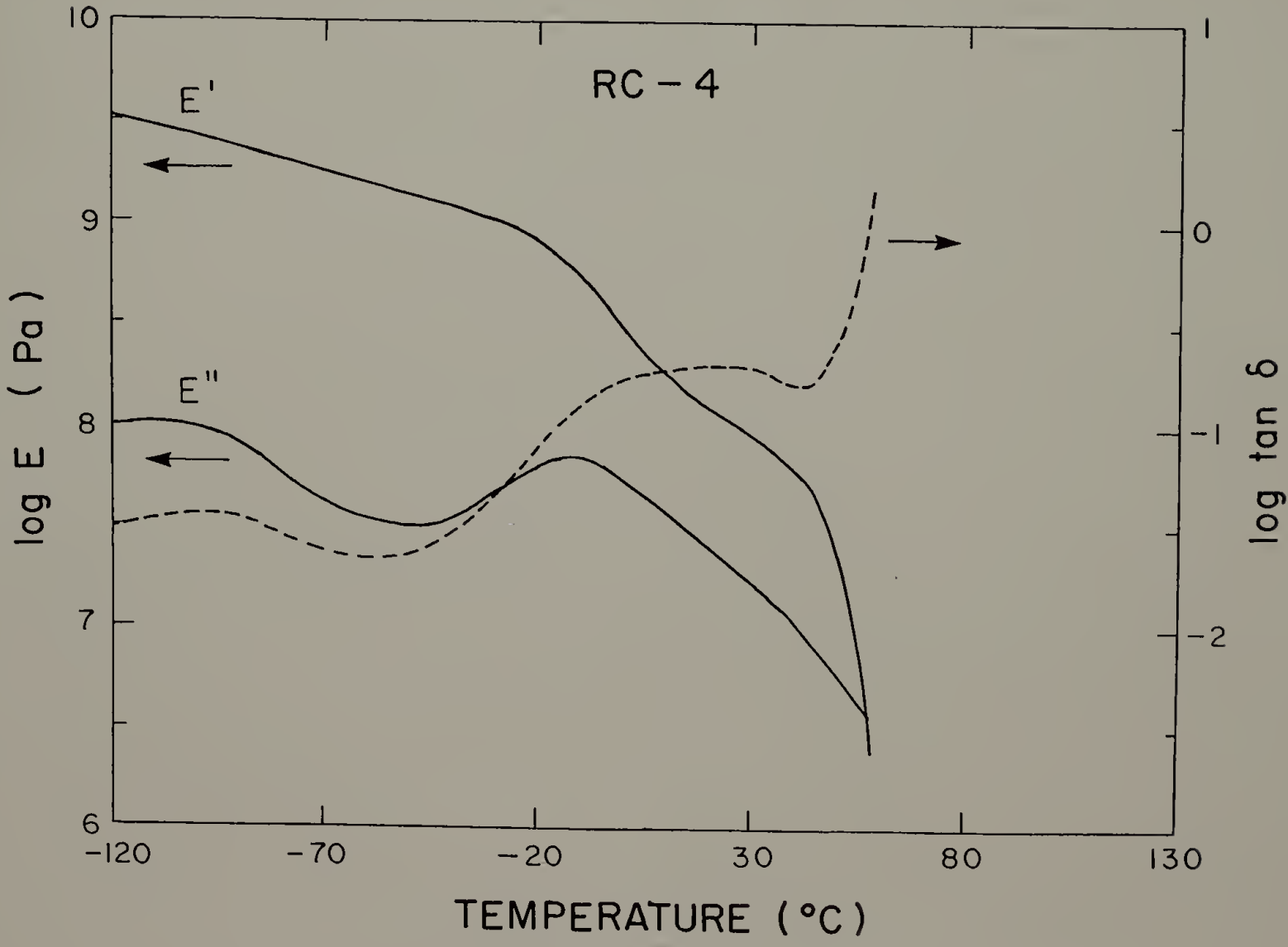
RC – 4
E'
E''
log E (Pa)
log tan δ
TEMPERATURE (°C)
10
9
8
7
6
1
0
-1
-2
-120
-70
-20
30
80
130

such peak was found for unbranched material. In all of the above polymers a glass transition (γ) peak was located at ca. -110 °C. The hydrogenated polybutadiene sample exhibited very different behavior than the above branched polymers. Instead of yielding three peaks, only two were detected, one at ca. -103 °C, and another at ca. 3 °C. It is conceivable that this latter peak corresponds to a "merger" of the α and β peaks.

Microscopy

Electron diffraction tilt studies of all undeformed films revealed high chain axis orientation along the draw direction as well as a single crystal-like texture with the a-axis preferentially oriented perpendicular to the film plane. For example, when the electron beam was initially oriented perpendicular to the film plane, and films were subsequently tilted about the chain axis, the (200) reflection increased in intensity while the (020) intensity decreased. This texture is analogous to that found previously for highly oriented linear polyethylene (Yang and Thomas, 1984; Smith et al., 1981b and 1985; Furuhata et al., 1986). Figs. 4.11, 4.12, and 4.13 show the morphology and corresponding diffraction patterns of HDPE and LLDPE. The diffraction patterns which were taken with the beam perpendicular to the film plane (all diffraction patterns shown except the inset in Fig. 4.11) resemble those obtained from blown films (Holmes and Palmer, 1958; Paulos and Thomas, 1980) as well as post drawn gels (Cannon, 1982; Smith

Figure 4.11

Brightfield micrograph of lamellar single crystal-like textured as-drawn HDPE film with electron diffraction patterns A) electron beam perpendicular to the film plane, and B) electron beam approximately parallel to the chain axis.


020
A
⊥c
B
∥ c
500nm

Figure 4.12

Brightfield micrographs of as-drawn polyethylene with corresponding electron diffraction patterns taken with the beam perpendicular to the film plane. A) HDPE (Marlex) and B) LLDPE (NTX-018, 2.29 mole % butyl branches). Note reduction of crystal size with increasing branch content. Chain axis vertical.

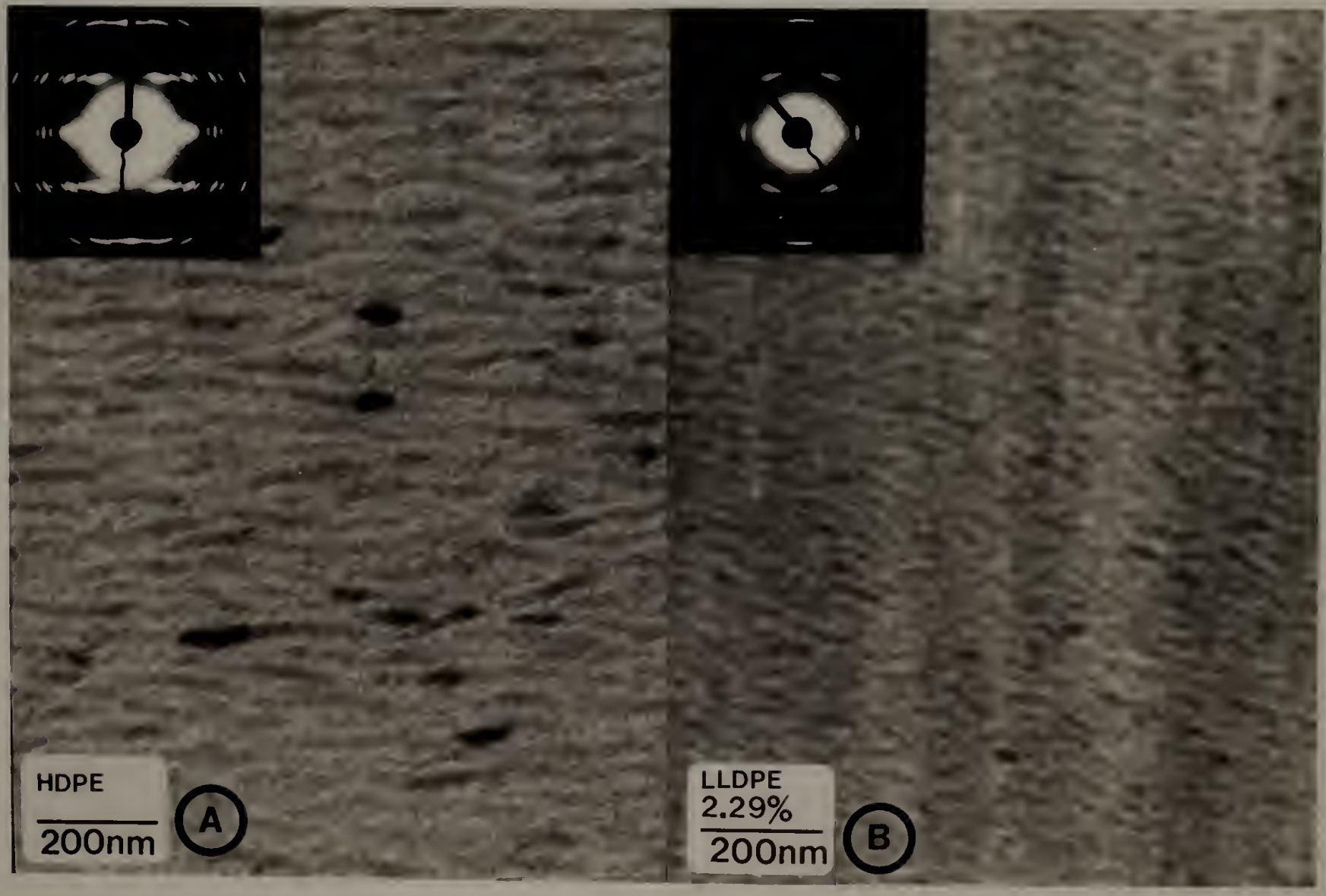
HDPE
200nm
A
LLDPE
2.29%
200nm
B

Figure 4.13

Brightfield micrographs of as-drawn polyethylene with corresponding electron diffraction patterns taken with the beam perpendicular to the film plane. A) LLDPE (RC-4, 2.36 mole % ethyl branches), and B) LLDPE (Dowlex, 0.3 mole% hexyl branches). Note absence of lamellar character at high branch contents. Chain axis vertical.

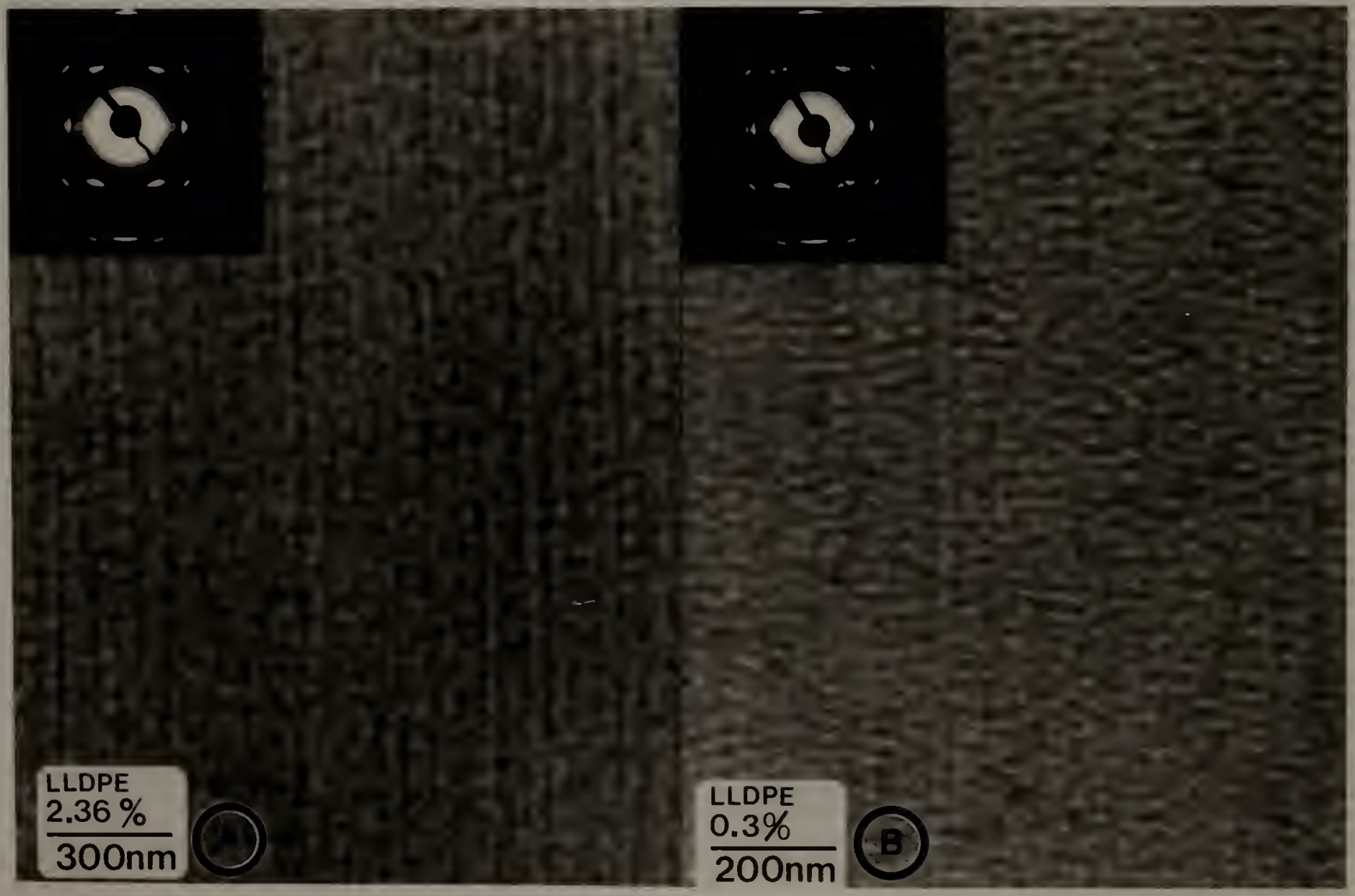
LLDPE
2.36 %
300nm
A
LLDPE
0.3%
200nm
B

et al., 1981b). The single crystal-like texture of these films is particularly evident in Fig. 4.11, inset B, where the beam was oriented nearly along the chain direction. Here the (200) and (020) reflections traced out arcs rather than rings, indicating that the films were not fiber symmetric. For example, the full angular width at half maximum intensity for the (020) reflection was 28 ± 5°.

Films were imaged in both brightfield and darkfield modes. Diffracting crystals appeared as bright areas in darkfield, whereas they appeared dark in brightfield. The mosaic block substructure of the lamellae was observed in both brightfield (Figs. 4.11, 4.12, and 4.13) and darkfield (Fig. 4.14) micrographs. The existance of such a substructure in polymers has been well established for some time (Hosemann et al., 1967). Brightfield images revealed increased lateral separation between mosaic blocks at high branch contents, in agreement with previous observations (Voight-Martin et al., 1986; Mandelkern, 1985). HDPE films (Figs. 4.11 and 4.12a) displayed a morphology of laterally aligned shish-kebabs (Petermann and Gohil, 1979). Such a morphology has been seen previously in drawn swollen gels of HDPE (Barham, 1982). In fact, it appears that similar morphologies and mechanical properties can be attained by several seemingly different drawing techniques (Smith and Lemstra, 1980). Shish-kebabs were also present in LLDPE films (Figs. 4.12b and 4.13). Note however, the poor lateral registration of mosaic block crystallites in LLDPE as opposed to HDPE. (A brightfield micrograph of NTX-017 was not included, since it was indistinguishable from NTX-018 (Fig. 4.12b)). In HDPE the alignment

Figure 4.14

Darkfield micrographs of as-drawn HDPE film (Marlex) using (110) + (200) + (210) + (020) diffraction reflections showing mosaic block structure. Arrows point to mosaic block interfaces. Inset was taken using the (002) reflection. Chain axis vertical.

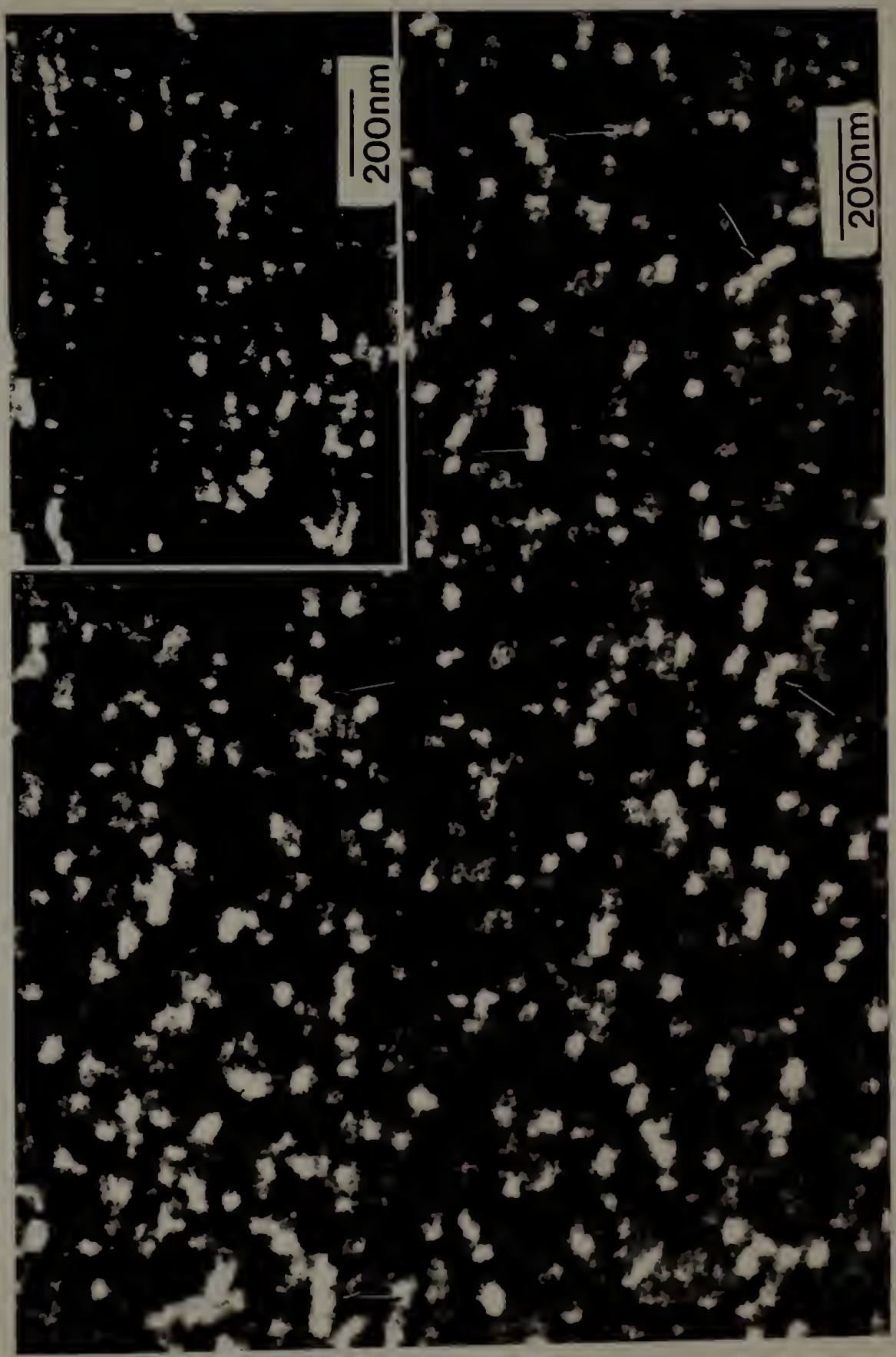
200nm
200nm

of crystalline regions obscured the shish-kebab morphology, and emphasized the lamellar nature of these films. In highly branched samples, on the other hand, the lack of lateral registration accentuated striations along the chain direction and obscured lamellar character (Fig. 4.13a).

Brightfield and darkfield images were used to determine crystal size. The decrease in crystal image contrast with increased branching, however, precluded accurate size measurement. The average crystal thicknesses of HDPE and LLDPE were in the range of 27 and 10 nm, respectively. In each sample, mosaic block widths were approximately equal to their thicknesses. In more highly branched polymers (e.g. 2.4 mole % ethyl branches, Fig. 4.13a) the lamellae did not form periodic stacks along the orientation direction.

Discussion

Gel Drawing

The state of films prior to drawing will now be addressed, in an effort to determine whether or not the precursor state was a gel. The linear increase of crystal dissolution temperature with increasing solution concentration reflected an increase of crystallization rate with concentration at a given crystallization temperature. Consider the process of nonisothermal crystallization. Crystals nucleate and grow throughout the cooling process. Crystalline regions which grow

from solution at high temperatures are thicker than those which grow later on in the cooling process. Due to their lower surface/volume ratio and greater perfection, the thick crystals have higher melting points than crystals formed at lower temperatures. When crystallized under nonisothermal conditions, the average crystal thickness depends on the relative rates of crystallization and cooling. In the present gelation studies, crystal nucleation was most probably heterogeneous. Therefore, the induction time for nucleation was assumed to be negligible.

The interpretation that higher dissolution temperatures are the result of a faster crystallization rate in concentrated solution parallels the arguments of Domszy et al. (1986), in which the dissolution temperature of a gel was found to depend mainly on crystal size and thus the crystallization temperature of the gel, rather than concentration. The increase of crystallization rate with increased concentration concurs with previous studies (Mandelkern, 1964a) on isothermal crystallization . This higher rate of crystallization is due to the lower entropy of mixing contribution to the bulk free energy of crystallization for concentrated versus dilute solutions. This data indicates that gelation could occur at a reasonable rate even at high temperatures provided polymer concentrations were sufficiently high.

As an extreme case, consider crystallization from the melt. HDPE is known to crystallize rapidly from the quiescent melt at 120 °C (Mandelkern, 1964). Crystallization from a concentrated solution would occur more slowly. However, whitening of film edges prior to the

drawing step of film processing indicated that crystallization had indeed commenced in these high surface area regions. This indicated that the precursor state of films (prior to drawing) could quite conceivably be a gel with crystalline crosslinks. The presence of a gel prior to drawing was further substantiated by the difficulty encountered when drawing films at temperatures exceeding the polymer melting range. Crystalline crosslinks apparently impart cohesion to the film. The presence of such crystalline crosslinks is supported by the deformation network structures seen in Figs. 5.6 and 8.2b. Thus, the film drawing process is a gel-drawing process, contrary to previous assertions that it involves melt-drawing (Petermann and Gohil, 1979; Yang and Thomas, 1984).

We have thus established that a gel was present prior to film drawing. Let us now direct attention to the crystallization which occurred during drawing. Crystallization is significantly enhanced in the presence of a strain field, as demonstrated by the crystallization of strained rubbers (Andrews, 1964). This enhancement was particularly evident when preparing solutions. When solutions maintained at 90 °C were vigorously stirred, they formed a vortex in which crystals rapidly nucleated and grew. A similar enhancement of crystallization due to chain elongation was present during film drawing, as evidenced by shish-kebab formation.

The increase in crystallization rate with applied strain becomes particularly significant in situations where crystallization is customarily slow, e.g. at high temperatures. Consider, for instance,

the crystallization of single crystals. Such crystals are routinely grown from a xylene solution at temperatures below approximately 96 °C, due to the slow rate of crystallization at higher temperatures (Domszy et al., 1986). However, fibers have been grown from xylene solution in a reasonable amount of time at 123 °C due to the application of a strain field (Zwijnenburg and Pennings, 1976). Subsequent investigations indicated that as concentration increased, the maximum temperature at which fibers could be grown also increased (Barham et al., 1980; Pennings, 1977).

Crystalline Phase Characterization

The effect of branching and processing history on sample crystallinity is shown in Fig. 4.4. For comparison, data taken from the literature was also plotted (Alamo et al., 1984). The results of the two experiments for undrawn samples agree quite well, especially considering the slower cooling rates employed in the present study. The difference in cooling rates between these two sets of data was only observable in those samples which crystallized slowly i.e. in highly branched samples.

Curiously, commercial samples (e.g. 2.05, 2.29 mole % branches) were more crystalline than hydrogenated polybutadienes of comparable branch concentrations (2.08, 2.36 mole %, respectively). The hydrogenated polymer crystallinities agreed very well with those of Alamo et al. in this branch content range. Since all of the polymers

used were branched essentially randomly along each chain, this suggested that the branch content in the commercially available materials varied considerably from chain to chain, resulting in a mixture of highly branched and slightly branched chains. Crystalline phase properties would then be dominated by the low branch content chains, which would fractionate by crystallizing first. This hypothesis was substantiated by the high melting temperatures (larger crystal sizes) of commercial polymers as seen in Fig. 4.5, where again the data of Alamo et al. was used for comparison.

Enthalpy of fusion measurements indicated that as-drawn films and melt-cooled samples had equivalent crystallinities. This, however, should not be taken as an indication that strain-induced crystallization was absent during film preparation. The high melting satellite peak found in some drawn samples indicated a high degree of noncrystalline phase extension. This "superheating" resulted from the lower change in conformational entropy, upon going from the crystalline to the chain-extended versus randomly-coiled noncrystalline state. Since the melting point is indirectly related to the change in entropy, the former case corresponds to a higher melting point than the latter (Zachmann, 1967; Flory, 1947). The absence of such satellite peaks in other drawn samples suggested that chain relaxation occurred during heating. Such chain reorganization has been well documented (Wunderlich, 1973d).

The greater number of melting peaks (at temperatures below the major endotherm) in drawn versus undrawn samples implied a greater degree of fractionation occurred in the drawn samples (Springer et al.,

1986). Moreover, in strained HDPE high molecular weight fractions are believed to form extended chain fibrils, which serve as nuclei for lamellar growth (Bashir et al., 1984 and 1986).

Endothermic peak breadth reflects the range of crystal sizes and perfection present in a given material. This in turn depends on the distribution of crystallizable units along each chain. To interpret the breadth of RC-4 melting peaks, each chain was assumed to possess the same branch content. Chains participating in crystallization would therefore be highly branched. These branches would significantly interrupt the crystallization process, resulting in a large "interphase" and a broad distribution of crystal sizes (as evidenced by multiple peaks at temperatures below the major melting peak of LLDPE) as well as the incorporation of some branch points in the crystal lattice. Furthermore, in the (highly branched) PBD samples, no single peak could be identified as a major melting endotherm, and crystals melted over a broad range of temperatures.

The nature of the interphase has been the subject of much theoretical activity (Flory, 1962; Flory et al., 1984). It is well known that the flux of polymer chains is dissipated in the interfacial region between the crystalline and amorphous phases. This dissipation occurs via chain reentry into the crystallite as well as by chain tilting within lamellae. In copolymers, chain reentry is restricted due to the presence of branch defects on chains. This means that reentry of chains is somewhat hindered, making the dissipation of chain flux occur over a greater distance from the crystal surface than for unbranched

material. Furthermore, the delegation of branches to crystal interfaces results in an additional increase in the number of atoms per unit area at the interface. Thus, not only is reentry hindered by branches, but the branches themselves take up space. Since the stable disordering of chain segments (from the perfect order at the crystal surface) requires an increase in volume available per chain, one can conclude that the presence of branches themselves interfered with the dissipation of order from the crystal surface. Both of these effects would result in a larger interphase and a more gradual dissipation of order from the crystal surface into the noncrystalline phase. In fact, it has been suggested that the β transition arises from the increased interphase content of branched polymers (Mandelkern, 1985). The increase of interphase size with branching was supported by the absence of a β peak in HDPE, and by the reduction in brightfield contrast between the crystal and amorphous phases as branch content increased.

The branch content dependence of the α transition revealed that the mechanical stability of the crystalline phase decreased with increasing branch content. In addition, very different DMTA curves were obtained for the RC-4 and NTX samples. The former sample yielded two loss peaks while the latter displayed three. It appeared that the α and β peaks in RC-4 merged. How would branching effect such a merger? The α_1 peak is believed to result from shear between mosaic blocks, or from chain mobility at the fold surface of crystals. The large separation distance between blocks in RC-4 samples may have reduced constraints to chain motion. This would reduce the activation energy needed for the α_1

mechanism, and thus the α_1 peak temperature. The α_2 process, on the other hand, is associated with chain motion within the crystalline phase. One would expect that the presence of branches on a chain would hinder chain slip through a crystal lattice. However, it is well known that the crystal lattice expands as branch content increases (possibly due to the inclusion of branch point defects). This would result in less interaction between chains when an unbranched portion of a chain slips through the lattice. The temperature at which the α_2 loss occurs would be reduced as well.

The increase in the β loss peak temperature with branching will not be interpreted here, as the actual mechanism of the β loss remains unclear. The relative invariability of the glass transition temperature with branch content suggested that long range chain mobility was not significantly affected by short branches. This supports the results in Fig. 4.5, that the crystallization of different LLDPE samples is not affected by the diffusion of chains to the crystallization site.

The above considerations proved useful in understanding why chain-folded crystals in LLDPE did not aggregate and laterally align in the same manner as was found for HDPE. It is believed that mosaic blocks aggregate into lamellae in order to reduce the total surface energy of the system (Yeh, 1976a). The LLDPE specimens apparently did not experience the same driving force to aggregate as HDPE crystals. This evidently arose from the fact that the lateral crystal surfaces of LLDPE differ from those of HDPE due to the expulsion of branches from the crystalline core (Voight-Martin et al., 1986). Since branched regions

of chains would neither be able to crystallize nor move to a new location, the epitaxial crystallization of chains onto lateral crystal surfaces and the associated "reeling in" of adjacent mosaic blocks would be hindered.

The α_1 transition can be used as an indicator of the degree of communication between lateral crystal surfaces, since it arises from shear between mosaic blocks. DMTA data indicated that such shear increased with branching, indicative of poorer "communication" and lateral cohesion between crystal blocks in highly branched samples.

Conclusions

It was shown that the films analyzed in this study were gel-drawn, as opposed to melt-drawn, and that the resultant morphology strongly resembled that obtained by other gel-drawing techniques. The morphology of both HDPE and LLDPE films was one of laterally aligned shish-kebabs, indicating a propensity for strain-induced crystallization even in branched material. Diffraction data indicated that crystallites were oriented with the c axis along the draw direction and the a axis preferentially perpendicular to the film plane, resulting in a single crystal-like texture. Thermal analysis indicated that branch length in randomly-branched LLDPE had no observable effect while branch content had a large effect on crystallization behavior. For instance, the lamellar character of as-drawn films became more and more obscured as branch content increased due to decreasing crystallinity and reduced

lateral crystallite aggregation. Thermal analysis indicated that the average crystallite thickness decreased and the range of thicknesses increased as branch content increased. TEM observations verified the reduction in crystal thickness with increasing branching. Moreover, although HDPE displayed periodically alternating crystalline and amorphous layers, such periodicity along the chain direction gradually disappeared as branch content increased.

In addition, the α transition temperature decreased with increasing branch content, indicating an increase in the mobility of mosaic blocks and chains within crystallites. Mosaic block motion was facilitated by an increase in the lateral separation between adjacent blocks with increased branching. In addition, LLDPE samples displayed a β relaxation, indicating an increase in interphase size with branching. HDPE displayed no such transition. The increase in interphase size also resulted in poor contrast between phases in brightfield TEM studies. In highly branched materials, the α and β peaks apparently merged into a single peak. Furthermore, branching had relatively little effect on the location of the γ (glass) transition.

It is quite clear that branches disrupted the crystallization process. In fact, the dependence of melting point on branch content was successfully explained by assuming that branches are excluded entirely from the crystalline phase and that crystal size depends solely on the limited availability of crystallizable units along a given chain. The fact that the extrapolated melting point at zero branch content equalled that measured for HDPE suggested that a very low percentage of branches

had been incorporated in the crystal lattice. No corrections for the effect of branches on chain diffusion to crystallization sites were invoked. The relative invariability of the glass transition temperature with branch type and content implied that such a transport correction would be negligible.

Differences in DSC melting endotherms made it apparent that two materials of essentially the same average branch content and both randomly sequenced can crystallize very differently due to fractionation between chains of high and low branch content. It is suggested that branching be characterized by a polydispersity index which identifies the variation of branch content between chains. This index could be determined by characterizing the branch content and branch sequencing of fractions of the material, isolated under standardized conditions. For instance, using temperature rising elution fractionation (Cady, 1987), quantized aliquots of eluted solution could be isolated at standard flow and heating rates. For a random distribution of branches along each chain, one could determine polydispersity from the ratio of the second to the first moments of the branch concentration versus corresponding weight of fractionated polymer.

CHAPTER V

ROOM TEMPERATURE DEFORMATION OF ORIENTED HIGH DENSITY POLYETHYLENE: NEAR ISOTHERMAL DECRYSTALLIZATION

Abstract

Thin, single crystal-like textured, shish-kebab morphology films of drawn high density polyethylene (HDPE) were prepared. These films were slowly uniaxially elongated at room temperature along or perpendicular to the chain direction and directly viewed by transmission electron microscopy (TEM). The drawing was assumed to be isothermal or near isothermal due to the slow elongation rate and thinness of films. For both deformation geometries, chains aligned along the local elongation direction. For materials deformed perpendicular to the chain direction, this corresponded to a 90 ° rotation of shish-kebabs. In fact, material deformed in this way underwent crazing whereas crazes nucleated but did not grow for material deformed along the chain direction. Apparently, crazing was facilitated in the former case due to the fact that craze propagation occurred between shish-kebabs, rather than perpendicular to them. In the latter case, shish-kebabs arrested such craze growth, and instead, stresses perpendicular to the chain direction were relieved by extensive cavitation in the noncrystalline phase and subsequent fibrillation of the film into bunches of shish-

kebabs. Meanwhile, chain-folded crystals were subject to mechanically-induced destruction, termed decrystallization. During decrystallization, internal defects were generated within crystallites, facilitating subsequent yielding. Defect generation also resulted in a reduction in crystal thickness along the chain direction, revealing that such a reduction can occur without a rise in temperature and subsequent melting. Crystals also underwent <001> crystal shear and chain slip, reducing crystal width, and martensitic transformation to the monoclinic crystalline form. Ultimately, the defect generation and chain unfolding associated with decrystallization would lead to a reduction in crystallinity. Subsequent recrystallization was not detected by darkfield studies. The structure and deformation of shish-kebabs was analyzed in detail. When strained, kebabs decrystallized and fed into the shish core. These resultant filaments were generally noncrystalline and of uniform diameter, with occasional crystalline remnants within them. A distribution of filament diameters indicated that draw-down (creep) occurred at high strains as well. These results suggested that room temperature, near isothermal deformation of HDPE does not bring about the formation of a continuous crystalline phase.

Introduction

Much research has been devoted to understanding the dependence of the mechanical properties of semicrystalline polymers on morphology and molecular topology (Samuels, 1985; Duckett, 1983; Peterlin, 1977 and

1979; Capaccio et al., 1976; Bowden and Young, 1974; Ward, 1984; Schultz, 1984; Smith et al., 1981b; see also J. Polymer Sci., Part C Polymer Symposia #32 (1971) for an overview of this area). In fact, much effort has gone into developing structural models which relate morphology to deformation behavior and overall mechanical properties. Specifically, numerous models have been devised to better understand the properties of semi-crystalline polymers such as polyethylene (PE). These models will be highlighted here. The structural models of PE can generally be divided into two main categories: those comprised of a single phase, and those comprised of two phases. The single phase models best represent materials which are ultradrawn or were crystallized under high pressure and have become almost entirely crystalline, whereas the two phase models are applicable to materials which have not been processed to this extreme.

First the two phase models will be addressed. One of the most well known models for semicrystalline polymers is the Peterlin model (1971, 1979). In this model, the lamellae of stressed isotropic spherulitic material shear into crystal blocks via chain tilt within lamellae and longitudinal slip at mosaic block interfaces. The blocks rotate such that the molecular axes align with the local strain direction. For PE, this deformation is often accompanied by crystal twinning and the conversion from orthorhombic to monoclinic crystals (Seto et al., 1968; Bevis and Crellin, 1971). (Other researchers consider this latter stress-induced crystalline form to be triclinic (Turner-Jones, 1962). In both cases, the same observed d-spacings were

cited.) The crystal blocks decrease in width by chain slip and unfolding until a microfibril of alternating crystal/amorphous regions is formed. A schematic of this process is shown in Fig. 5.1. Each lamellar stack forms numerous micronecks once the yield stress is reached. Each microneck, in turn, is associated with the formation of a microfibril, the basic structural element of this model. Some small angle x-ray scattering measurements have indicated that the average crystal thickness and long period in the deformed material are quite often different than that in the undeformed material (Cornelluissen and Peterlin, 1967; Peterlin and Sakaoku, 1967; Peterlin, 1972). This was originally interpretted to mean that the conversion of lamellae to microfibrils involved a rise in temperature and subsequent melting and recrystallization (Peterlin and Sakaoku, 1967; Peterlin, 1967). Later calculations revealed however, that the temperature rise associated with necking was insufficient to melt lamellae (Peterlin, 1972). Instead, the reorganization of the crystalline phase was believed to be mechanically induced. The nature of the mechanical destruction of crystallites in fibrillar HDPE will be a focal point of interest here.

Microfibrils which have experienced approximately the same local strain history coalesce to form a fibril in which the registry between microfibrils is quite good. The ends of microfibrils are viewed as defect regions, capable of giving rise to microcracks. Different fibrils result from different local strains on neighboring lamellar stacks. Therefore, their draw ratios are not equal and crystal/amorphous registry between fibrils is quite poor. This leads to

Figure 5.1

Peterlin molecular model (1971) of drawing in a semicrystalline polymer with a) lamellar stacks within a spherulite, b) chain tilt and slip within lamellae, c) mosaic block shear and necking, and d) resultant microfibrillar structure. Elongation direction vertical.

Molecular Model of Drawing in Semicrystalline Polymers

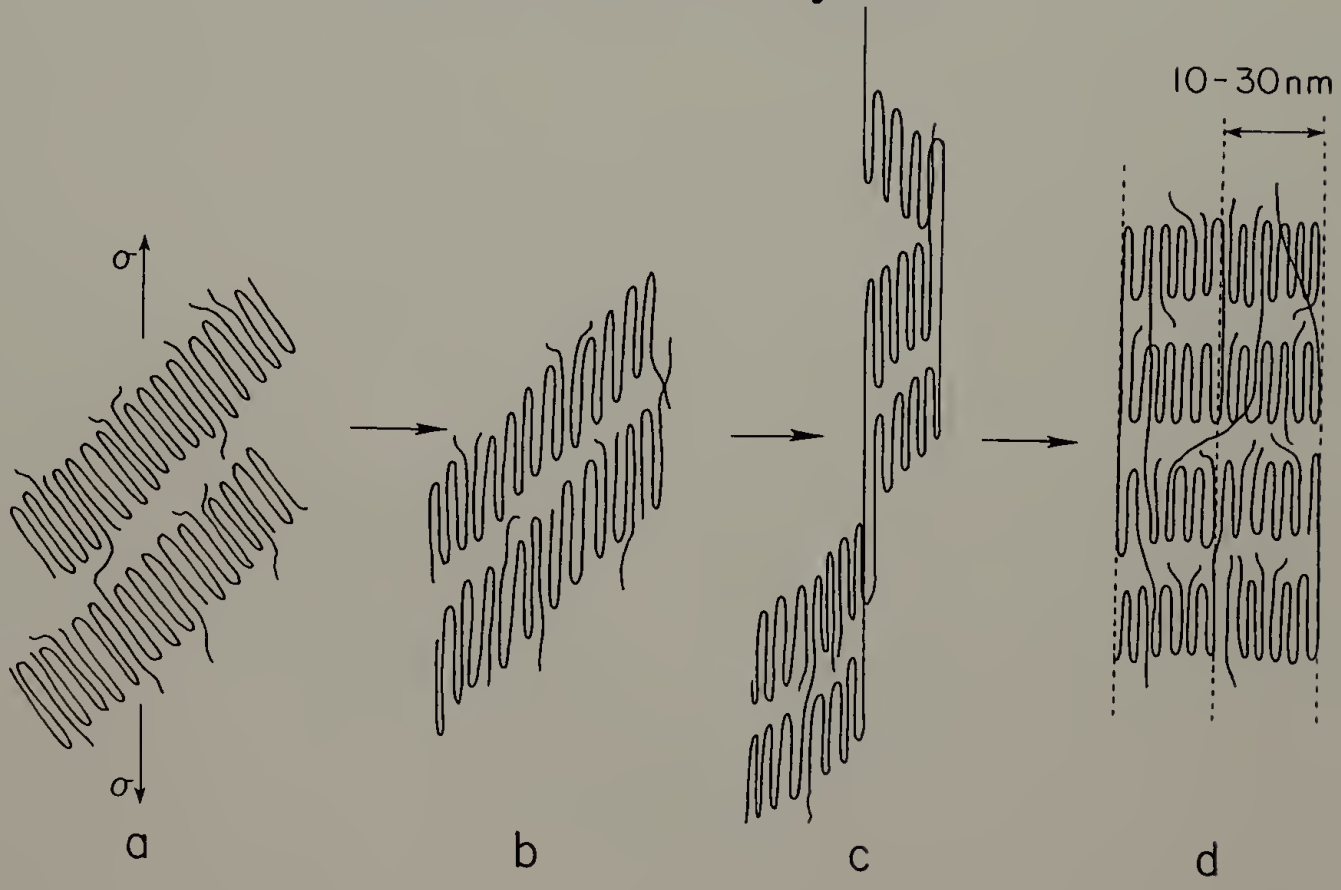

After Peterlin (1971)

poor "adhesion" between fibrils. When the fibrillar material is further strained, slip between fibrils is believed to occur to a greater extent than slip between microfibrils, due to the enhanced "friction" between microfibrils. Interfibrillar tie molecules connect both adjacent fibrils as well as microfibrils, and in addition to Van der Waals forces comprise the frictional forces which resist longitudinal slip. Intermicrofibrillar tie molecules arise not only from the tie molecules which interconnect lamellae in the original structure, but also are formed by the unfolding of chains during microfibrillar slip. This results in a large number of tie molecules being located on the outer surface of microfibrils (Meinel and Peterlin, 1971).

A tie molecule is defined as a noncrystalline chain which is incorporated in more than one crystallite, forming an intercrystalline connection. Though they have never actually been imaged, their existance is supported by the mechanical and crystallization behavior of semi-crystalline polymers. For instance, tie molecules are believed to serve as nucleation sites for intercrystalline links, which are fibrous 1 - 2 micron long extended-chain crystals which interconnect lamellae (Keith et al., 1966 and 1971). It is generally believed that upon straining, tie molecules become taut by undergoing gauche to trans conformational changes (Peterlin, 1979). Further straining results in bond angle distortion and the stretching of covalent bonds. Ultimately, some taut tie molecules undergo chain scission while other ones take on the additional load as strain increases. The number of taut tie

molecules increases with strain. This is believed to be (at least in part) responsible for the increase in tensile modulus with draw ratio.

In the current Peterlin model (Peterlin, 1977 and 1979), reinforcing elements consist not only of interfibrillar tie molecules, but also of crystalline bridges and taut intrafibrillar tie molecules which span the amorphous layers between lamellae within a microfibril. The incorporation of crystalline bridges has proven particularly useful in explaining the time dependence of mechanical properties in PE. For instance, the tensile modulus of PE decreases during annealing, and subsequently recovers upon cooling and aging at room temperature (Peterlin, 1977 and 1978). It is believed that the crystalline bridges melt during annealing, and subsequently recrystallize upon cooling. In addition, it has been found that the tensile modulus of as-drawn PE increases and the permeability decreases as the material is aged (for ca. 2 hours) at room temperature (Decandia et al., 1985). This is believed to be due to the crystallization of taut tie molecules, and the formation of crystalline bridges following drawing. Previous studies showed that room temperature chain reorganization and crystallization was possible in PE (Miles et al., 1976). All of these studies indicate that time dependent morphological and mechanical changes can occur at room temperature.

In a modification of the Peterlin model, it has been suggested that intermicrofibrillar tie molecules are lax, rather than taut as in the Peterlin model (Kausch and Devries, 1975). However, Peterlin (1979) showed by electron spin resonance (ESR) studies on Nylon 6 that a

detectable fraction of taut tie molecules fractured at only 40% strain to break. As fully extended aliphatic chains resist rupture up to 35% strain to break by bond stretching, this implies that no significant chain extension occurred before rupture. This of course assumes that affine deformation prevailed. Another variation of the early Peterlin model invoked lax tie molecules between lamellae within microfibrils and taut tie molecules interconnecting microfibrils (Prevorsek et al., 1973). In this way, strength-determining elements were present between microfibrils. This model does not account for the ease of fibrillation in necked materials.

Let us now consider some of the mechanical models which have been used to predict the tensile modulus of HDPE. Using the approach of Takayanagi et al. (1966), the crystalline phase can be treated as a (continuous) matrix phase, being simultaneously in parallel and in series with the amorphous phase. Structural detail must be incorporated into any two phase composite model to adequately predict mechanical properties (Halpin and Kardos, 1972). A continuous crystalline phase can form either by including crystalline bridges between lamellae, or by placing very long (sample-spanning) extended-chain crystals in an amorphous matrix. The former model was developed in the work of Gibson et al. (1978). Small angle x-ray scattering (SAXS) was used to determine the average long period of PE as a function of draw ratio while wide angle x-ray scattering (WAXS) was used to measure the average crystal size along the chain direction. This data was used in conjunction with a morphological model, equivalent to the Peterlin model

(Fig. 5.1d) except that the amorphous layers were spanned by crystalline bridges, to determine the probable distribution of crystals with thicknesses equal to or greater than the long period. A fiber composite mechanical model was then introduced in which the apparent fiber phase consisted of these long crystals, and the matrix phase consisted of the remaining chain-folded and amorphous phases. The results were used to interpret the dependence of modulus on temperature and draw ratio. An important aspect of this model is that a continuous crystalline phase formed even though most of the crystalline phase remained chain-folded, the structural building blocks being microfibrils.

The use of two phase composite models to describe semi-crystalline polymers is not as straight forward as it may seem. As indicated by Gibson et al. (1978), difficulties are often encountered when defining the two phases with respect to specific load-bearing morphological elements. Indeed, the mechanical models commonly used are often primitive representations of the actual morphology of the sample, individual phases of known volume fraction being treated as springs of a given force constant (the analog of modulus). Typically, these springs are arranged in series and/or parallel combinations, whichever best represents the mechanical data.

The concept of a continuous crystalline phase was introduced long ago (Hess and Kiessig, 1943; Staudinger, 1932), although at that time the actual morphological data to support this model was lacking. Such a chain-extended continuous crystalline phase has been cited in contemporary literature to explain the generation of a new class of

ultrahigh modulus materials. For example, ultradrawn polyethylene has recently been made with a crystallinity exceeding 90% and room temperature tensile modulus of over 220 GPa (Kanamoto et al., 1983a). For comparison, consider the modulus of isotropic HDPE cooled from 180 °C at room temperature (1.5 GPa, see Fig. 4.7) versus the crystalline phase modulus of HDPE along the chain axis direction (ca. 300 GPa). The achieveable modulus has become so high as to warrant the use of a single phase model. Although morphological observations (by TEM) indicated alternating crystalline and amorphous regions in PE samples, Fischer and Goddar (1969) viewed polyethylene as a single phase crystalline material interspersed with nonrandomly-placed defects (tie molecules, chain folds and ends). This continuous crystalline phase model was based on darkfield micrographs which yielded stacks of lamellae simultaneously diffracting and therefore probably interconnected by crystalline bridges. Still other models espoused randomly-placed defects in the form of chain ends (Porter, 1971) or buried folds (Clark and Scott, 1974). These latter models were based on mechanical as well as morphological data such as the loss of SAXS long period peaks with draw. Up until this point, however, no direct TEM evidence of an extensive (sample-spanning) crystalline phase had been found.

In the following development, it will become apparent that the applicability of a given model depends on the processing conditions used as well as the degree to which the material has been drawn. For instance, iodine staining has indicated the presence of a periodic

arrangement of alternating crystalline and amorphous layers in microfibrils (Peterlin et al., 1965). Periodicity along the microfibril axis in deformed materials was further verified by small angle x-ray scattering (SAXS) (Hay and Keller, 1966; Peterlin, 1977). However, ultradrawn materials display no such periodicity by darkfield microscopy (Smith et al., 1985) or SAXS (Porter, 1971). What is generally accepted, is that the population of long crystals and crystal bridges increases with draw (Frye et al., 1979; Sherman et al., 1982; Van Hutten et al., 1985; Smith et al, 1985). The main debate centers around whether or not extended chain crystals or simply crystal bridges interconnecting lamellae are needed to attain ultrahigh modulus along the draw direction.

The deformation behavior of shish-kebab-reinforced, highly oriented thin films will be discussed next. First, however, the formation and structure of shish-kebabs will be elucidated. One theory of shish-kebab formation has been proposed in which the shish-kebabs are generated by the deformation of an entirely chain-folded, spiral crystalline structure. This initial spiral structure was believed to have formed via a screw dislocation mechanism (Nagasawa and Shimomura, 1974). Alternatively, it has been suggested that the high molecular weight component of a polymer gives rise to fibrous extended chain crystals which serve as nuclei for lamellar growth (Hoffman, 1979; Bashir et al., 1984 and 1986). Note that this latter view is applicable to crystallization from stirred solution, but not to the formation of shish-kebabs from the solid state via deformation. Instead of viewing

the chain-folded overgrowth as "decorative lamellae", it is believed that chains which constitute the crystalline core ("shish") are molecularly integrated with the chain-folded-overgrowth lamellae (Grubb and Keller, 1978; Van Hutten et al., 1984; Yeh, 1976b; Pennings, 1977; Krueger and Yeh, 1972). In addition, shrinkage studies on shish-kebabs have indicated that the shish core is best viewed as a series of longitudinally aligned fringed micelles which in some regions have grown sufficiently thick along the chain direction to "fuse" together (Grubb and Keller, 1978). This is equivalent to a long chain-extended crystal with defects interspersed along its length (Fig. 5.2). When deformed, the kebab size decreases and the spacing between kebabs increases until fibers of uniform diameter are obtained (Krueger and Yeh, 1972; Van Hutten et al., 1984). This indicated that kebabs feed into the shish. These electron microscopy studies were done using gold decoration and in the case of Krueger and Yeh, a polyethylene terephthalate substrate.

In previous studies by others, HDPE films of the type used here were mechanically tested, and stress/strain curves obtained (Petermann and Gohil, 1979). The films displayed a yield point and slight strain hardening, as identified by an increase in the slope of the stress/strain curve with increasing strain. In the bulk, HDPE deformed at room temperature typically exhibits strain hardening (Gent and Jeong, 1986). This is generally attributed to the extension of chains and the generation of taut tie molecules and crystalline bridges with draw. In this context, it is important to note that not only the crystalline but also the noncrystalline phase is transformed during deformation, as made

Figure 5.2

Grubb and Keller (1978) model of a shish-kebab, in which defects have been incorporated in the shish core, and kebabs are covalently linked to shish. Chain axis vertical.

SHISH-KEBAB

after D.T. Grubb and A. Keller (1978)

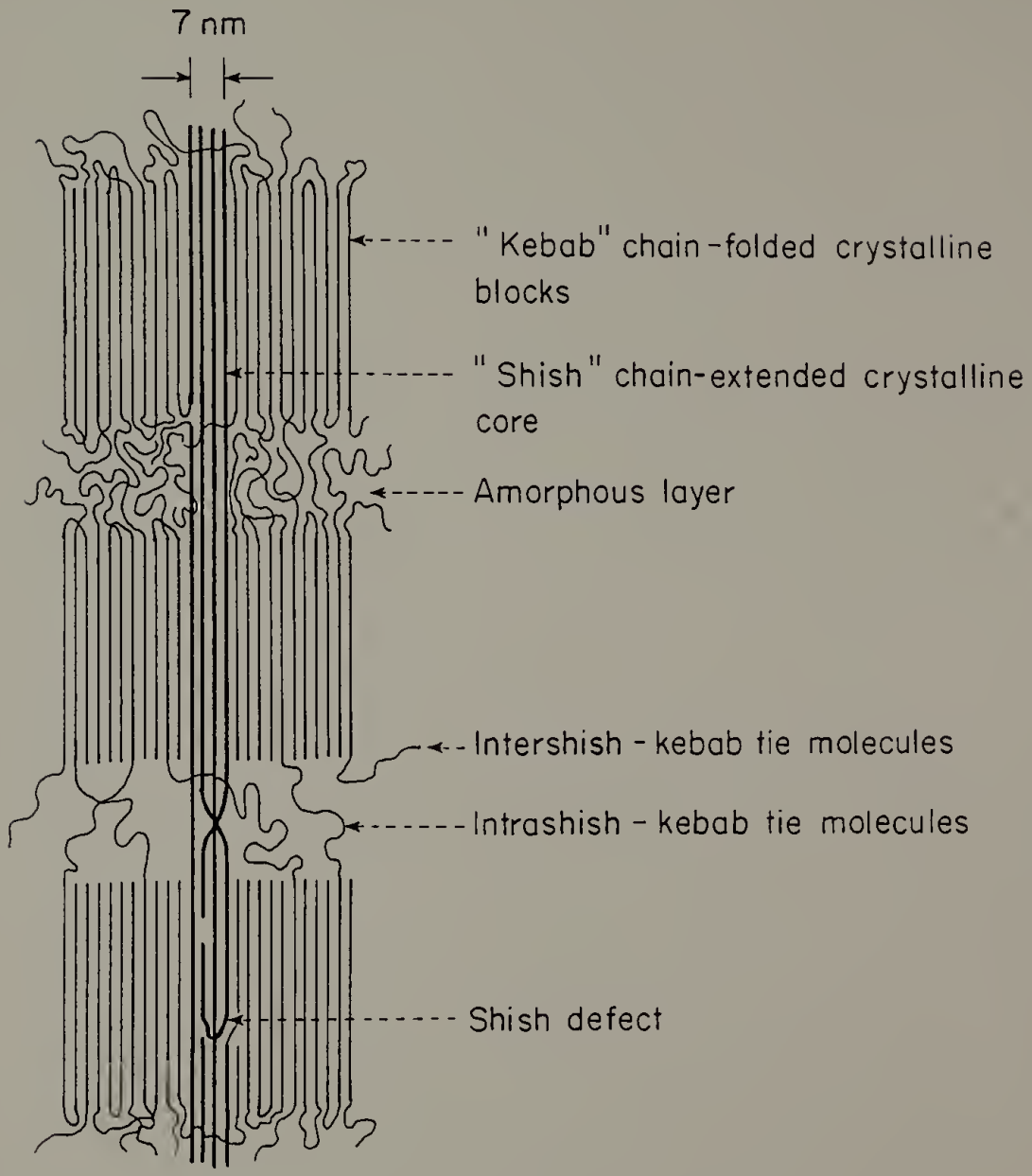

evident by changes in both the mechanical and thermal stability of the material (Sumita et al., 1977; Dhawan et al., 1980).

Experimental

Materials and Processing

The polymer used was Marlex 6003, obtained from Phillips Petroleum Corporation, with M_w= 200,000 and M_w/M_N= 7 - 13. A full description of the film preparation techniques used in this study, as well as the characterization of as-drawn films can be found in chapter 4.

Microscopy

Sample preparation procedures were discussed in Chapter 4. For deformation studies, samples were placed on annealed (typically 700 °C for 18 hrs in vacuo) electroformed copper deformation grids which were purchased from Interconics of St. Paul, Minnesota. These grids were pretreated by immersion into hot polyethylene solution to promote film adhesion. The grid and supported film were uniaxially elongated at a rate of 5×10^{-4} mm/s at room temperature using a JEOL SEH deformation stage.

Although films were subjected to an elongational force along the chain direction, a biaxial planar stress field developed due to hindered lateral contraction of the film. The transition from uniaxial to

biaxial tension increases the probably that the films will behave in a brittle manner (Sandiford and Willbourn, 1960). Typically, a 0.5 - 1.0 mm guage length sample was elongated by 0.6 mm. The local strain within these films was usually very inhomogeneous and could not be related to the nominal strain. Near isothermal conditions were assumed to persist during deformation due to the slow elongation rate employed and to the thinness of films. This would result in a slow rate of energy release, and a relatively fast rate of heat dissipation, respectively.

Films were viewed using a JEOL 100CX TEM, operated at 100 kV. To avoid the introduction of artifacts and to get the best resolution, no heavy metal stains, gold decoration, replication techniques, or substrate films were used. As indicated in Chapter 3, low electron dosage precautions were taken to mitigate the beam damage incurred by the sample.

Results

First, the morphology of undeformed films will be reviewed. The brightfield image of HDPE appeared lamellar (Fig. 4.11). Closer scrutiny revealed however, that the lamellae were comprised of mosaic blocks which were approximately as wide (perpendicular to the chain axis) as they were thick (parallel to the chain axis) (Fig. 4.14). When diffracting, these individual blocks appeared as dark regions in brightfield mode, and bright regions in darkfield mode. Crystallites

which were not diffracting appeared as grey regions in brightfield mode. Electron diffraction indicated a high degree of chain orientation as well as a single crystal-like texture in which the a axis was preferentially oriented perpendicular to the film plane and the c axis was oriented along the draw direction. The shish-kebab nature of these films was generally not apparent until they were deformed.

In the following, it will be useful to refer to a schematic representation of the deformed film microstructure (Fig. 5.3). At low strains, these materials deform elastically by elongation of the noncrystalline phase (Miles et al., 1976). The details of deformation at low strains were not observable by TEM here. However, such elongation would occur freely only in regions not reinforced by shish-kebabs, and would therefore not occur uniformly throughout the sample. For instance, longitudinal forces (parallel to the chain direction) would elongate material at the ends of shish-kebabs while lateral forces (perpendicular to the chain direction) would elongate material between shish-kebabs. At high strains, an increase in the separation distance between lamellae (kebabs) was seen (Fig. 5.4a), resulting in what can be termed craze formation. Crazing necessarily involved deformation of the crystalline phase. Crazes have been seen previously in PE (Friedrich, 1983; Postema et al., 1987). The numerous short crazes in the present case of elongation along the chain direction did not propagate, however, growth being arrested by shish-kebabs.

The noncrystalline phase was subject to fewer constraints to lateral rather than longitudinal extension. Lateral stresses were

Figure 5.3

Schematic of HDPE film uniaxially elongated parallel to the chain direction at 25 °C. Chain axis vertical. Elongation direction (E) as indicated.

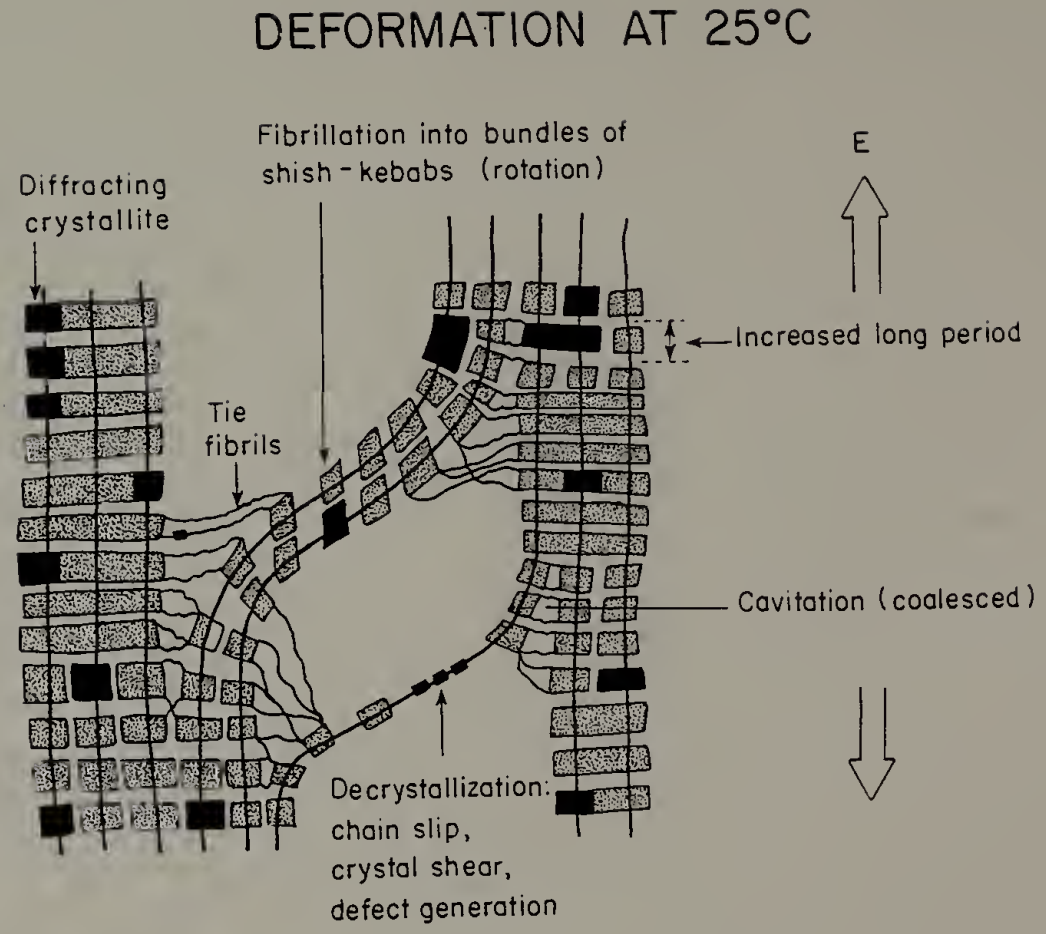
DEFORMATION AT 25°C
Fibrillation into bundles of shish-kebabs (rotation)
E
Diffracting crystallite
Increased long period
Tie fibrils
Cavitation (coalesced)
Decrystallization: chain slip, crystal shear, defect generation

Figure 5.4

Brightfield micrograph of early stages of deformation in HDPE film, uniaxially elongated parallel to the chain axis at 25 °C showing A) cavitation and craze initiation, and B) longitudinal coalescence of cavities prior to fibrillation. Chain axis vertical.

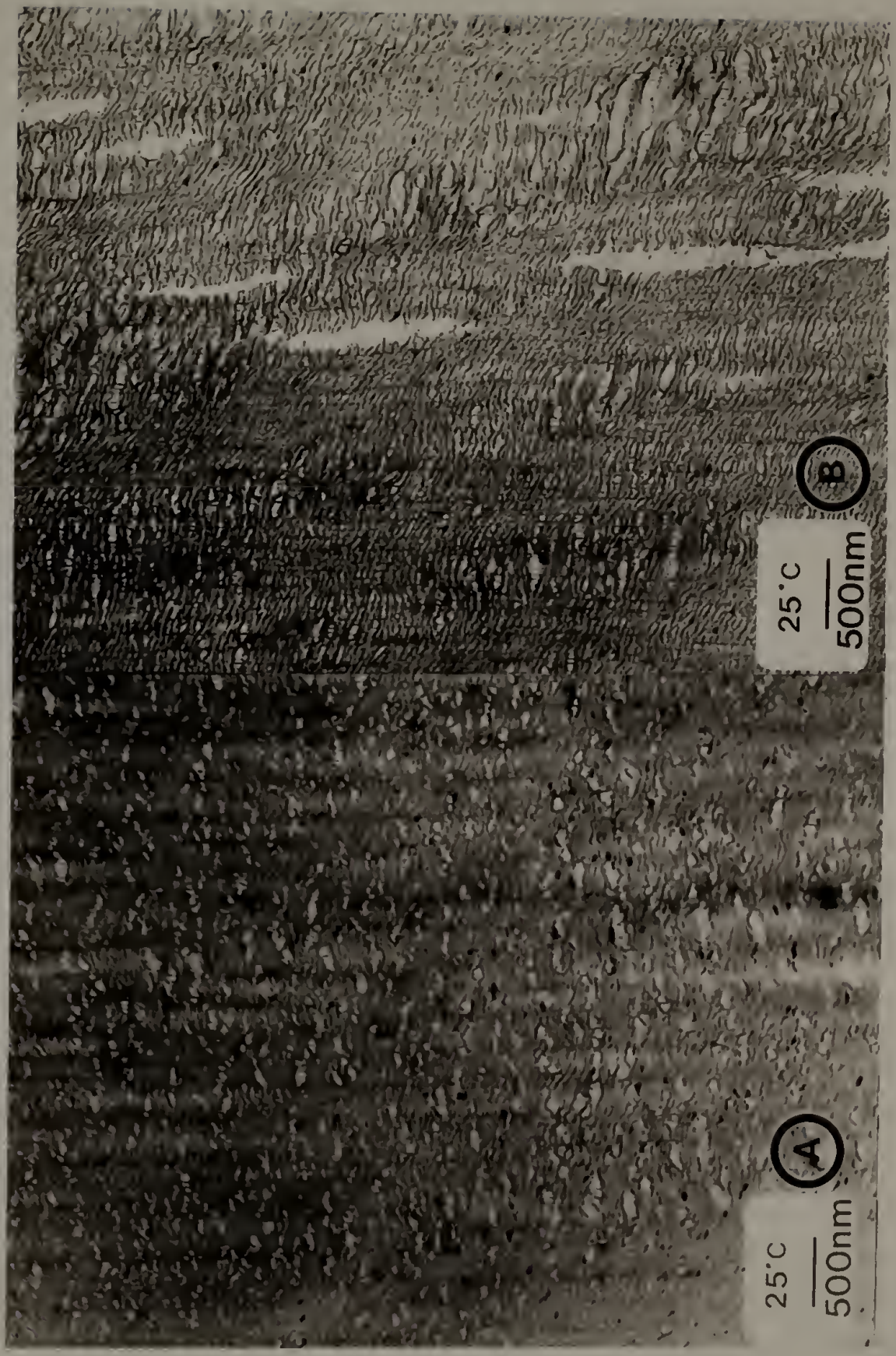
25°C
500nm
A
25°C
500nm
B

relieved by film thinning, which is visible as the light/dark striations in Fig. 5.4a, followed by cavitation. Eventually, these cavities coalesced, resulting in the growth of long voids between shish-kebabs (Fig. 5.4b). These voids were commonly spanned by tie fibrils, which are believed to consist of tie molecules and entangled chains as well as free chain ends. Eventually, fibrillation occurred (Fig. 5.5). The interconnected nature of the various structural elements in these films ultimately resulted in a network-like structure similar to that found elsewhere (Heise et al., 1980) (Fig. 5.6). This structure further supported the conclusions of chapter 4 that these films were drawn from a precursor gel state. The process of fibrillation, in which cavities preferentially nucleated in noncrystalline areas and shish-kebabs peeled apart kebab by kebab, is summarized in Fig. 5.7. Details of the later stages of fibrillation were best seen at higher magnification (Fig. 5.8).

The heterogeneous fibrillation shown here resulted from the inherent structural heterogeneity of these films. Since shish-kebabs are crystalline, they remained relatively rigid as the noncrystalline phase extended and cavitated. Subsequent fibrillation occurred nonuniformly, some fibrils being several shish-kebabs wide while others were comprised of a single shish-kebab. It appears that heterogeneities also existed within the noncrystalline phase, making one region more susceptible to cavitation than another. These heterogeneities could arise from such things as film thickness variations or uneven

Figure 5.5

Brightfield micrograph of HDPE film uniaxially elongated along the chain axis at 25 °C showing extensive fibrillation into bundles of shish-kebabs. Chain axis (in thick fibrils) vertical.

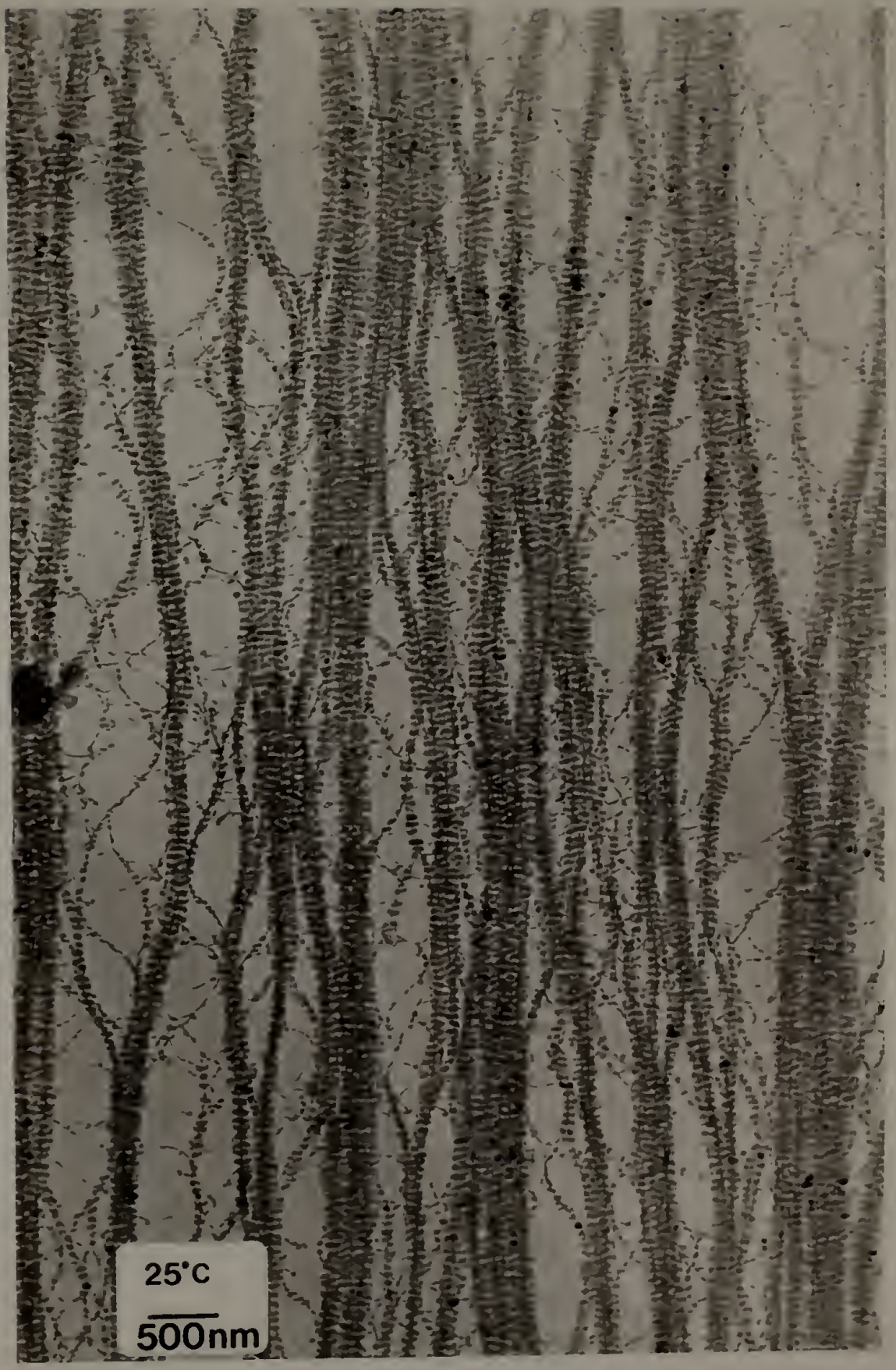
25°C
500nm

Figure 5.6

Brightfield micrograph of HDPE film, uniaxially elongated parallel to the chain axis at 25 °C showing network-like structure. Chain axis (in thick fibrils) vertical.


25°C
500nm

Figure 5.7

Composite of figures 5.4A (A), 5.4B (B), 5.5 (C), and 5.6 (D) showing cavitation between shish-kebabs and the eventual fibrillation which followed.

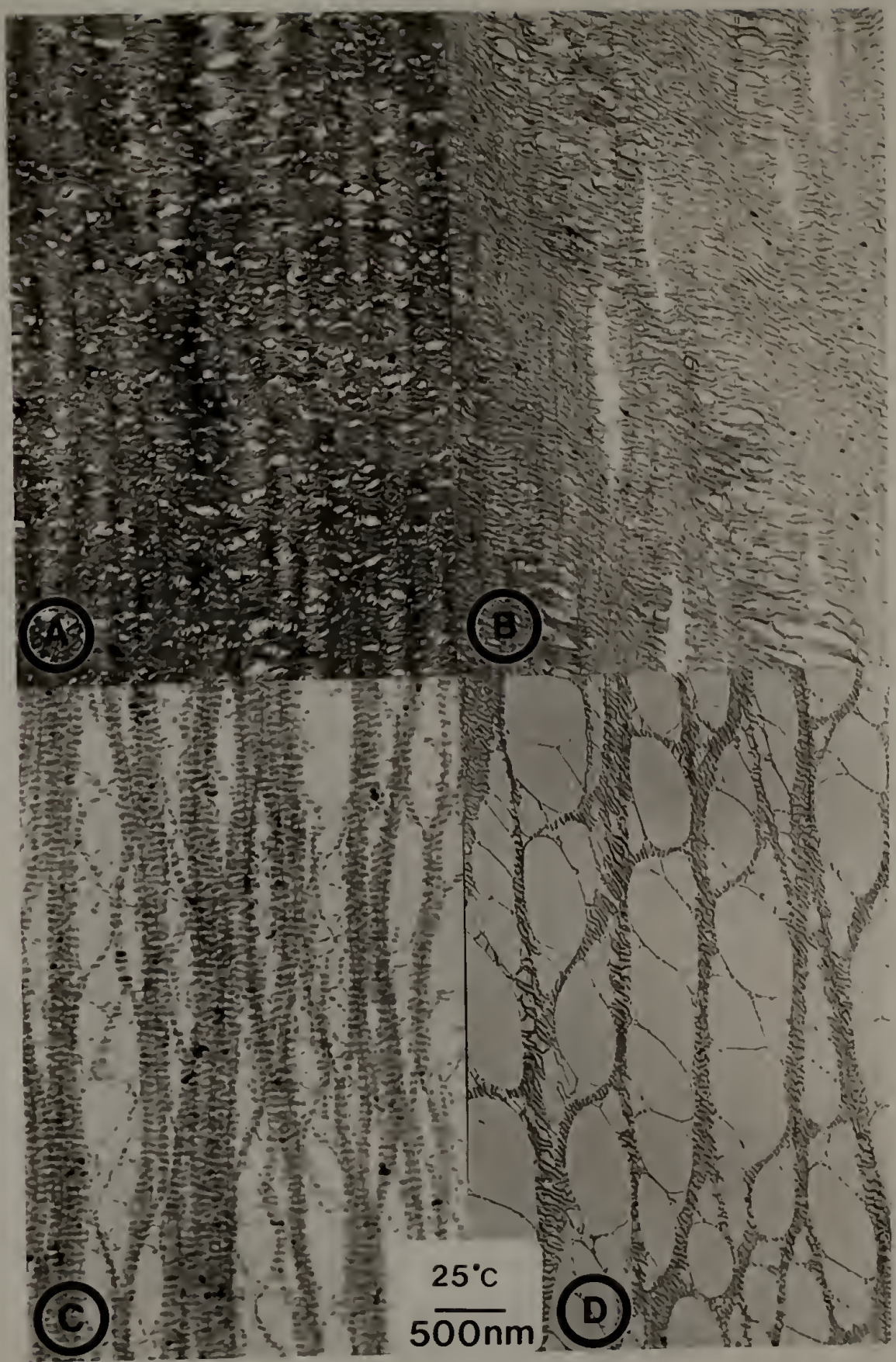
A
B
C
D
25°C
500nm

Figure 5.8

Higher magnification of Fig. 5.5. Brightfield micrograph of HDPE film uniaxially elongated parallel to the chain axis at 25 °C showing tie fibrils (A), change in mosaic block shape at early stages of crystal shear (B), crystal shear (C), resulting in a reduction in crystal width, and D) defective regions within crystals. Chain axis vertical.


A
B
B
B
B
B
C
C
C
C
D
25°C
200nm

reinforcement of the noncrystalline phase (high concentration of shish-kebab ends or defects in a given region or low number density of crystals). The resultant stress concentrations in these regions brought about premature yielding.

Tie fibrils spanned cavities and interconnected neighboring shish-kebabs. Shish crystals were clearly visible as dark striations running along the elongation direction (Fig. 5.8). They almost exclusively originated and terminated at kebab fold surfaces (Fig. 5.8, region A). It is clear that lateral strength ultimately depends on the number density and strength of these load-bearing tie fibrils. Fibrils, on the other hand, were comprised of bunches of shish-kebabs which spanned cavities. The location of fibrils and tie fibrils between shish-kebabs suggested that very little shear occurred between shish-kebabs. Shear between shish-kebabs was observed, however, in subsequent studies in which the film was elongated at an angle of 14 ° to the chain axis, resulting in a higher shear stress (Fig. 5.9).

Eventually, stresses transferred by the tie fibrils became sufficiently large to induce the mechanical destruction of the crystals to which they were attached (Fig. 5.8, regions B - D). The mechanical destruction of the shish-kebabs was accompanied by a transition to a monoclinic crystalline phase, as evidenced by the appearance of the (001), 4.55 Å monoclinic reflection for a unit cell of dimensions: 8.09 Å, 2.53 Å, and 4.79 Å for the a, b, and c axes, respectively (Seto et al., 1968) where the b axis refers to the molecular axis. Chain

Figure 5.9

Brightfield micrograph of HDPE film uniaxially elongated at an angle of 14 ° to the chain axis at 25 °C showing extensive shear. Chain axis vertical.


25°C
500nm

scission is likely to have occurred as well, at sufficiently high stress levels.

The decrystallization process is schematically outlined in Fig. 5.10. Decrystallization occurred via chain slip, crystal shear, and defect generation. The onset of crystal shear within mosaic blocks was identified by changes in block shape from orthorhombic to that of a parallelopiped (Fig. 5.8, regions B). Subsequent shear resulted in a decrease in crystal width (perpendicular to the chain direction) (Fig. 5.8, regions C). In addition to the shear of crystallographic planes, decrystallization also involved the generation of defects within the interiors of mosaic blocks (Fig. 5.8, regions D). Ultimately the thickness of crystals (parallel to the chain direction) was reduced in this way without invoking a rise in temperature. Strain-induced defect generation has been detected previously by wide angle x-ray scattering (Reck et al., 1985; Adams et al., 1985). Thus, decrystallization brought about a reduction in crystal size, perfection, and crystallinity.

As the load on tie fibrils increased, they elongated by incorporating new material into the fibril, analogous to the surface drawing mechanism of fibril growth seen in polystyrene crazes (Lauterwasser and Kramer, 1979). The cannibalization of kebabs by shish crystals during drawing was clearly indicated by the presence of (ca. 10 nm thick) crystal remnants throughout tie fibrils. (Note that this is approaching the resolution limits of ca. 7 nm in these micrographs.) In

Figure 5.10

Schematic of decrystallization starting with chain-folded lamellae and ending with a much more chain-extended continuous crystal. Extensive crystalline regions were only seen in linear polyethylene deformed at 93 °C and 129 °C. Chain axis vertical.

DECRYSTALLIZATION

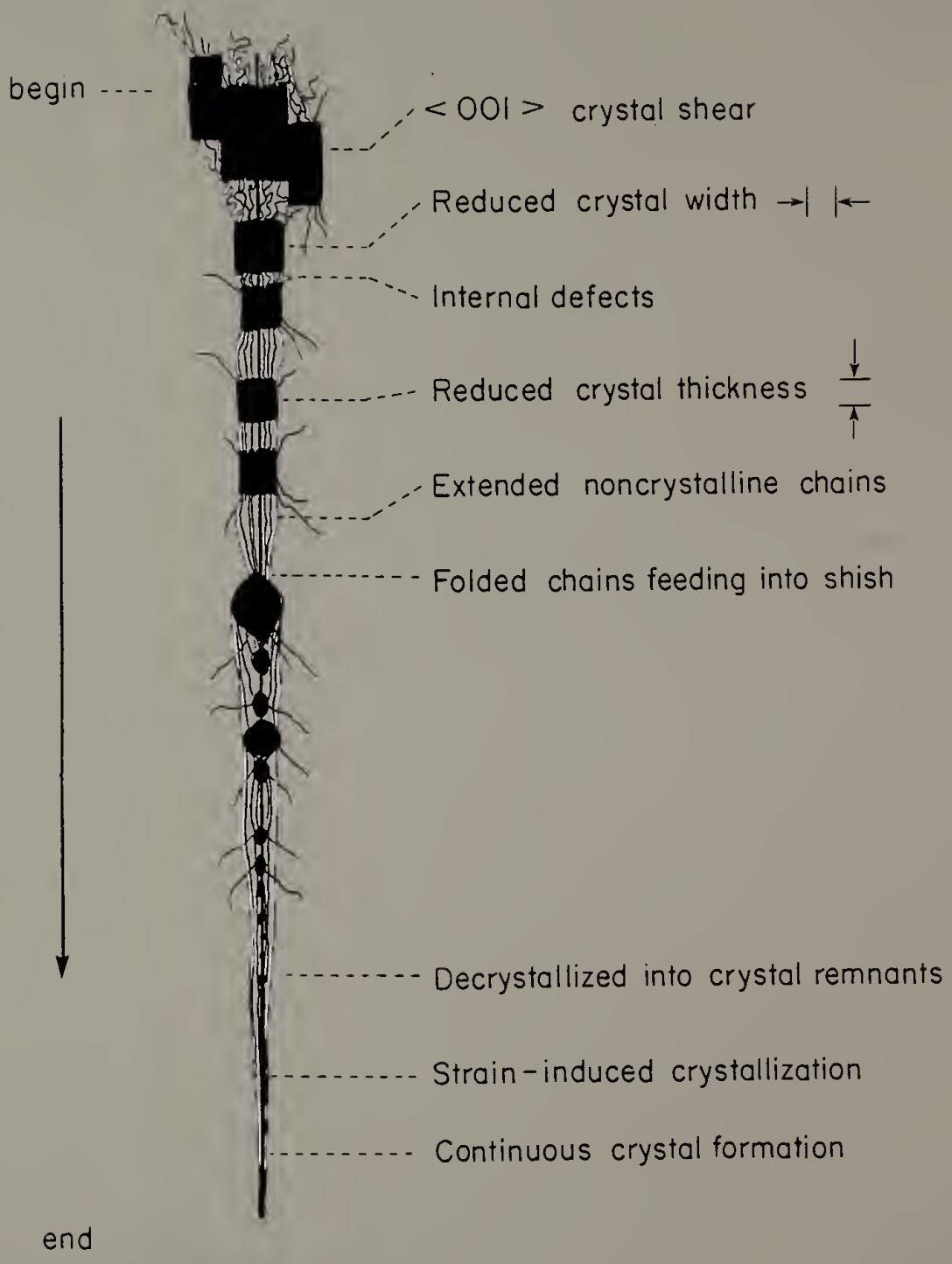

addition, the polydispersity in tie fibril diameter suggested that draw-down (creep) also occurred. It is believed that both mechanisms were operative, surface drawing being followed by draw-down (creep). At very high strains, the tie fibrils broke by chain scission and/or disentanglement.

Additional experiments were performed to determine the effect of applying stress perpendicular to the chain direction. Initially, cavities grew between shish-kebabs. This enabled the shish-kebabs to then rotate by 90°, forming a craze in which shish-kebabs served as craze fibrils and the chain axis became aligned with the draw direction (Fig. 5.11). The small arrows in Fig. 5.11 indicate the direction of lamellar normals on either side of the craze interface. The rotation of shish-kebabs within the craze was indicative of a high stress level along craze fibrils. Apparently, craze growth occurred because the crazes could propagate between shish-kebabs in the relatively ductile noncrystalline phase. Within the craze, deformation was essentially identical to that for films which were deformed along the chain direction. Crystal blocks appeared relatively undeformed until the bulk/neck interface was reached, in contrast to the prenecking deformation reported elsewhere (Peterlin, 1971). The experimental microstructure shown in Fig. 5.11 displays all of the schematic components proposed by Friedrich (Fig. 5.12) except Friedrich did not include lateral tie fibril connections between craze fibrils. Such connections are clearly seen in Fig. 5.11. In fact, the lateral separation of craze fibrils, and the high tension in tie fibrils often

Figure 5.11

Brightfield micrograph of HDPE film elongated perpendicular to the chain axis at 25 °C showing craze formation as well as 90 ° rotation of shish-kebabs at craze interface. Arrows indicate direction of lamellar normals. Insets show the electron diffraction pattern of craze fibrils, as well as the "zigzag" appearance of shish-kebabs under tension within a craze. Elongation direction vertical.


500nm
25 °c
1μm

Figure 5.12

Friedrich model (1983) of craze initiation and propagation in a semicrystalline polymer showing the rotation of the chain axis towards the direction of draw and the reduction in crystallite width as crystallites are drawn into craze fibrils.

Craze Formation in Semicrystalline Polymers

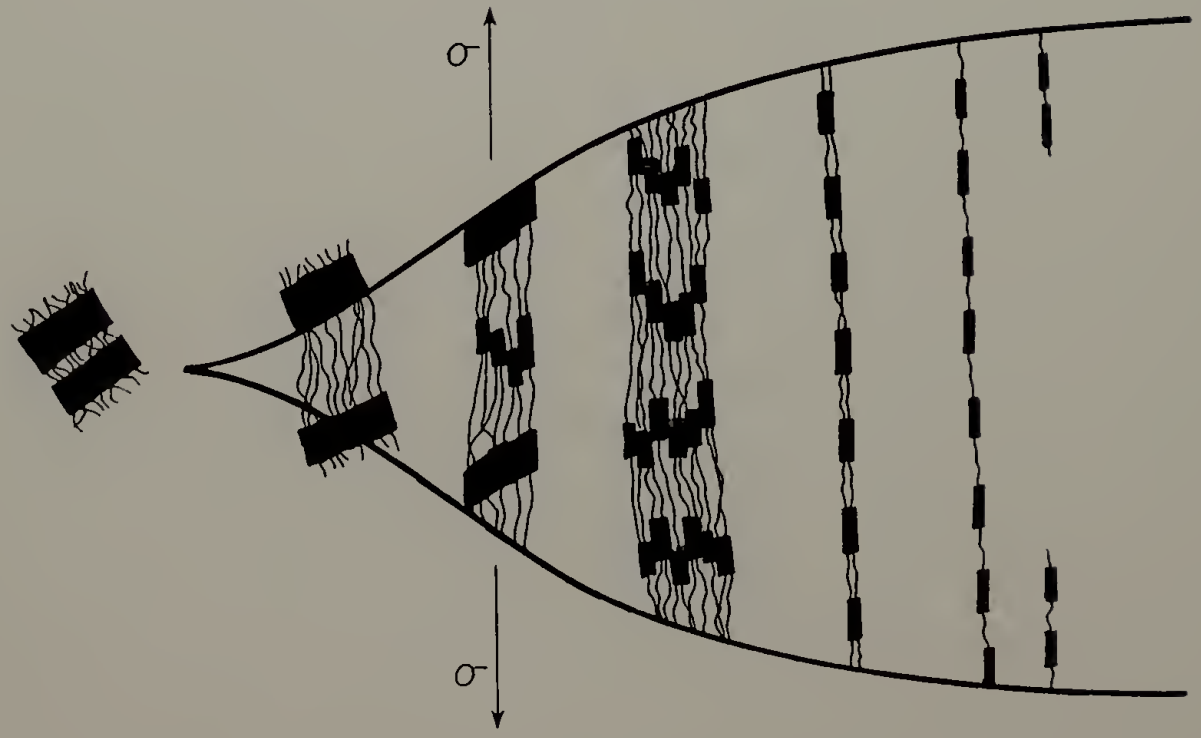

After K. Friedrich (1983)

imparted a "zig-zag" appearance to crazed regions (Fig. 5.11, inset). Deformation within crazed regions led to changes in kebab size, shape, and lateral registration, destroying the original lamellar character of this material.

Electron diffraction was used to determine the chain axis orientation within these highly deformed regions. The rotation angle between images and diffraction patterns was measured by comparing the orientations of the image and corresponding shape transform of MgO single crystals, vapor deposited onto a carbon film. Diffraction reflections from craze fibrils were weak and broad (Fig. 5.11, inset). The large angular (2θ) breadth along the equator, and absence of essentially all reflections except one ((110) and (200), merged) indicated that the samples had undergone significant decrystallization. Such diffraction patterns resembled those of heavily beam-damaged (and highly defective) material (recall Fig. 3.2). However, under the exposure conditions used, the material deformed at 90 ° was not heavily beam damaged. This corroborated the assessment that these fibrils had undergone extensive decrystallization. The crystals within craze fibrils were highly oriented along the local draw direction. The weakness of reflections is believed to be due to the small number of crystals in a given projected volume, a result of film thinning, cavitation, and extensive chain slip within the highly deformed region.

Consider now those processes which occurred in the noncrystalline phase during deformation. Initially, the noncrystalline phase became extended and oriented. When chain mobility was sufficiently high, these

chains aligned and crystallized (Miles et al., 1976) by a process known as "strain-induced crystallization". (See review symposia in Polym. Eng. and Sci., 16(3), 125 (1976)). It was not possible to observe in real time the above processes due to the fast crystallization rate and beam sensitivity of HDPE. However, darkfield microscopy (of samples viewed directly followed by deformation several hours (>) after deformation) did not reveal any noticeable strain-induced crystallization as a consequence of the deformation applied during these particular studies. Apparently, the mobility and extension of chains at 25 °C was not high enough to bring about strain-induced crystallization or the generation of long crystalline regions. Under appropriate conditions, however, HDPE is capable of strain-induced crystallization, as indicated by the presence of chain-extended shish crystals in as-drawn films. In fact, strain-induced crystallization was observed in polyethylene deformed at higher temperatures, as will be made evident in the following two chapters.

Discussion

The deformation behavior observed here agreed with previous microfibrillar models in that crystal blocks broke apart and fed into fibrils. In this case, however, the initial undeformed films consisted of highly oriented aligned shish-kebabs as opposed to isotropic spherulitic films. This morphology served as a useful model of fibrillar morphologies (such as those found in blown film and extruded

material), and was used to determine how such materials deform. Likewise, these experiments relate to the deformation behavior of spherulitic material at high strains.

The destruction of crystals in previous studies has been followed both by direct viewing (Adams et al., 1986) and by line broadening wide angle x-ray scattering (WAXS) studies (Reck et al., 1985). In the former case, crystal shear in polyethylene was identified to be of the (100) <001> and (010) <001> type. In addition to a decrease of crystal size with draw ratio, WAXS studies indicated that upon straining new grain boundaries developed within crystals by dislocation formation. It was also found that the number of dislocations present increased with strain. It has been suggested that crystal shear in polyethylene occurs by a dislocation mechanism analogous to metal deformation (Petermann and Gleiter, 1973b). In the following, the evolution of crystalline phase morphology with deformation will be discussed in detail.

The near isothermal process of "decrystallization" and the subsequent feeding of crystal remnants into fibrils involved the mechanical destruction and thermodynamic destabilization of the crystalline phase. Crystal block size was reduced by crystal shear and chain unfolding, whereas crystal perfection was reduced via defect generation. All of these factors serve to reduce the melting point.

The extent of melting point depression depends not only on crystal size and the local stress state, but also on the degree of amorphous phase extension. Such extension would increase the melting point by reducing the conformational entropy of the noncrystalline phase (Flory,

1947). In the extreme, the crystal size could become so small as to be thermodynamically unstable (due to both small size and internal imperfections) that the (depressed) melting point would reach the deformation temperature.

Analogies can be drawn between decrystallization and pressure-induced melting whereby a negative pressure reduces the melting point according the Clausius-Clapeyron equation:

$$dT_m/dP = T_m/\Delta H_f \, (V_2 - V_1)$$

where T_m is the equilibrium (atmospheric pressure, quiescent) melting temperature, P is hydrostatic pressure, ΔH_f is heat of fusion, V_2 is the specific volume of the "melt", and V_1 is the specific volume of the crystalline phase. For polyethylene, one can take T_m to equal 141.4 °C, ΔH_f to be 69 cal/gm, V_2 to be $1/(0.854\ g/cm^3)$, and V_1 to be $1/(1.0\ g/cm^3)$ (Wunderlich, 1973f). Then the change in melting point with hydrostatic pressure would be 2.45×10^{-7} °K/Pa. Such low temperature, pressure-induced melting has been used to interpret the necking process in Nylon 6.6 (Hookway, 1957) as well as the change in crystal size with deformation in polyethylene (Peterlin, 1972). In the present experiments, the stress tensor is comprised not only a hydrostatic pressure component, but deviatoric components as well.

In the following discussion, the term "melting" will be associated with the thermally-induced phase change which occurs at atmospheric pressure under quiescent conditions. When describing the evolution of

morphology with deformation in thin films, the term "decrystallization" will be employed, referring to the localized, near isothermal, stress-induced reorganization of the crystalline phase. Moreover, although decrystallization is believed to lead to a loss in crystallinity, the overall change in crystallinity of the sample will depend on how much strain-induced (re)crystallization and annealing occurs as chains reorganize.

The debate over whether or not polyethylene melts during deformation is not a new one (Chuah et al., 1986; Juska and Harrison, 1982; Meinel and Peterlin, 1971; Flory and Yoon, 1978). It has been suggested that the deformation of bulk polymers results in a temperature rise sufficiently large to bring about thermally-induced melting (Peterlin and Sakaoku, 1967; Corneluissen and Peterlin, 1967; Swallowe et al., 1986; Phillips and Philpot, 1986), and to facilitate crystal shear by thermal expansion of the crystalline lattice (Peterlin, 1972; Swan, 1962). The occurrence of such melting and recrystallization during deformation has been used to explain the changes in crystalline phase morphology accompanying drawing. Alternatively, others believe that changes in crystalline phase morphology can be explained in terms of stress-induced yielding. In the present set of experiments, essentially isothermal conditions prevailed. As such, the observed disruption of crystallinity was straight forwardly attributed to decrystallization and the generation of defects rather than to temperature rise and subsequent melting. Other researchers have shown that lattice expansion accompanies deformation and attributed this to a

loss in crystal perfection (Adams et al., 1985). Here the effects of defect generation on the crystalline phase were actually seen. The resultant lattice expansion in defective areas would reduce the constraints to chain motion within the crystalline phase, much as thermally-induced lattice expansion facilitates flow processes and yielding.

Much research has centered on the change of crystallinity with deformtion. Numerous conflicting reports have arisen concerning the effect of deformation on crystallinity. When comparing these reports, it must be kept in mind that not only deformation temperature, but also draw ratio and the nature of the undeformed material varies from one study to the next. For instance, it has been stated that when spherulitic PE is deformed, no change in crystallinity occurs at all. However, spherulitic PE deforms differently than the HDPE films in the present case in that a high degree of chain orientation exists in the latter. In spherulitic polyethylene, a significant amount of crystal reorientation and amorphous phase extension preceeds decrystallization. Observations made here indicated that once strained and yielded, spherulitic PE would probably experience a loss in crystallinity at a given stage via chain unfolding and stress-induced defect generation within crystals (and due to the absence of strain-induced crystallization) without invoking the temperature rise associated with melting. Such a loss in crystallinity with deformation has been found by density measurements (Chuah et al., 1983).

In closing, some remarks relating these morphological observations to the known mechanical behavior of HDPE at room temperature will be made. The studies done here are mainly applicable to highly oriented (and therefore post-yield) HDPE. During yielding, lamellae feed into fibrils. Further straining typically results in a significant increase in stress level (strain hardening) as a large portion of the chains become extended and stresses are taken up by covalent bonds along the extended chain backbone. Subsequent elongation occurs at the expense of the crystalline phase, which undergoes decrystallization and brings about a further increase in chain extension. No identifiable strain-induced crystallization was observed here, implying that strain hardening in PE can occur even in there is (at least initially) a loss of crystallinity, provided chain extension increases with draw. However, since these materials were not drawn to failure, it is unclear whether strain-induced crystallization would occur at higher strains than those accessed.

Conclusions

Thin, oriented, single-crystal-like textured, shish-kebab morphology films of HDPE were uniaxially extended both parallel and perpendicular to the chain direction. At low strains, the films crazed, forming cavitated regions spanned by fibrils. In material elongated perpendicular to the chain direction, these crazes grew and were

accompanied by the lateral separation and a 90 ° rotation of shish-kebabs, such that the chain axis became aligned with the elongation direction (Fig. 5.11). This craze structure resembled that outlined by Friedrich (Fig. 5.12), except that tie fibrils interconnected craze fibrils in the present case. On the other hand, craze growth was not detected in films elongated along the chain direction. Here, it was apparent that the high yield stress of the crystalline phase hindered craze propagation. In the former case, crazes propagated between shish-kebabs in the amorphous phase, the rotation of shish-kebabs within the crazes resulting from the high stresses along craze fibrils. In HDPE elongated along the chain direction, lateral stresses were relieved by cavitation between bundles of shish-kebabs (leading to fibrillation) and by a decrystallization process (Fig. 5.10) which enabled kebabs to feed into shish crystals, resulting in shish-kebab elongation. At high strains, shish-kebabs were transformed into fibrils, each one having uniform diameter, which subsequently underwent draw-down.

Near isothermal decrystallization resulted in the mechanical destruction of crystals by <001> crystal shear, chain unfolding and slip, and the generation of defects within crystals. Crystal shear brought about a distortion in crystal block shape followed by a decrease in crystal width (perpendicular to the chain axis). More importantly, it was shown that a reduction in crystal thickness (parallel to the chain axis) could be brought about mechanically, without requiring a rise in temperature, by means of defect generation. The incorporation of defects within the lattice would in turn facilitate yielding. Both

chain unfolding and defect generation would probably lead to a loss of crystallinity as well. In addition, the crystalline phase underwent a martensitic transformation from the orthorhombic to monoclinic phase. Although noncrystalline phase elongation occurred, no crystalline regions indicative of strain-induced crystallization were detected in darkfield micrographs. It appears that negligible if any strain-induced crystallization occurred at room temperature, although it is known to occur in HDPE deformed at higher temperatures.

The structural transformations observed during deformation can be used to explain the evolution of mechanical properties with draw. HDPE deformed at room temperature is known to strain harden following necking (Fig. 1.1, region III). At low strains, the noncrystalline phase becomes extended and oriented, increasing the number of load-bearing covalent bonds (Fig. 1.1, region I). This may be responsible for the strain hardening observed at high strains. In addition, upon yielding (Fig. 1.1, region II) decrystallization and chain unfolding occur, increasing the degree of chain extension. The absence of observable strain-induced crystallization suggested that polyethylene comprised of two discontinuous phases prior to deformation will not develop a continuous crystalline phase upon isothermal deformation at room temperature. A continuous crystalline phase would develop if crystalline bridges interconnecting crystallites formed. Although Keith et al. (1966 and 1971) have shown that such bridges can form from concentrated polyethylene solution without applying stress, it is difficult to imagine their formation from the solid state without such

stimulation, especially in view of the fact that decrystallization and the associated chain reorganization is stress-induced.

The above findings are applicable to studies of bulk PE because they show that changes in crystal thickness cannot be used as proof of thermally-induced melting during deformation. In fact, a loss of crystallinity can occur at temperatures below the (atmospheric pressure, quiescent) melting range when under the influence of stress. This is particularly relevant to bulk material deformed at low temperatures and low strain rates.

C H A P T E R VI

THE CONVERSION OF SINGLE CRYSTAL MATS TO ULTRAHIGH MODULUS POLYETHYLENE: THE FORMATION OF A CONTINUOUS CRYSTALLINE PHASE

Abstract

Ultrahigh modulus and strength (≥ 175 GPa and 3 GPa, respectively) ultrahigh molecular weight (UHMWPE) films, which were formed by solid state coextruding and post-drawing (SSE/PD) single crystal mats to draw ratios up to 250, were analysed by transmission electron microscopy (TEM). The high performance properties of these samples were attributed to the formation of a continuous (sample-spanning) crystalline phase of laterally coalesced protofibrils. Indeed, crystalline regions displaying a protofibril substructure were observed by darkfield TEM to be up to 3 microns long. The fact that darkfield TEM gives only a lower bound of crystal size, coupled with the known ultrahigh tensile modulus of this material, suggested that the limited extent of observed crystalline regions resulted from variations in crystalline phase orientation, and not from discontinuities within the crystalline phase. Moreover, the lateral coalescence and simultaneous diffraction of adjacent protofibrils suggested that crystal/crystal junction points were present between protofibrils. Such a coupling would enable a sample-spanning crystalline phase to form even if individual protofibrils were not sample-spanning themselves.

The protofibril structure (Fig. 6.5) resembled that of shish-kebabs (Fig. 5.2), with very narrow kebabs. The protofibrils themselves were made up of a series arrangement of ca. 8 nm thick kebabs and crystalline bridges, were hundreds of nanometers long (along the chain direction), and were no wider than 10 nm. The observed evolution of morphology from a draw ratio of 6 to 250 indicated that protofibrils formed by the decrystallization of the original single crystal structure and subsequent strain-induced crystallization of noncrystalline chains. Decrystallization occurred via <001> crystal shear, chain slip and unfolding, and defect generation (Fig. 5.10).

Current structural models of a continuous crystalline phase do not adequately represent the observed protofibril morphology. For instance, the model of Gibson et al. (1978), which is a modification of the basic Peterlin model (Fig. 5.1) depicts the continuous crystalline phase as being comprised of lamellae interconnected by crystalline bridges. TEM observations indicated that such a model is satisfactory for polyethylene drawn to a draw ratio (DR) of ca. 6. However, this model does not apply in the case of ultradrawn PE since ultradrawn PE displays no long period. Other continuous crystalline phase models recognize the absence of a long period, although they do not incorporate a fibrous substructure (Clark and Scott, 1974). However, TEM observations indicated that a continuous crystalline phase is best depicted by the lateral coalescence of protofibrils.

Introduction

Recent advances in processing techniques have enabled polyethylene to be drawn to extremely high draw ratios. Draw ratio, however, is a macroscopic measure of sample extension. Strain-induced crystallization and the attainment of ultrahigh modulus depends on the extension of individual chains. Drawing is efficient when chains are extended and do not relax or undergo chain scission appreciably. Nuclear magnetic resonance (NMR) studies have indicated that the efficiency of draw decreases as temperature increases (Ito et al., 1981). However, since the yield stress increases as temperature decreases, low temperature deformation is accompanied by high tension along chains, which leads to deleterious chain scission instead of plastic deformation (Porter and Casale, 1985). It has been shown that it is desirable to draw at or above the alpha loss temperature, where crystal shear and chain slip is facilitated by a relatively low yield stress, and chain scission is minimized (Perkins and Porter, 1977; Zachariades et al., 1980).

NMR studies have shown that chains in the noncrystalline phase become less mobile as the draw ratio increases, mobility decreasing sharply with draw (at room temperature) up until an extrusion draw ratio of ca. 12, and then gradually approaching a limiting value at higher draw ratios (Ito et al., 1981). The sharp reduction of amorphous phase mobility can be related to the high degree of amorphous phase orientation and extension accompanying yielding. Upon reaching a draw ratio of ca. 10 (for room temperature drawing), initially isotropic HDPE

has been completely transformed into a fibrillar morphology (Gibson et al., 1974) and has reached its "natural draw ratio". Subsequent draw is accompanied by a rapid increase in draw stress. Crystallite size along the chain direction is known to increase steadily with draw at this stage of deformation (Ito et al., 1981), suggesting that the high modulus of drawn material is due to a high degree of noncrystalline chain extension and strain-induced crystallization.

Conventional tensile drawing is often viewed as an impractical way to achieve high draw ratios, since materials tend to cavitate and undergo premature brittle failure (Chuah et al., 1983). SSE offers an alternative way by which one can achieve high draw ratios and correspondingly high tensile moduli. The major and perhaps most significant difference between SSE and tensile drawing is that SSE is accompanied by a high hydrostatic pressure. Kanamoto et al. (1983b) indicated that in both processes, the maximum achievable draw ratio increases with temperature, and similar draw ratios and tensile moduli can be achieved, at least up to a draw ratio of 100. However, at high draw ratios, the efficiency of draw becomes limited by the number density of entanglements and tie molecules, which are required for proper stress transfer. For instance, efficient draw was limited to a draw ratio of 120 for HDPE of a molecular weight of 2×10^6 (Irvine and Smith, 1986). In the SSE technique, such a dependence on entanglement density appears to be absent (Kanamoto et al., 1979). The high lateral pressure which is present during SSE increases the friction between microfibrils, and stress is believed to be transferred between

microfibrils even in regions where they are not interconnected by tie molecules or entanglements.

Kanamoto et al. (1983b) also found that drawing efficiency, as measured by the tensile modulus achieved for a given draw ratio, increased if samples were solid state extruded prior to tensile drawing. For instance, material drawn to a draw ratio of 230 (without prior SSE) had a tensile modulus of 110 GPa, while material solid state extruded to a draw ratio of 6 followed by post-drawing (PD) to yield a total draw ratio of 250, had a modulus of ca. 220 GPa. It is possible that the higher modulus accompanying SSE "pre-treatment" resulted from the compaction of fibrils and microfibrils (Peterlin, 1976). This densification would give rise to a greater number of covalent bonds per cross sectional area, and therefore higher tensile moduli.

Ultradrawn (draw ratio = 247) SSE/PD samples have been shown to exhibit crystallinities as high as 90%, as determined using conventional density methods (Kanamoto et al., 1983a). Wide angle x-ray scattering studies have indicated that crystals deform by <001> shear mechanisms during SSE, whereby crystallite dimensions along the a and b axes initially decrease and subsequently remain constant with draw (Kanamoto et al., 1981; Tsuruta et al., 1985; Adams et al., 1985). Similar mechanisms have been noted during tensile drawing (Adams et al., 1986; Peterlin, 1976; Kanamoto et al., 1984). Furthermore, crystal perfection, crystallinity, and crystallite dimensions along the c axis decrease and then increase with draw (Chuah et al., 1983; Tsuruta et al., 1985). In fact, calculations using Peterlin's morphological model

(1971) as well as scattering and density data (on materials drawn up to a draw ratio of 30), have indicated that the number of crystalline tie fibrils interconnecting lamellae increases with draw (Tsuruta et al., 1985). More importantly, the population of thick crystals as well as crystalline tie fibrils has been shown by darkfield TEM to increase with draw (Sherman et al.,1982; Smith et al., 1985; Frye et al., 1979; Van Hutten et al., 1985). Small angle x-ray scattering (SAXS) has revealed that the long period peak scattering intensity decreases as the material is drawn beyond a draw ratio of 10, when the fibrillar texture itself begins to deform (Kanamoto et al., 1984; Adams et al., 1985). In fact, no long period reflections have been discerned in ultradrawn material (T. Kanamoto, private communication), indicating that the Peterlin and Gibson models are no longer applicable. This loss of intensity concurs with other studies in which the SAXS long period peak vanished entirely when drawn to a draw ratio of 80 at 100 °C (Furuhata et al., 1986). At the same time, infrared measurements have indicated a fractional crystallinity approaching unity, implying the formation of a continuous crystalline phase.

For the present purposes, a continous crystalline phase will be defined to be a sample-spanning crystalline phase. Such a phase can form in more than one way. For instance, the continuous crystalline phase can be comprised of much smaller crystalline elements which, through interconnections, attain crystalline phase continuity. To attain an ultrahigh modulus, such coupling points would be required to transfer stress between crystallites efficiently. Alternatively, the

sample could be comprised of a single crystallite, pervaded by occasional defects.

The disappearance of SAXS scattering intensity with draw has been interpretted in several ways. It has been suggested that instead of measuring SAXS peak heights or areas, it is fundamentally more meaningful to determine the integrated scattering intensity or invariant (Adams et al., 1985). The invariant itself is directly related to the mean square electron density fluctuation: $\langle(p - \dot{p})^2\rangle$ where p is the density at a given point and $\dot{p}$ is the bulk sample density. Most importantly, the invariant is model independent. For a two phase system with sharp boundaries, in which no scattering arises from electron density fluctuations within a single phase, the mean squared density fluctuation is given by :

$$(p_c - p_a)^2 V_c(1 - V_c)$$

where p_c is the crystalline phase density, p_a is the amorphous phase density, and V_c is the volume fraction crystallinity. Thus, the integrated scattering intensity depends only on the density of the two phases, and the amount of each phase. The density of the amorphous phase is known to increase upon drawing, while the opposite is true for the crystalline phase (Adams et al., 1985; Chuah et al., 1983). Moreover, crystallinity initially decreases and subsequently increases with extrusion draw ratio (Adams et al., 1985). Both of these effects

would significantly reduce SAXS intensity with draw ratio, at high strains.

To determine if changes in the density difference between the crystalline and noncrystalline phases were responsible for the loss of SAXS peak intensity, highly drawn UHMWPE was heated and analyzed by SAXS (Furuhata et al., 1986). Since the amorphous phase expands much more than the crystalline phase, the SAXS peak should have reappeared (i.e. the integrated scattered intensity should have increased). Furuhata et al. observed no such behavior. It is conceivable that the amorphous layers between lamellae strained inhomogeneously, reflecting local stress concentrations. This would give rise to long period polydispersity, which would broaden the SAXS peak and reduce the maximum intensity of the long period reflection, as well as change the position of the peak depending on long period distribution (Wang and Harrison, 1980). One other possibility involves a randomization of the placement of chain folds (via chain slip and crystal shear) to the extent that highly deformed regions can no longer be characterized by a long period (Beresford and Bevan, 1963). Such a reduction in the amount of periodic material would further reduce peak intensity.

The multitude of explanations for the disappearance of a long period peak illustrates a major weakness of scattering experiments, namely morphological models derived from scattering data are nonunique. Electron microscopy, on the other hand, yields unique detailed information. Indeed, diffracting crystallites along can be viewed (by darkfield TEM), elucidating the evolution of microstructure with draw.

Experimental

SSE/PD samples were obtained from Dr. T. Kanamoto for the present set of experiments. The SSE/PD techniques have been described elsewhere (Kanamoto et al., 1983a and 1979; Perkins and Porter, 1977; Zachariades and Porter, 1981). The specific samples used here were formed from single crystals of ultrahigh molecular weight polyethylene (Hizex Million 240M, $M_v = 1.5 \times 10^6$). Kanamoto grew these crystals under nitrogen for 20 hours at 85 °C from a 0.2 % (w/w) xylene solution, containing 0.5 % (w/w polymer) (2,6-di-t-butyl-p-cresol) as an anti-oxidant. The single crystal supsension was cooled to room temperature, filtered slowly, dried at room temperature, and then extracted with acetone, and dried for 20 hours at 60 °C. The mat was then solid state coextruded to a draw ratio of six at 110 °C and subsequently post-drawn at 125 °C to total draw ratios as high as 250. Polyethylene drawn to draw ratios of 97 and 250 displayed tensile moduli exceeding 175 GPa and strengths exceeding 3 GPa (T. Kanamoto, private communication).

For TEM studies, thin sections were removed from the bulk materials obtained from T. Kanamoto. This was accomplished by etching the films in fuming nitric acid at ca. 80 °C for 6 hrs. The films were rinsed in distilled water and then soaked in fresh distilled water overnight (15 hrs.). The samples were then rinsed once again with fresh water, and subsequently dried in a vacuum oven. Pieces of these films were detached from these samples using standard detachment replication techniques. Specifically, a 5.0 % (w/w) solution of polyacrylic acid

(PAA, M_w = 450,000) in water was placed on a glass slide. The glass slide had been cleaned and then "pretreated" by rubbing with a lint-free cloth onto which one drop of glycerol had been placed. The surface treatment with glycerol enabled the PAA to be removed from the glass slide at a later stage. Nine drops of PAA solution were placed on the glass slide with a disposable pipette, avoiding the introduction of air bubbles whenever possible. The previously prepared polyethylene films were cut into very thin strips (ca. 1 mm wide) and laid on top of the wet PAA, taking care that the film made good surface contact with the PAA. Alternatively, the PAA can be air-dried for one hour (until it becomes tacky) before placing the films onto its surface.

After air-drying for at least 24 hours, the polyethylene strips were removed from the PAA surface, and a thin carbon coating was evaporated onto the PAA surface. The areas of PAA where no polyethylene strips had been placed were then trimmed off of the replica with a sharp razor blade. The areas potentially containing polyethylene remnants were scraped off of the glass slide and then cut into ca. 2 mm square pieces. These pieces were floated onto the surface of distilled water, making sure that the PAA side was in contact with the water. To dissolve the PAA film, the samples were left floating in water for at least 6 hrs. (Longer times may be required, depending on PAA film thickness. After 6 hours, residual PAA was still present in films. Therefore, it is recommended that the samples be floated for 12 - 24 hrs.) The remaining carbon film and polyethylene remnants were then

picked up from the water surface with copper grids, dried in a vacuum oven, and viewed by TEM.

The best TEM contrast was obtained in darkfield mode, as these materials were highly crystalline, and residual PAA could be excluded from the image. The (110) + (200) + (210) + (020) reflections were used. Crystal sizes determined by darkfield TEM were taken as lower bounds, since slight bending out of the Bragg condition (by as little as a couple of degrees), or degradation of defective crystalline regions by nitric acid would keep such crystalline regions from being imaged in darkfield mode.

Results and Discussion

The following addresses the evolution of morphology with SSE/PD for draw ratios ranging from 6 to 250. Special attention was given to the identification of those structural elements likely responsible for the ultrahigh modulus of these samples.

Solid state extrusion of UHMWPE single crystal mats to an extrusion draw ration of 6 led to a morphology consisting of diffracting lamellae stacked along the chain direction (Fig. 6.1, regions A). Typically, the lamellae consisted of only a few laterally coalesced mosaic blocks, the mosaic blocks being ca. 20 nm thick (parallel to the chain axis) and wide. In some cases, still thicker lamellae (ca. 37 nm) were seen (Fig. 6.2A, region A), although mosaic blocks of 20 nm thickness were present nearby. The lamellae in Fig. 6.2 appeared to be

Figure 6.1

Darkfield micrograph of solid state extruded UHMWPE, draw ratio of 6, showing lamellar stacks. A mosaic block can be seen breaking away from the uppermost stack. Chain axis vertical.


A
A
A
DR6
200nm

Figure 6.2

Darkfield micrograph of solid state extruded UHMWPE, draw ratio of 6, showing A) lamellar stacks and B) defective regions between mosaic blocks. Chain axis vertical.

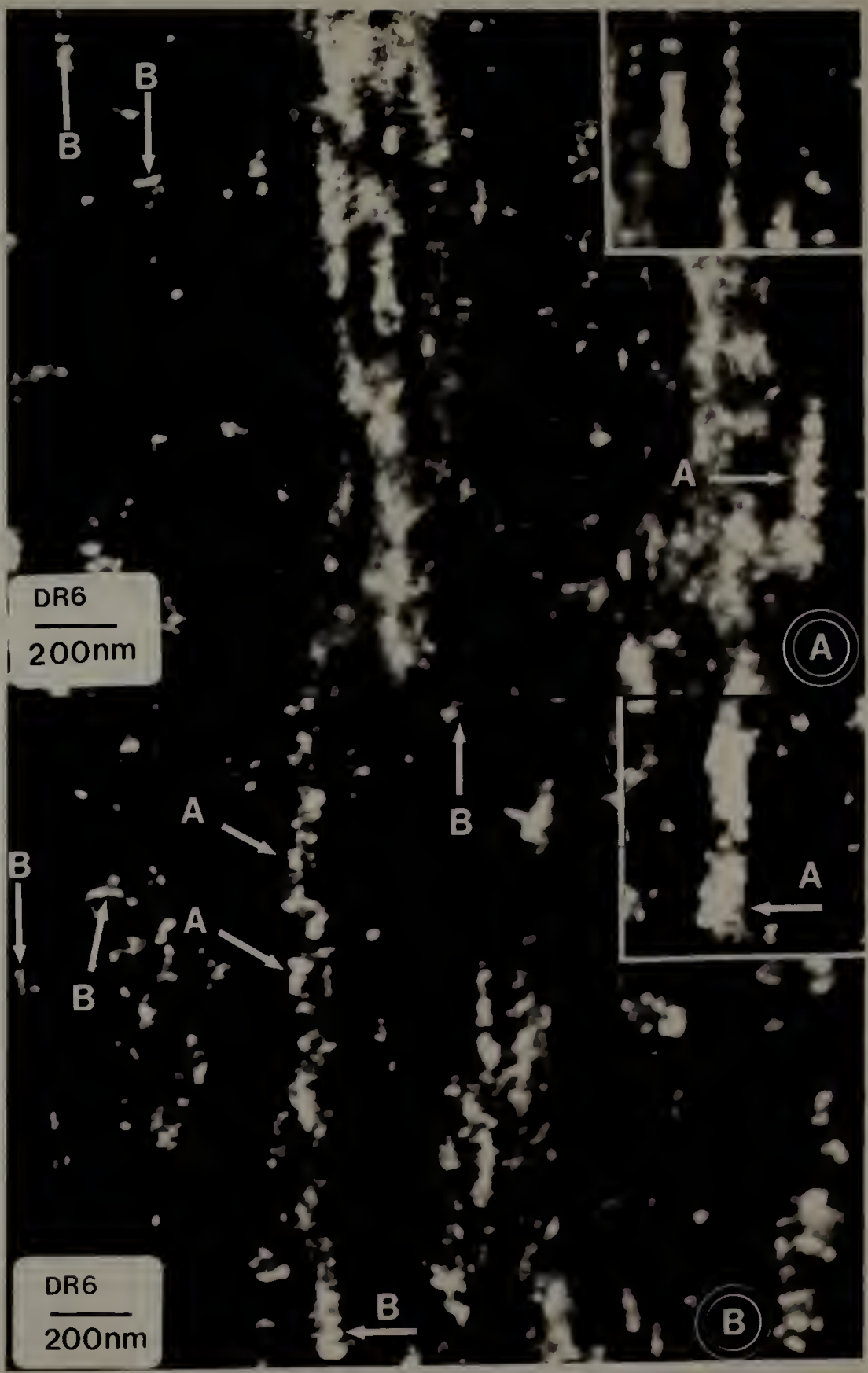
B
B
B
A
DR6
200nm
A
A
B
B
A
B
A
B
DR6
200nm
B
B

largely disrupted by applied stresses, leaving behind numerous mosaic blocks with a wide distribution of sizes. Regions A consisted of vestiges of lamellar stacks.

The fact that stacks of lamellae were simultaneously diffracting indicated that they were in crystallographic registry. It is improbable that this would occur unless crystalline bridges were interconnecting the lamellae. This indicated that a shish-kebab morphology was present at a draw ratio of 6, and that some strain-induced crystallization had accompanied the SSE of single crystal mats. Upon extrusion, these single crystals are believed to have developed grain boundaries and a mosaic block substructure. At higher strains, the mosaic blocks sheared apart along the <001> direction. Defective regions between mosaic blocks were discerned (Fig. 6.2, regions B). In addition, mosaic blocks were observed breaking off of lamellae (Fig. 6.1, uppermost region A). Meanwhile, chains in the noncrystalline phase became oriented, extended, and underwent strain-induced crystallization. This latter process led to the formation of crystalline bridges between lamellae. Indeed, the previously cited reduction and subsequent increase in average crystal thickness (along the chain direction) and crystallinity with draw can be explained in terms of differing degrees of decrystallization and strain-induced (re)crystallization.

Likewise, material drawn to a draw ratio of 42 was comprised of very large crystalline regions which displayed a lamellar morphology (Fig. 6.3, regions A). When deformed, these lamellae exhibited a mosaic block substructure (region B). These films appeared to be very fibrous.

Figure 6.3

Darkfield micrograph of SSE/PD UHMWPE, draw ratio of 42, showing large crystalline regions composed of lamellae (A), and mosaic block substructure (B). Chain axis vertical.

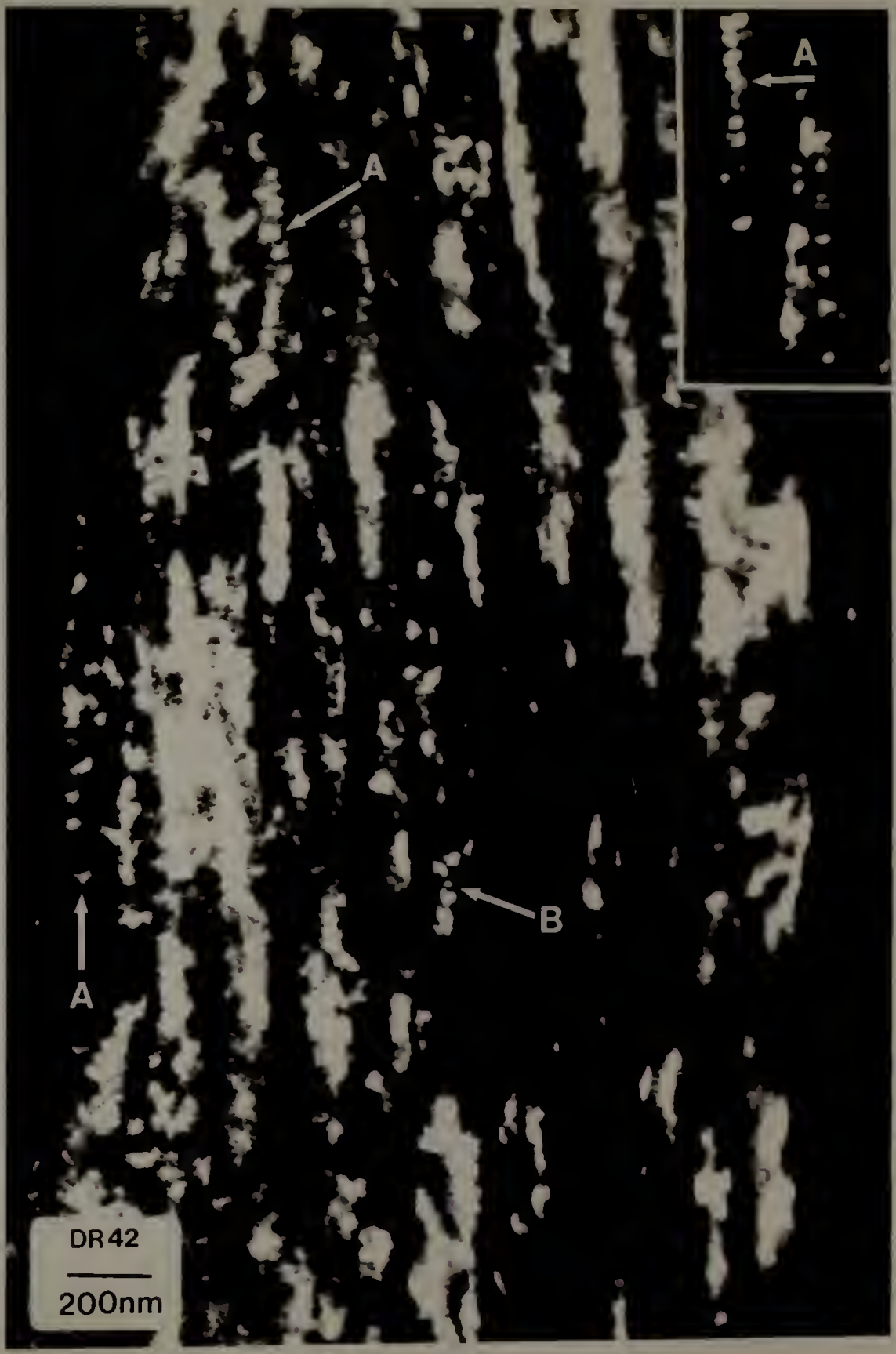
A
A
A
B
DR42
200nm

The increase in fibrous nature with draw was detected during the preparation of detachment replicas, as the material drawn to a draw ratio of 250 fibrillated readily while that drawn to a draw ratio of 6 did not. In Fig. 6.4A, the conversion of lamellae, interconnected by crystalline bridges (region A), to a series of mosaic blocks (region B) and subsequently to highly crystalline fibrils (protofibrils) which were $\leqslant$ 10 nm wide (regions C), was seen. Close scrutiny of the protofibrils indicated that they were composed of a series arrangement of crystalline blocks of ca. 8 nm thickness.

The formation of protofibrils is depicted in Fig. 6.5. Decrystallization occurred by the same mechanisms as indicated in Chapter 5 (Fig. 5.10): <001> crystal shear and chain slip (chain unfolding and pullout), which reduced the lateral crystal width, as well as defect generation, which reduced crystal thickness. Moreover, strain-induced crystallization accompanied protofibril formation, as evidenced by the fact that protofibrils were in crystallographic registry for hundreds of nanometers. Fig. 6.5 illustrates the two types of kebab top surfaces present in protofibrils. Those surfaces which arose from defect generation within crystals were of a fringed micellar type to the extent that chains at the surfaces were not folded, while the original kebab surfaces retained chain folds. This suggests that protofibrils formed from originally thicker single crystals would have fewer folded chain surface "defects". Note the similarity between the protofibril model and the shish-kebab model of Grubb and Keller (1978) (Fig. 5.2). The main difference is that the protofibrils have been

Figure 6.4

Darkfield micrograph of SSE/PD UHMWPE, draw ratio of 42, showing A) lamellae interconnected by crystalline bridges (A), series of mosaic blocks (B), and protofibrils (C); and B) microstructure of SSE/PD UHMWPE not exposed to nitric acid. Chain axis vertical.

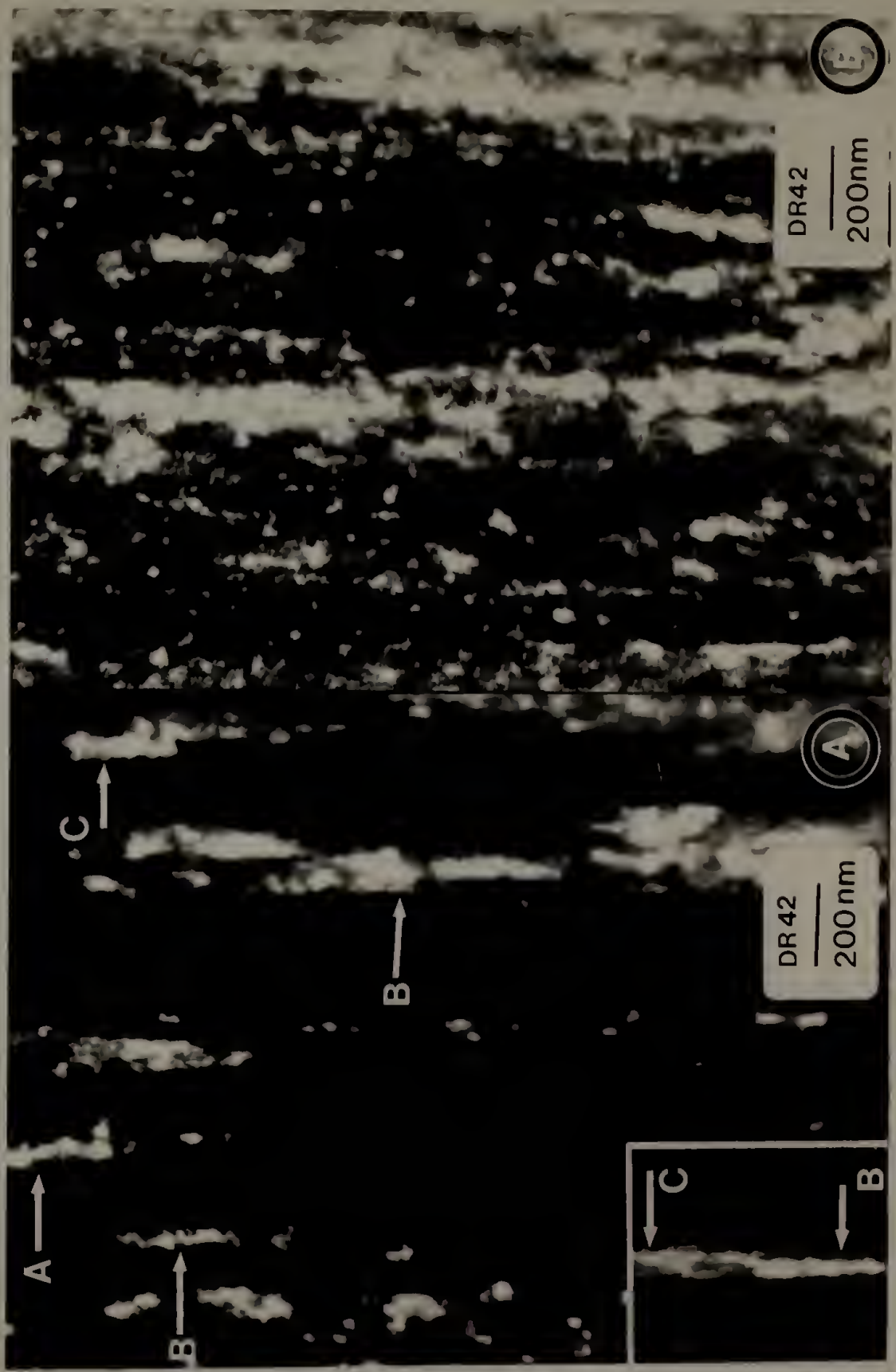
A
B
C
B
C
DR42
200nm
A
DR42
200nm
B
C
B

Figure 6.5

Schematic of protofibril formation via decrystallization and strain-induced (re)crystallization. Chain axis and elongation direction vertical.

Protofibril Formation

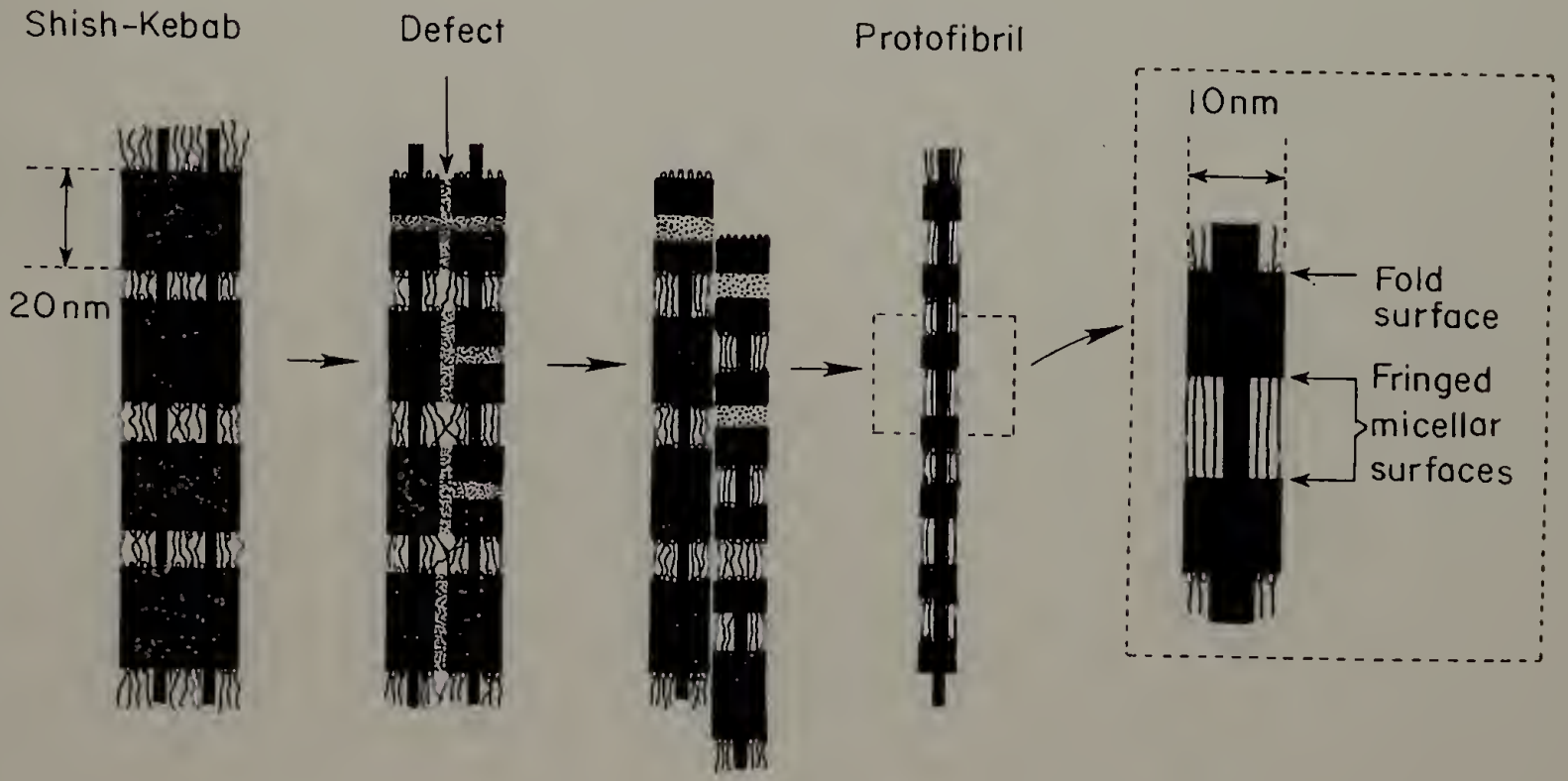

drawn to the extent that they are almost all shish core, kebabs appearing only slightly wider than the crystalline bridges interconnecting them. These similarities suggest that shish-kebabs are formed during solid state deformation by the same yielding and the associated decrystallization and strain-induced crystallization processes which brought about protofibril formation.

The formation of protofibrils in ultrahigh tensile modulus polyethylene is consistent with the Peterlin model of deformation (Peterlin, 1971) in which the increase in tensile modulus with draw ratio at high strains can be explained in terms of an increase in the number of taut tie molecules, which in turn are formed by decreasing microfibril diameter through shear and chain slip. In the present case, such shear (decrystallization) processes led to protofibril formation.

To ascertain that the observed morphology was not an artifact of nitric acid etching, samples which had not been exposed to nitric acid were viewed. The conversion of lamellae to their mosaic block components and the decrystallization of these blocks led to a broad distribution of crystal thicknesses (Fig. 6.4B). Exposure to nitric acid apparently had little effect on the crystalline phase microstructure.

At a draw ratio of 97, SSE/PD polyethylene displayed crystalline bridges interconnecting long crystalline regions (Fig. 6.6, regions A). In addition, protofibrils up to hundreds of nanometers long had formed (Fig. 6.6, regions B). The variation in the diameter of an individual protofibril was clearly depicted. Indeed, lamellae were converted to

Figure 6.6

Darkfield micrograph of SSE/PD UHMWPE, draw ratio of 97, showing long crystalline regions interconnected by crystalline bridges (A), and protofibrils (B). Chain axis vertical.

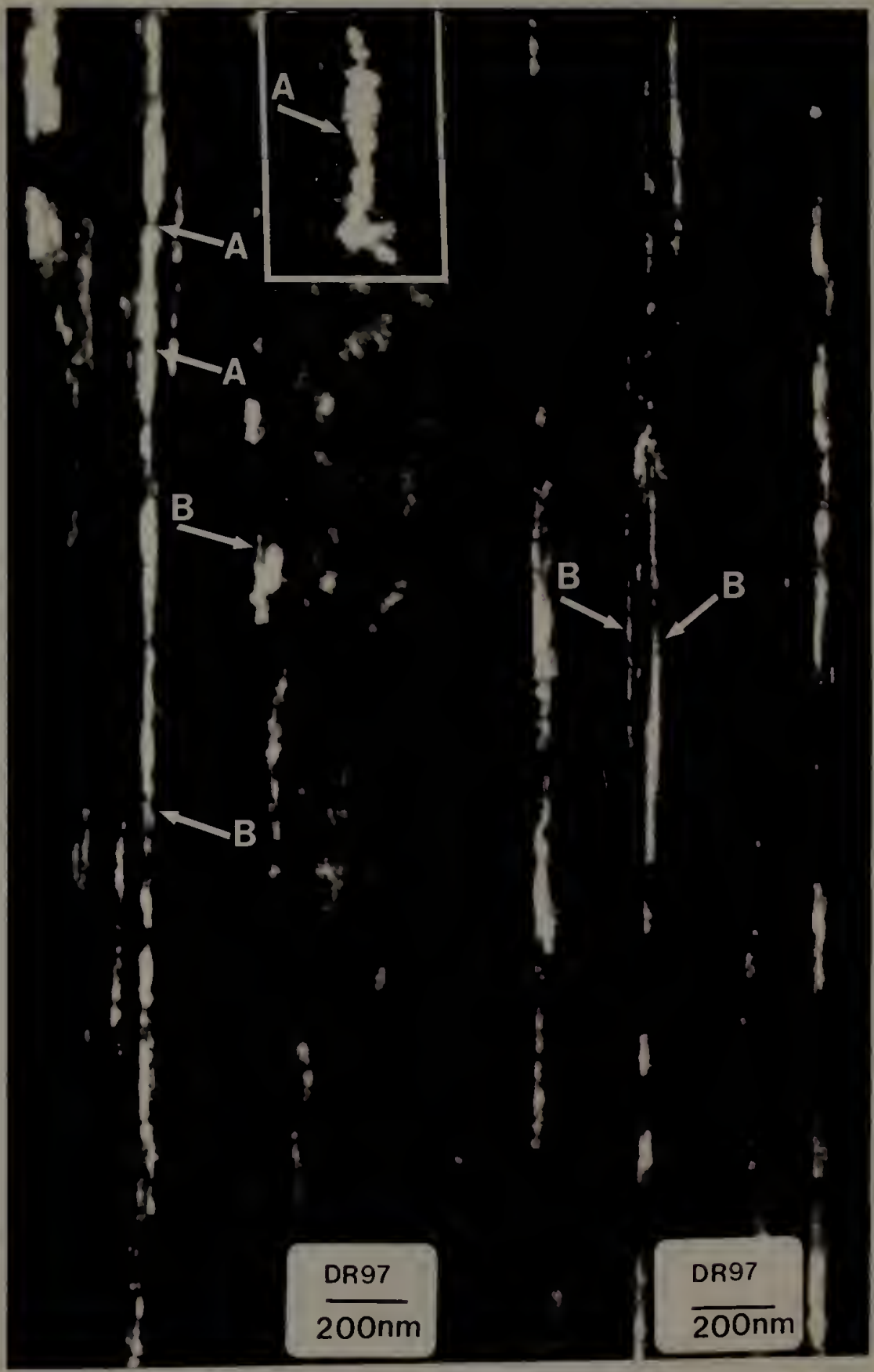
A
A
A
B
B
B
B
DR97
200nm
DR97
200nm

mosaic blocks which subsequently decrystallized and fed into protofibrils (Fig. 6.7, regions A). Occasionally, the protofibrils laterally coalesced, forming wider crystalline regions (Fig. 6.7A, regions B). This coalescence is particularly important, since the simultaneous diffraction of adjacent protofibrils suggests that they may be coupled by lateral crystal/crystal junction points.

Though not readily apparent, the observation of protofibril coalescence implied that the thick crystalline regions shown in Fig. 6.7B (regions B) were composed of protofibrils. This was in contrast to material drawn to a draw ratio of 6, where crystalline regions were comprised of lamellae (interconnected by bridges) of greater width than thickness. Here, the lamellae themselves had been transformed into crystalline bridges (protofibrils), which were thick (along the chain direction), but not very wide.

Observations at a draw ratio of 250 further indicated the formation of protofibrils (Figs. 6.8 and 6.9, regions A), as well as the generation of large crystalline regions (up to 3 microns long along the chain direction) composed of coalesced protofibrils rather than lamellae (Figs. 6.8 and 6.9, regions B). In fact, at this draw ratio, discrete lamellar regions were no longer present. This concurred with previous reports that the crystallite microstructure of ultradrawn polyethylene bore little resemblance to the precursor morphology (Smith and Lemstra, 1980; Capaccio et al., 1979). The shish-kebab-like nature of these protofibrils was particularly evident (Fig. 6.8, region C). Moreover, protofibrils bridged discontinuities in long crystalline regions (Fig.

Figure 6.7

Darkfield micrograph of SSE/PD UHMWPE, draw ratio of 97, showing mosaic blocks being drawn into protofibrils (A), and laterally coalesced protofibrils as well as wide crystalline regions (B). The inset indicates that lamellae are still present. Chain axis vertical.


A
200nm
B
A
B
B
B
B
B
B
B
A
A
A
A
DR97
200nm
A
B
DR97
200nm

Figure 6.8

Darkfield micrograph of SSE/PD UHMWPE of draw ratio 250, showing protofibrils (A), large crystalline regions comprised of protofibrils (B), shish-kebab-like protofibrils (C), and protofibrils interconnecting large crystalline regions (D). Chain axis vertical.

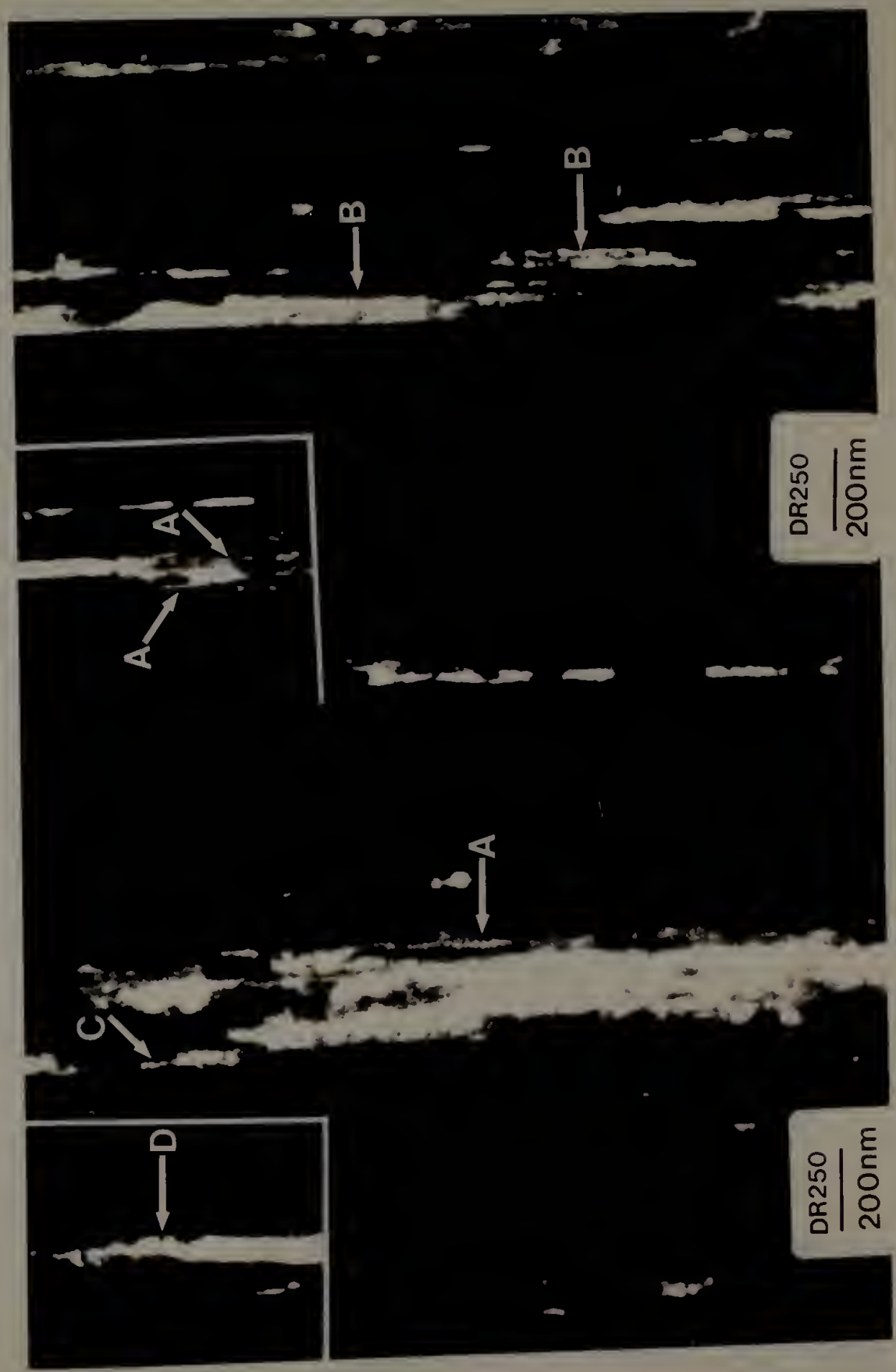
B
B
A'
A
DR250
200nm
A
C
D
DR250
200nm

Figure 6.9

Darkfield micrograph of SSE/PD UHMWPE of draw ratio 250, showing protofibrils (A) and large crystalline regions comprised of protofibrils (B). Chain axis vertical.

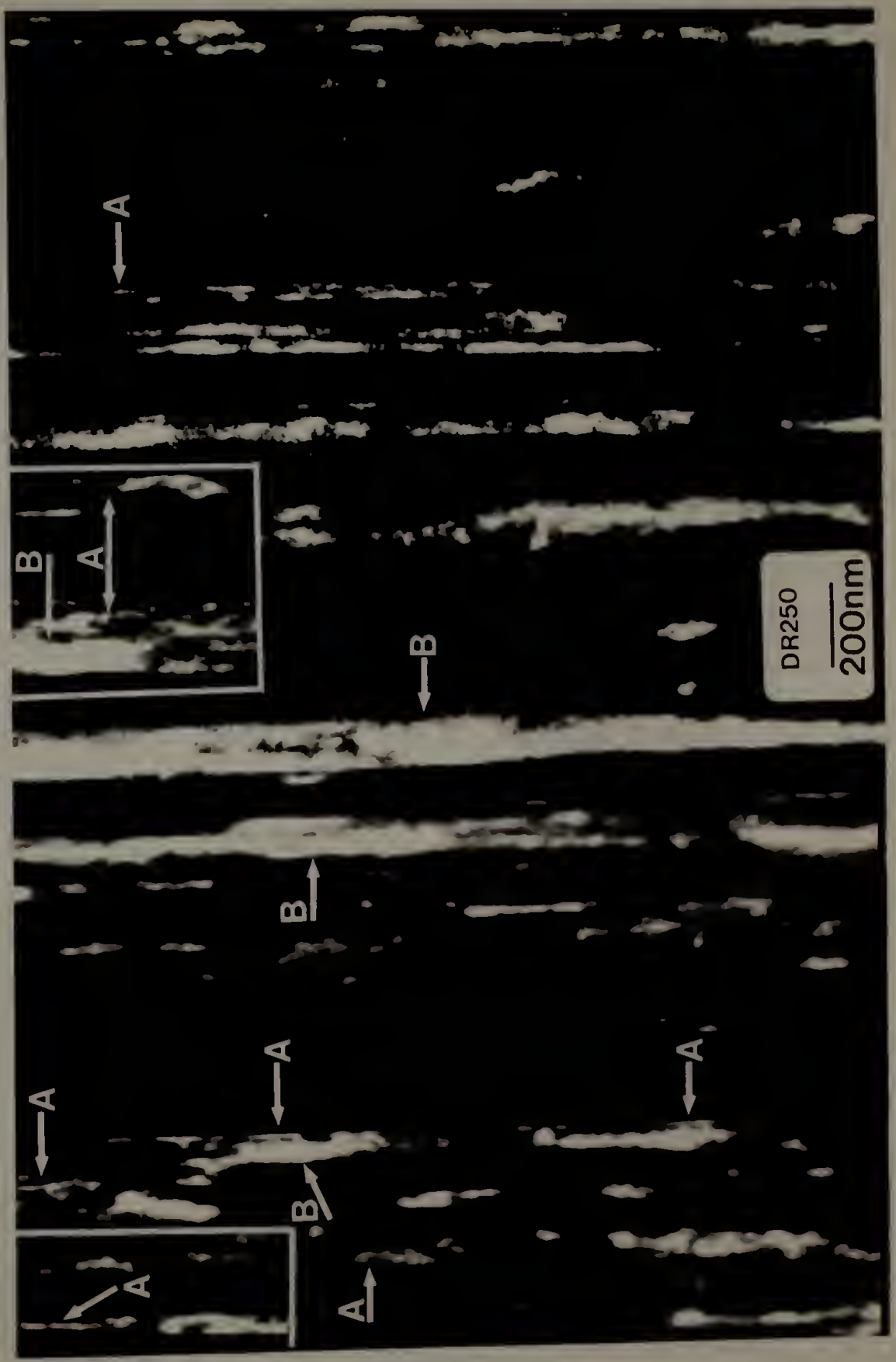
A
A
B
A
A
B
A
B
A
B
A
DR250
200nm

6.8, region D). Observations of samples not subjected to nitric acid etching concurred with these findings. For example, Fig. 6.10 displayed individual protofibrils (regions A) as well as coalesced protofibrils (regions B). The overall morphology was fibrous (region C).

Electron diffraction data on these samples indicated a high degree of chain axis orientation in the crystalline phase at all draw ratios (Fig. 6.11). A comparison of the azimuthal arcing of equatorial reflections indicated that crystalline phase orientation increased with draw. Moreover, the 2θ breadth of the crystalline equatorial reflections increased with increasing draw ratio, indicating that deformation brought about a reduction in the average crystallite size and/or perfection perpendicular to the chain axis.

To summarize, the observations made here, coupled with the mechanical and morphological characterization data of others strongly support the formation of a sample-spanning crystalline phase in ultradrawn (SSE/PD) single crystal mats. The SSE process brought about decrystallization of the original single crystal mats, as well as strain-induced crystallization of (extended and highly oriented) chains interconnecting the lamellae. This led to a shish-kebab structure by a draw ratio of 6, as evidenced by the simultaneous diffraction of lamellae within a stack. Such a morphology is well-represented by the structural model of Gibson et al., (1978), in which lamellae within microfibrils are interconnected by crystalline bridges.

At higher draw ratios, the periodic alternation of chain-folded crystals and amorphous phases gave way to the highly crystalline

Figure 6.10

Darkfield micrograph of SSE/PD UHMWPE of draw ratio 250, not exposed to nitric acid. Note protofibrils (A), coalesced protofibrils (B), and fibrillar morphology (C). Chain axis vertical.

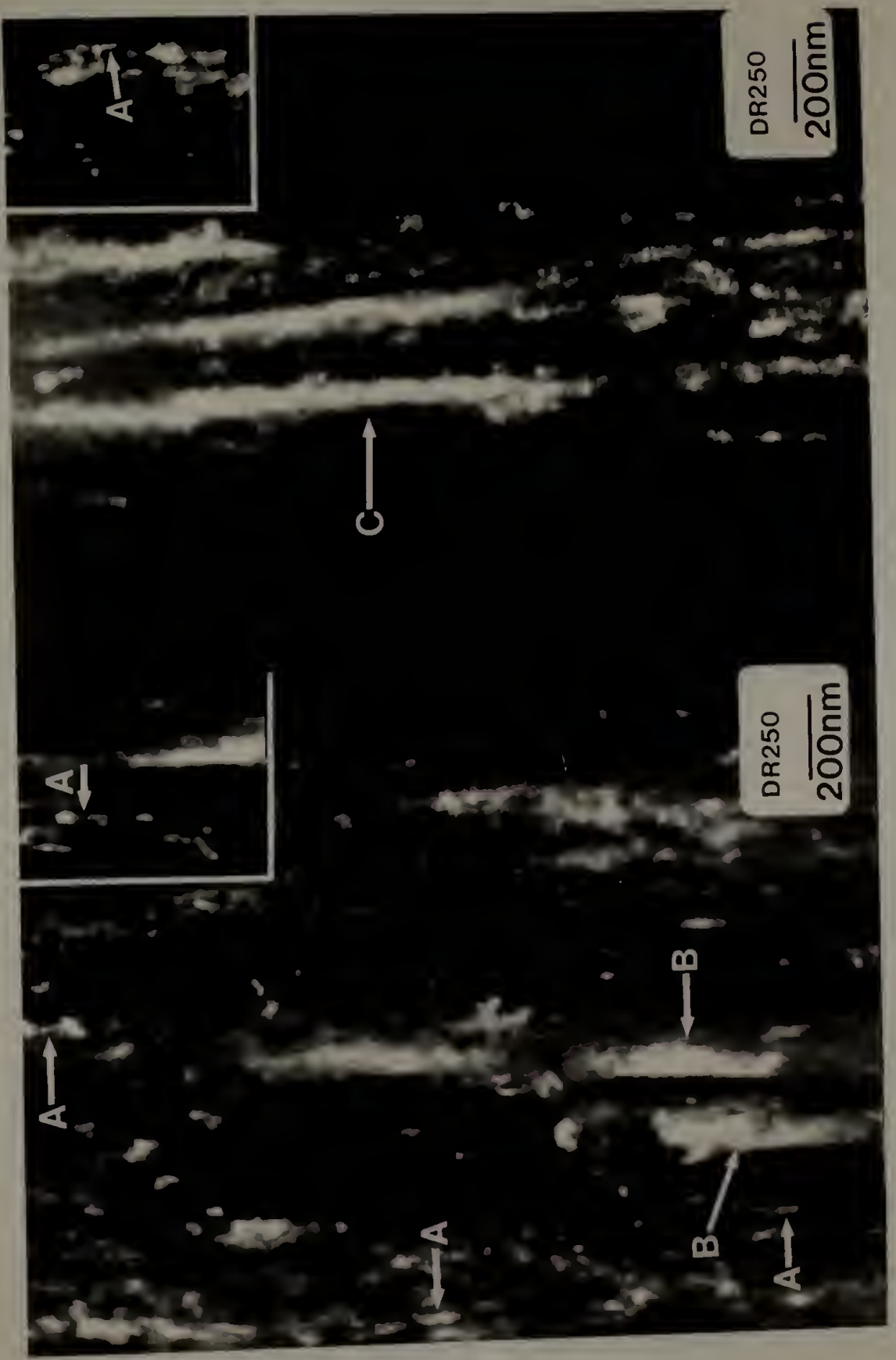
A
A
A
A
A
B
B
C
DR250
200nm
DR250
200nm

Figure 6.11

Electron diffraction patterns taken with beam perpendicular to chain axis of UHMWPE solid state extruded to A) a draw ratio of 6, and B) a draw ratio of 250. Each diffraction pattern is shown at two different exposures. Chain axis vertical.

DR6
DR250
A
B

protofibril morphology. At a draw ratio of 42, protofibrils coexisted with chain-folded lamellae and mosaic blocks, whereas material drawn to a draw ratio of 250 exhibited no lamellae. This explained the known reduction in SAXS long period peak intensity and eventual total disappearance of the peak with draw. In addition, decrystallization and concommitant strain-induced crystallization explained the variation of sample density and crystal thickness with draw, whereby the reduction in density at low extrusion draw ratio most likely corresponded to a loss of crystallinity and crystal perfection during decrystallization (assuming cavitation to be minimized by the hydrostatic pressure accompanying SSE).

The combined use of SSE and PD led to a high degree of chain extension, and increase in crystallinity, and ultimately to an ultrahigh tensile modulus material with a morphology of laterally coalesced protofibrils. Moreover, the simultaneous diffraction of adjacent protofibrils suggested that they were laterally coupled by means of a crystal/crystal contact. Resolution limitations did not allow the nature of this coulpling to be determined in detail. However, the high modulus and strength of these ultradrawn materials supports the existence of such interconnections which would efficiently transfer stress between protofibrils and impart continuity to the crystalline phase.

Conclusions

The evolution of morphology with draw was shown for ultrahigh molecular weight polyethylene single crystal mats which were solid state extruded to a draw ratio of 6 and post-drawn to draw ratios as high as 250 at elevated temperatures. Crystalline regions as extensive as 3 microns (along the chain direction) were observed at high draw ratios ($\geq$ 97) by darkfield TEM. In view of the fact that darkfield microscopy gives only a lower bound of crystal size, and taking into consideration the fact that these ultradrawn samples have previously been shown to exhibit tensile moduli of $\geq$ 175 GPa and strengths of $\geq$ 3 GPa at room temperature, and weight average crystallinities of ca. 90 %, one can conclude that a continuous (sample-spanning) crystalline phase was indeed present. Moreover, the morphology of the extensive crystalline regions seen here indicated that such a continuous crystalline phase is composed of laterally coalesced "protofibrils". The fact that adjacent protofibrils were shown to simultaneously diffract implied that they were laterally coupled at crystal/crystal junction points. This is significant in that it indicates that the protofibrils themselves need not necessarily be sample-spanning for a continuous crystalline phase to form.

Protofibrils were identified as long, highly crystalline morphological elements. Each protofibril was typically hundreds of nanometers long and consisted of a series arrangement of ca. 8 nm thick crystalline blocks interconnected by crystalline bridges. Protofibrils

formed via decrystallization and strain-induced (re)crystallization processes. The decrystallization process was equivalent to that outlined in Chapter 5 and summarized in Fig. 5.10. Lamellae were reduced to their mosaic block components, which sheared apart along the <001> direction. Mosaic block thickness was reduced to less that 10 nm by defect generation within thicker (20 nm) blocks. These smaller blocks were then drawn into the protofibrils. It is believed that the strain-induced crystallization processes which led to shish-kebab formation upon drawing chain folded crystals to an extrusion draw ratio of 6, were equivalent to those which led to protofibril formation at still higher draw ratios.

It was concluded that the crystalline bridge model of Gibson et al. (1978), is a good representation of material drawn to a draw ratio of ca. 6, but is not applicable of ultradrawn material where no long period is observed by either SAXS or TEM. Instead, ultradrawn material can be represented by a model consisting of the lateral coalescence of protofibrils. This is consistent with the known fibrous nature of ultradrawn material. Previous models of a continuous crystalline phase have not incorporated such a fibrillar substructure.

C H A P T E R VII

THE DEFORMATION OF ORIENTED HIGH DENSITY POLYETHYLENE AT ELEVATED TEMPERATURES: CRAZING AND CONTINUOUS CRYSTAL FORMATION

Abstract

Thin, single crystal-like textured films of HDPE were uniaxially elongated at 56, 93, and 129 °C along the chain direction. In all cases, the initial shish-kebab morphology was transformed via decrystallization processes to a more extended chain microstructure. Shear between shish-kebabs was observed at all temperatures and was identified by a rotation of lamellar normals away from the elongation direction. Crazes nucleated at all temperatures, but only propagated at temperatures above the alpha transition temperature (93, 129 °C), where the yield stress was low and chain mobility in the crystalline phase was high. Indeed, shish-kebabs elongated within crazed regions and were drawn into microfibrils (craze fibrils) via the surface drawing of kebabs, which decrystallized by <001> crystal shear, chain slip, and defect generation. At temperatures below the alpha loss temperature, sample elongation was much more uniform, and was accompanied by large scale fibrillation.

The evolution of the crystalline phase during deformation was imaged in detail by darkfield TEM. This technique proved particularly

useful when observing HDPE deformed above the alpha transition temperature, in which the noncrystalline phase underwent strain-induced crystallization. Long ($\geq$ 3 micron), thin crystalline fibrils of ca. 7 nm diameter, called protofibrils, were observed. Lateral connections between the original kebabs were retained during drawing in many cases, and constituted tie fibrils between adjacent microfibrils. In some cases, neighboring microfibrils laterally coalesced.

The processes which occurred in thin films at temperatures above the alpha transition and which gave rise to long crystals were shown to be analogous to the deformation processes occurring in the bulk (above the alpha transition temperature). Most importantly, they provided insight into the generation of the continuous crystalline phase present in the SSE/PD ultrahigh modulus PE fibers of Chapter 6. In both cases, protofibrils constituted the fundamental microstructural element. Moreover, the fact that microfibrils (precursors of protofibrils) were observed to be laterally interconnected by tie fibrils, and in some cases laterally coalesced, supported the conclusions of Chapter 6 that protofibrils were laterally interconnected.

Long crystalline microfibrils did not form in materials elongated at temperatures (25, 56 °C) below the alpha transition temperature, as poor chain mobility (and therefore more chain scission) as well as a more uniform longitudinal strain did not favor strain-induced crystallization. In fact, the dependence of the resultant average crystal thickness and long period on deformation temperature was interpretted in terms of decrystallization, (re)crystallization, and

annealing without invoking a rise in temperature, thermally-induced melting, and recrystallization during deformation. Furthermore, the reduction of crystalline phase yield stress at 56 °C with respect to that at 25 °C was made evident by the extensive shear and lack of mosaic block definition in fibrillated regions. This led to a network structure in which each network fibril was of uniform diameter and contained crystal block remnants.

Introduction

It has been shown that highly drawn polyethylene can exhibit a modulus of up to 220 GPa (Kanamoto et al., 1983a) which is of the same order of magnitude as the theoretical crystalline modulus (along the chain direction, room temperature) variously estimated to be 235 to 340 GPa (Sakurada et al., 1966; Shimanouchi et al., 1962). Mechanically, a material of such high modulus must have the noncrystalline phasein parallel with the crystalline phase, with crystals of high aspect ratio contributing most significantly to reinforcement of the composite material. In the extreme case of highly crystalline ultradrawn materials, one can envision the formation of an essentially single phase crystalline material. In Chapter 6, the existence of such material was shown to be plausible. The present chapter will address those processes which give rise to the formation of a continuous crystalline phase, as well as the optimum temperature range required for its formation.

The high crystallinity and crystalline phase continuity found in ultrahigh modulus PE is a result of extensive strain-induced crystallization. Strain-induced crystallization in polymers has been a topic of research for many years (Peterlin, 1976; Yeh, 1976 a and b; Nagasawa and Shimomura, 1974; Pennings, 1977; Andrews, 1964). As stated above, much of the recent resurgence of interest in this topic derives from its relevance in the production of ultrahigh modulus PE (Pennings and Meihuizen, 1979; Kanamoto et al., 1983a; Smith and Lemstra, 1980; Zachariades et al., 1980). Here too, the strain-induced crystallization of PE will be studied. What will make these studies unique is the method of observation. The conversion of lamellar HDPE to a more chain-extended morphology will be imaged in detail using TEM in both darkfield and brightfield modes.

Since strain-induced crystallization is necessary for the attainment of ultrahigh modulus in PE, it is important to determine the processing conditions which favor it. In the present set of experiments, the effect of temperature on strain-induced crystallization was probed. The temperature dependence of strain-induced crystallization has been previously studied by Andrews (1964). He showed that natural rubber crystallizes at temperatures well below room temperature (-28 °C) when uniaxially strained, the lower the temperature and the higher the strain, the faster the nucleation rate. Evidently, the degree of chain reorganization and alignment required for strain-induced crystallization can be achieved at such temperatures provided the material is well above the glass transition temperature.

Apparently, chain "flow" accompanied deformation, enabling chains to extend and align. This implies that an important prerequisite for strain-induced crystallization is the achievement and retention of chain extension until nucleation and crystallization occur.

Strain-induced crystallization is known to occur at room temperature in PE (Miles et al., 1976; Decandia et al., 1985). In semicrystalline polymers such as polyethylene, the motion of noncrystalline chains is constrained by both entanglements and crystals, much as crosslinks constrain chain motion in a crosslinked rubber. The application of stress perturbs the equilibrium distribution of conformations at a given temperature, making it possible to achieve low energy (trans) conformations even at high temperatures, and resulting in chain orientation and extension. When a sufficient number of chains laterally align, a stable chain-extended crystal nucleus forms and further crystal growth ensues. This results in the formation of an extended chain crystal. However, if molecules disengage from crystals or disentangle and undergo chain relaxation, they will not strain crystallize.

The crystalline phase of strained material is believed to consist of highly aligned fringed micellar crystals (Grubb and Keller, 1978). These crystals are believed to grow in thickness along the elongation direction until they coalesce (along the chain direction) to form very long (several microns) crystals. Such crystals are typically on the order of 10 nm wide. Hoffman (1979) theorized that the size of strain-induced crystals is limited by the stresses which build up in the

crystalline phase, due to repulsion between chains in the amorphous phase. The propensity of a material to undergo strain-induced crystallization, and the resultant crystal perfection varies with the number density of entanglements, crosslinks, branches, or other hindrances to the crystallization process which constitute defects in the crystal lattice. In the present case, HDPE films of low entanglement density were used, as discussed in Chapter 4.

Experimental

HDPE films of the type discussed in Chapter 4 were floated on the surface of water and caught on deformation grids. These grids were then secured to a JEOL model SEH deformation stage. The stage was then inserted into an air oven, and equilibrated to the desired temperature for at least fifteen minutes. Temperatures were considered accurate to within 2 °C. The films were then strained as described in Chapter 5. When the deformation was completed, the materials were allowed to cool for one hour and were then carbon coated (while still strained in the stage) and viewed by TEM. The deformation temperatures used were 56, 93, and 129 °C.

In one additional experiment, the examination of the microstructure of as-drawn film at elevated temperatures was undertaken by using an electron microscope stage (purchased from GATAN of Warrendale, Penn.), heated to 122 °C.

Lastly, it should be noted that great care should be employed while handling as-drawn films to avoid accidental room temperature deformation. This is particularly important since the fibrillation could easily be misinterpreted as a response to the applied deformation at elevated temperatures.

Results

Since deformation at 129 °C constituted an extreme case of high temperature deformation, it will be discussed in detail below. The results from deformation at temperatures of 56 and 93 °C will be interjected where appropriate.

As with deformation at room temperature (Fig. 5.4a), the initial observable stages of deformation at 93 and 129 °C involved cavitation of the noncrystalline phase and craze initiation (Fig. 7.1). At this stage, the films appeared similar to deformed hard elastic fibers (Sprague, 1973; Cannon et al., 1976; Cayrol and Petermann, 1974). This degree of deformation was necessarily accompanied by shish-kebab elongation. Unlike low temperature deformation along the chain direction (25, 56 °C), where shish-kebabs arrested craze growth, high temperatures (93, 129 °C) fostered craze growth and microfibrillation (Fig. 7.2). In fact, when previously-fibrillated films were deformed at high temperatures, the fibrils themselves microfibrillated. It is believed that crazes nucleated in areas of noncrystalline phase weakness, where reinforcement of the noncrystalline phase was poor.

Figure 7.1

Brightfield micrograph of HDPE elongated parallel to the chain axis at 93 °C showing the early stages of crazing. Chain axis vertical.


93°C
500nm

Figure 7.2

Brightfield micrograph of HDPE elongated parallel to the chain axis at 129 °C revealing craze microstructure and shish-kebabs being drawn into microfibrils at A) low magnification showing how shish-kebabs are drawn into microfibrils (white arrows), and B) high magnification showing relatively undeformed lamellae (A), lamellae being surface drawn into microfibrils (B), and strain-induced crystallization in microfibrils (C). Chain axis vertical.

129°C
500nm
A
129°C
200nm
B

Stress concentrations in such flawed areas facilitated noncrystalline phase extension, cavitation, and eventually the decrystallization of nearby crystals. The films deformed very nonuniformly. Crazed (microfibrillated) regions were highly strained while uncrazed regions appeared essentially undeformed. Indeed, relatively undeformed crystals can be seen diffracting in Fig. 7.2b in uncrazed regions (region A) whereas crystallites were deformed at the craze interface as they were drawn into microfibrils (regions B). In some microfibrils, the strain was high enough to bring about strain-induced crystallization (Fig. 7.2B, region C). It is probable that some yielding occurred in uncrazed regions, but to a much lesser extent than in crazed ones. The structure of microfibrillated material is shown schematically in Fig. 7.3. This closely resembled the depiction of crazing in semicrystalline polymers by Friedrich (1983) (Fig. 5.12) except very long crystals formed within crazes in the present case.

Microfibril diameters ($\leqslant$ 10 nm) and lateral separation distances (ca. 15 - 30 nm) were essentially the same as those of shish-kebabs in the undeformed film. This suggested that each microfibril arose from an individual shish-kebab. This was verified by the observation that shish-kebabs in uncrazed regions led directly into microfibrils (Fig. 7.2A, arrows). This same analogy between shish and craze fibril diameters was made for gel-spun fibers of UHMWPE elsewhere (Postema et al., 1987). At high stresses, the original shish-kebabs were transformed into a more chain-extended form, in which the average kebab thickness was reduced from ca. 30 nm to 7 nm (Fig. 7.4) and the extended

Figure 7.3

Schematic of HDPE elongated parallel to the chain axis at 129 °C. Chain axis vertical. Elongation direction (E) as indicated.

DEFORMATION AT 129°C

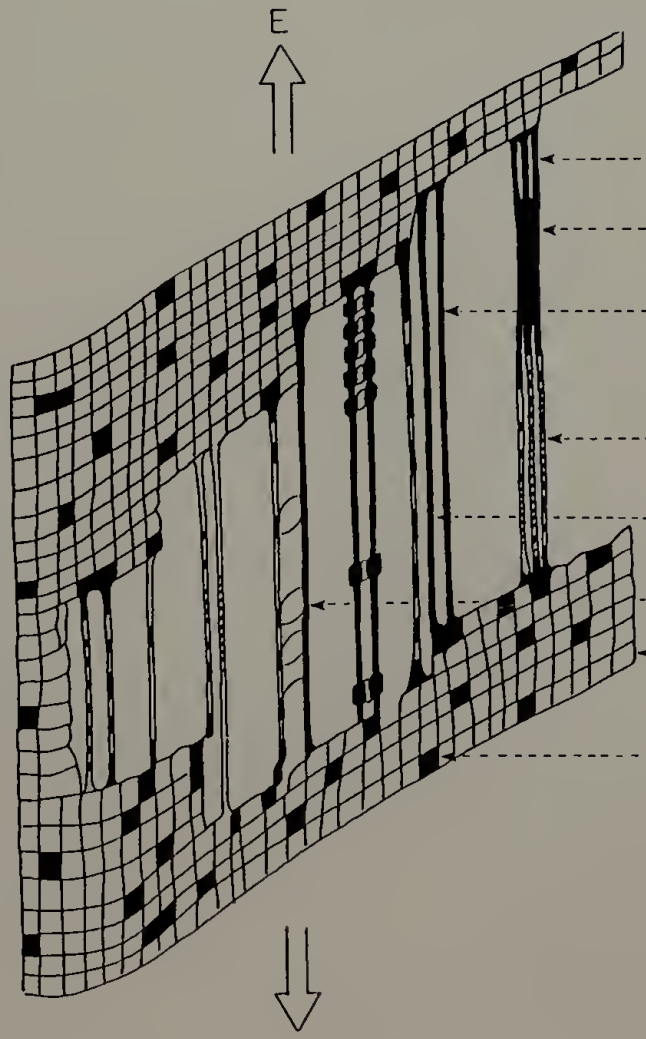

*Microfibril

Coalesced microfibrils

Strain-induced crystallization
(continuous crystal)

Decrystallization

Cavitation

Intermicrofibrillar tie molecules

Sheared mosaic block

Diffracting mosaic block

* Microfibrils: 10nm wide, 15-30nm apart, 2 micron thick crystols, oriented along elongation direction

Figure 7.4

Darkfield micrograph of HDPE elongated parallel to the chain axis at 129 °C showing extensive strain-induced crystallization in crazed regions. Chain axis vertical.

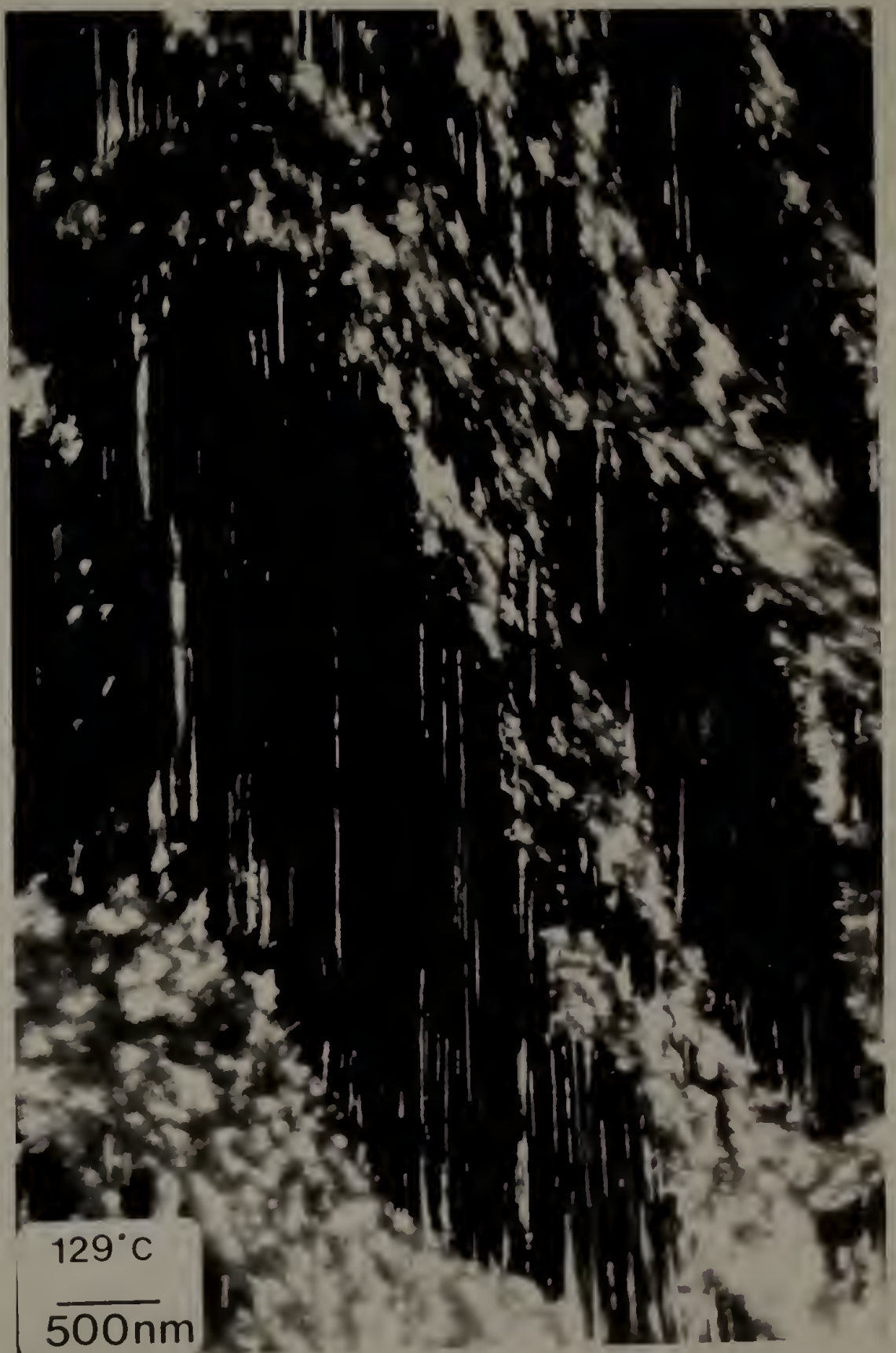
129°C
500nm

chain shish core appeared more prominent. As this latter size borders on the resolution limits of the diffraction constrast darkfield imaging technique used, the kebabs were often difficult to detect. In fact, the elongated shish-kebabs were eventually transformed into crystalline fibrils of essentially uniform diameter. Such long, thin crystalline microfibrils will be henceforth called protofibrils. They are believed to constitute the fundamental structural element in ultradrawn polyethylene.

In many cases, protofibrils appeared by darkfield TEM to be entirely uniform along their length, being single crystals.In other cases, however, protofibrils were shown to be comprised of a series arrangement of very small simultaneously diffracting crystalline blocks, as was previously depicted in Chapter 6 for SSE/PD material (Fig. 6.5). The simultaneous diffraction of all of these blocks suggested that they were interconnected by (unresolvable) crystalline bridges which could have formed by strain-induced crystallization. Furthermore, the presence of similar blocks during decrystallization implied that they were remnants of the original chain-folded kebabs, organized into a fibrillar structure.

Microfibrillation involved the decrystallization and elongation of shish-kebabs. This decrystallization process is shown schematically in Fig. 5.10. Darkfield micrographs provided the most detailed information yet on the decrystallization and drawing of kebabs into shish crystals (Figs. 7.4 - 7.7). The early stages of crystalline phase deformation involved <001> crystal shear from the main kebab block (Figs. 7.5, 7.6,

Figure 7.5

Darkfield micrograph of HDPE elongated parallel to the chain axis at 129 °C showing crystal shear (A), more extensive shear (B), protofibrils (C), defects within crystals (D), and diamond-shaped crystallites (E). Chain axis vertical.


C
C
B
A
B
A
B
C
A
A
D
D
E
129°C
200nm

Figure 7.6

Higher magnification of Fig. 7.4. Darkfield micrograph of HDPE elongated parallel to the chain axis at 129 °C showing crystal shear (A), more extensive shear (B), protofibrils (C), microfibrils which have laterally coalesced (D), and laterally interconnected microfibrils (E). Chain axis vertical.

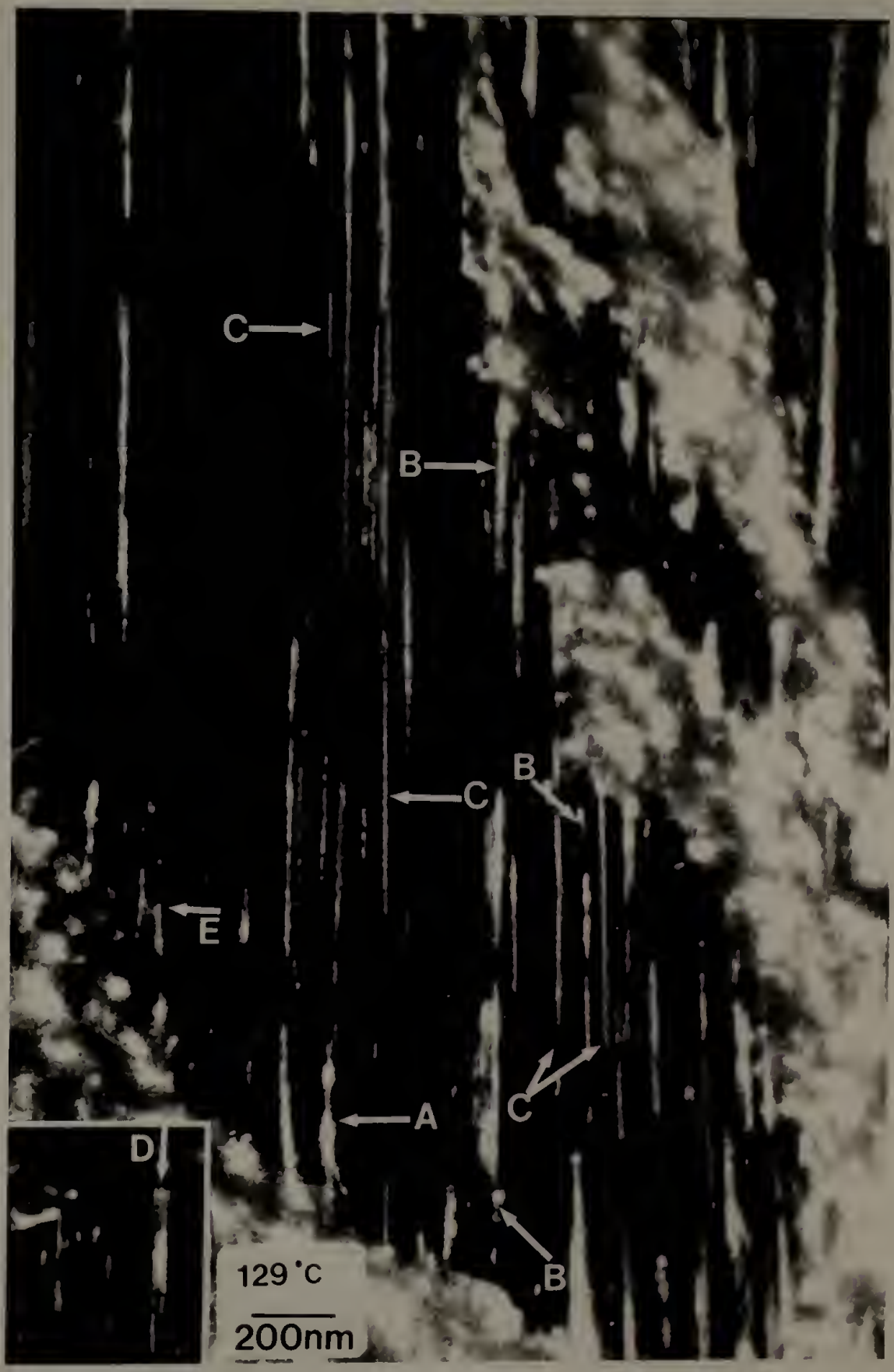
C
B
C
B
E
A
C
B
D
129 °C
200nm

Figure 7.7

Darkfield micrograph of HDPE elongated parallel to the chain axis at 93 °C showing crazing and diamond-shaped kebabs (inset). Chain axis vertical.

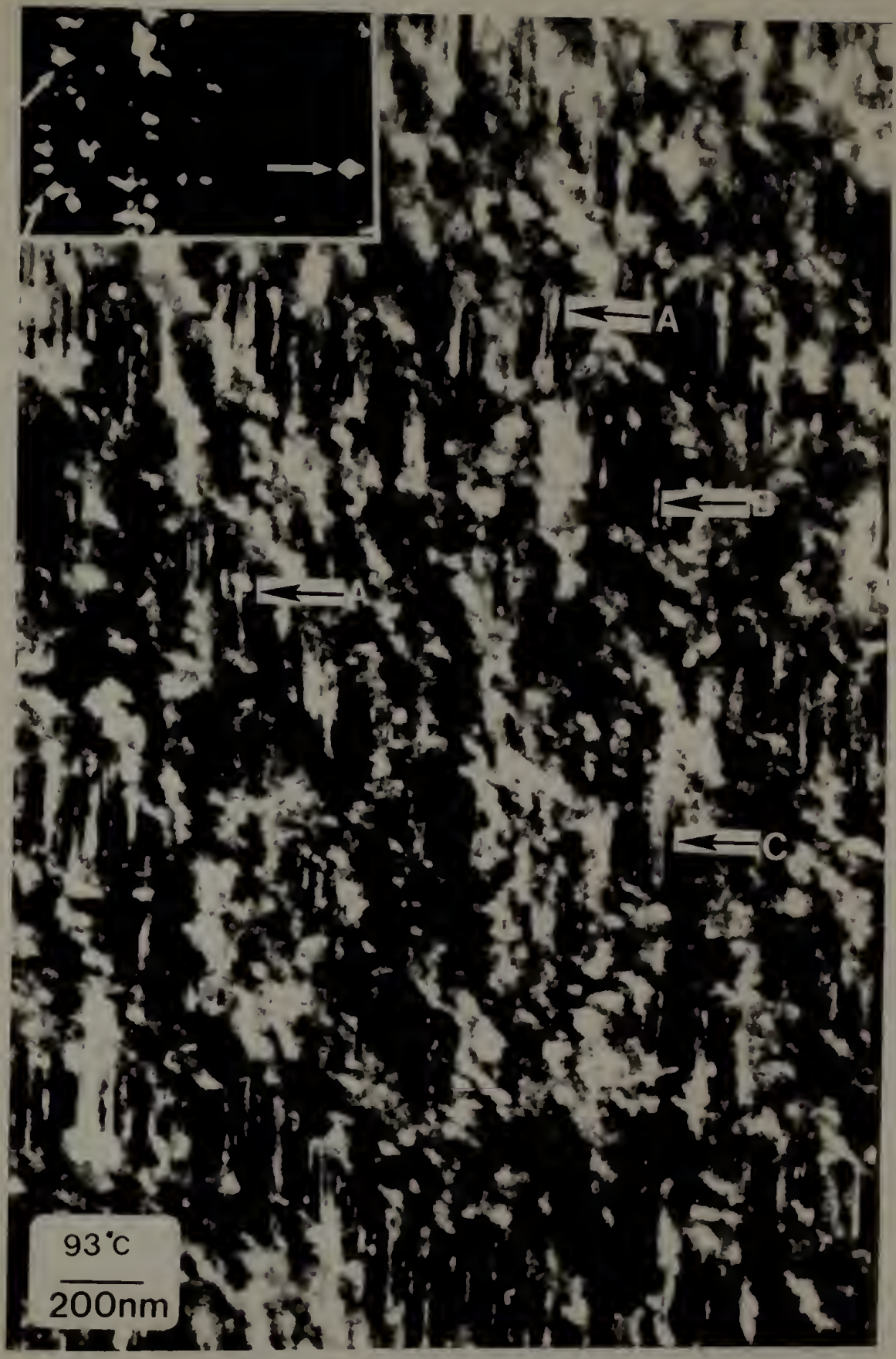
A
A
C
93°C
200nm

regions A). Occasionally, the kebab became diamond-shaped (Fig. 7.5, region E and Fig. 7.7, inset). This was followed by additional shear until the kebab had been transformed into a number of very narrow crystal remnants; positioned sequentially one after another along the draw direction (Figs. 7.5, 7.6, and 7.7, regions B). This gave the appearance of a nonperiodic alternation of crystalline and amorphous phases along the microfibril. Chain-folded kebabs decomposed into mosaic blocks of reduced crystal thickness (along the chain direction) by the generation of defects within crystals (Fig. 7.5, regions D). Strain-induced crystallization subsequently occurred where the noncrystalline phase had become extended and aligned. The final result was the formation of protofibrils in crazed regions (Figs. 7.5, 7.6, and 7.7, regions C). The fact that uncrazed material, which was much less strained than crazed material, did not contain long crystalline regions indicated that protofibril formation involved strain-induced crystallization. In some cases, microfibrils laterally coalesced as well (Fig. 7.6, region D), while in other cases microfibrils appeared to be laterally interconnected with tie fibrils (Fig. 7.6, region E). In brightfield micrographs, protofibrils appeared as faint striations (Fig. 7.8). Darkfield and brightfield micrographs indicated that crystals up to 3 microns long were present in microfibrillated regions (Fig. 7.6, regions C). The reader is again referred to Fig. 7.3 for a summary of the microfibrillar structure.

During microfibrillation, lateral stress (perpendicular to the chain axis) was relieved by cavitation between microfibrils, while

Figure 7.8

Brightfield micrograph of HDPE elongated parallel to the chain axis at 129 °C showing craze microstructure and faint striations corresponding to protofibrils at A) low magnification and B) high magnification. Chain axis vertical.

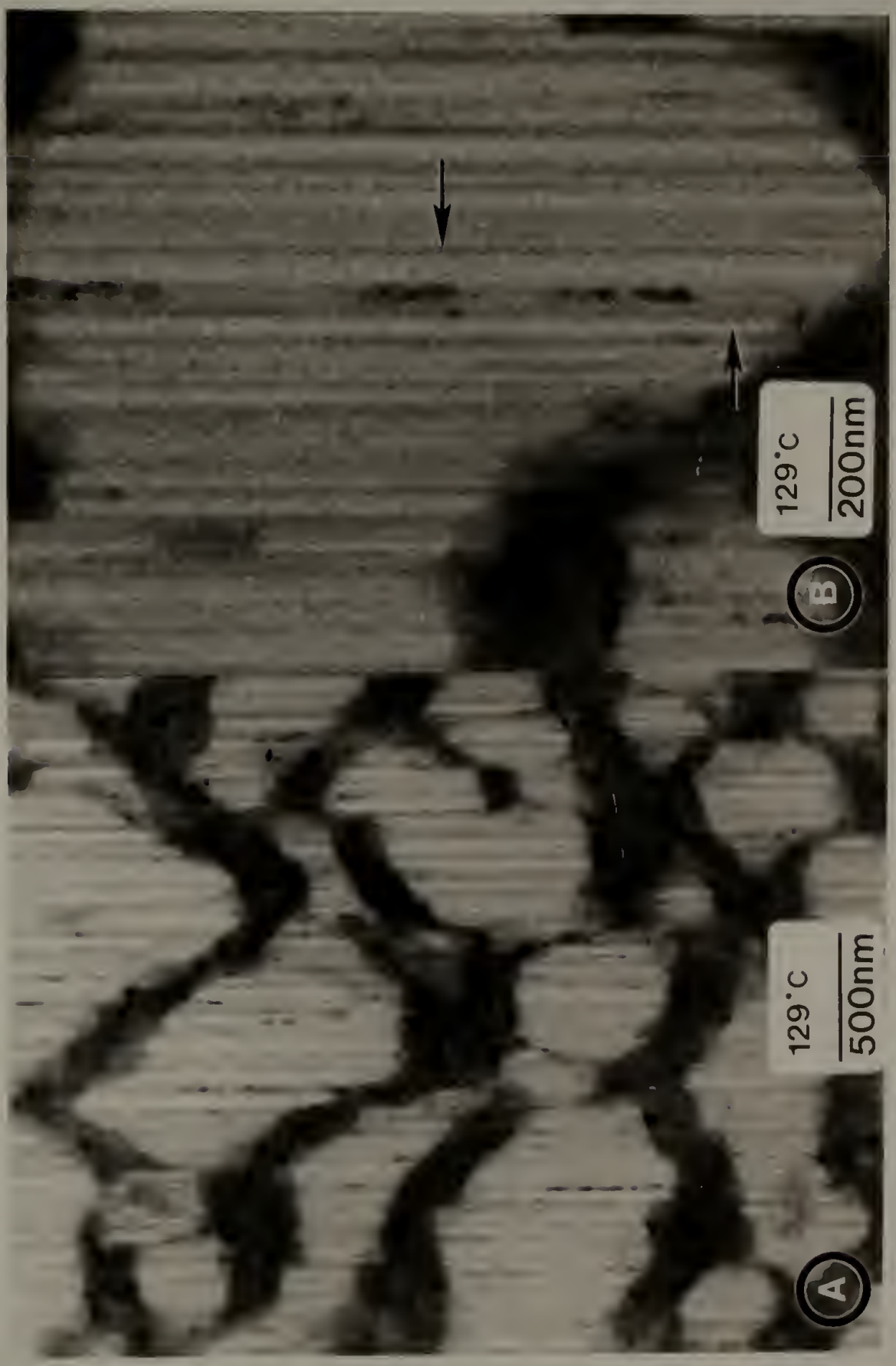
A
129°C
500nm
B
129°C
200nm

longitudinal stress (parallel to the chain axis) was relieved by shish-kebab elongation. The nonuniform extension of shish-kebabs in crazed regions resulted in a significant amount of shear between neighboring shish-kebabs in uncrazed regions. This was detected by the rotation of lamellar normals away from the elongation direction (Fig. 7.2), in a manner seen previously (Fig. 5.9). This resulted in a jagged craze interface which had an overall wavy nature, forming an angle ranging from ca. 30 to 90 degrees with the elongation direction (Fig. 7.8b). Lamellae laid along the craze interface while shish-kebabs retained their initial orientation, the chain axis remaining parallel to the elongation direction. Shish-kebabs constituted lateral borders between crazed and uncrazed material, and reduced the "sharpness" of craze tips (Figs. 7.2 and 7.8).

The deformation of HDPE at 93 °C paralleled that at 129 °C (Fig. 7.7). In both cases the material microfibrillated and formed long crystalline regions. It is believed that the major difference in deformation at these two temperatures involves the level of draw stress during microfibrillation.

Deformation at 56 °C resembled that discussed in Chapter 5 in room temperature studies. Elongation along the chain direction occurred globally throughout the film, and the material fibrillated into bundles of shish-kebabs. However, there was significantly more shear and flow at this temperature as a whole than found for room temperature deformation. This resulted in a network-like appearance. Individual crystal blocks were relatively undefined, and the interface between

highly deformed and slightly deformed material was quite diffuse (Fig. 7.9). Each fibril in the network was of approximately constant diameter and contained crystal block remnants. The chain mobility at 56 °C was apparently high enough to facilitate crystal shear, but not so high as to effect microfibrillation, significant strain-induced crystallization, protofibril formation, and the generation of extensive crystalline regions.

The fact that evidence of extensive strain-induced crystallization was observed for material deformed at high temperature appears to contradict the known behavior of natural rubber, in which crystal nucleation rates are extremely low at low undercoolings (Andrews, 1964). In this context, it must be emphasized that even though films were deformed at high temperatures, crystallization most probably occurred during and after cooling to room temperature. Therefore, chains had only to extend and remain extended until the sample was cooled, for strain-induced crystallization to occur.

To better understand the high temperature deformation of as-drawn films, these materials were directly viewed by TEM using a microscope stage set at 122 °C. The main microstructural feature observed at this temperature was that the films had lost their lamellar character (Fig. 7.10). In addition, electron diffraction patterns displayed a prominent amorphous halo, indicating that a significant amount of thermally-induced melting had occurred. The diffraction pattern of HDPE at 122 °C (Fig. 7.10, inset) had only one equatorial reflection, which appeared to arise from the merger of the (110) and (200) reflections.

Figure 7.9

Brightfield micrograph of HDPE elongated parallel to the chain axis at 56 °C showing fibrillation and network-like structure. Chain axis vertical.

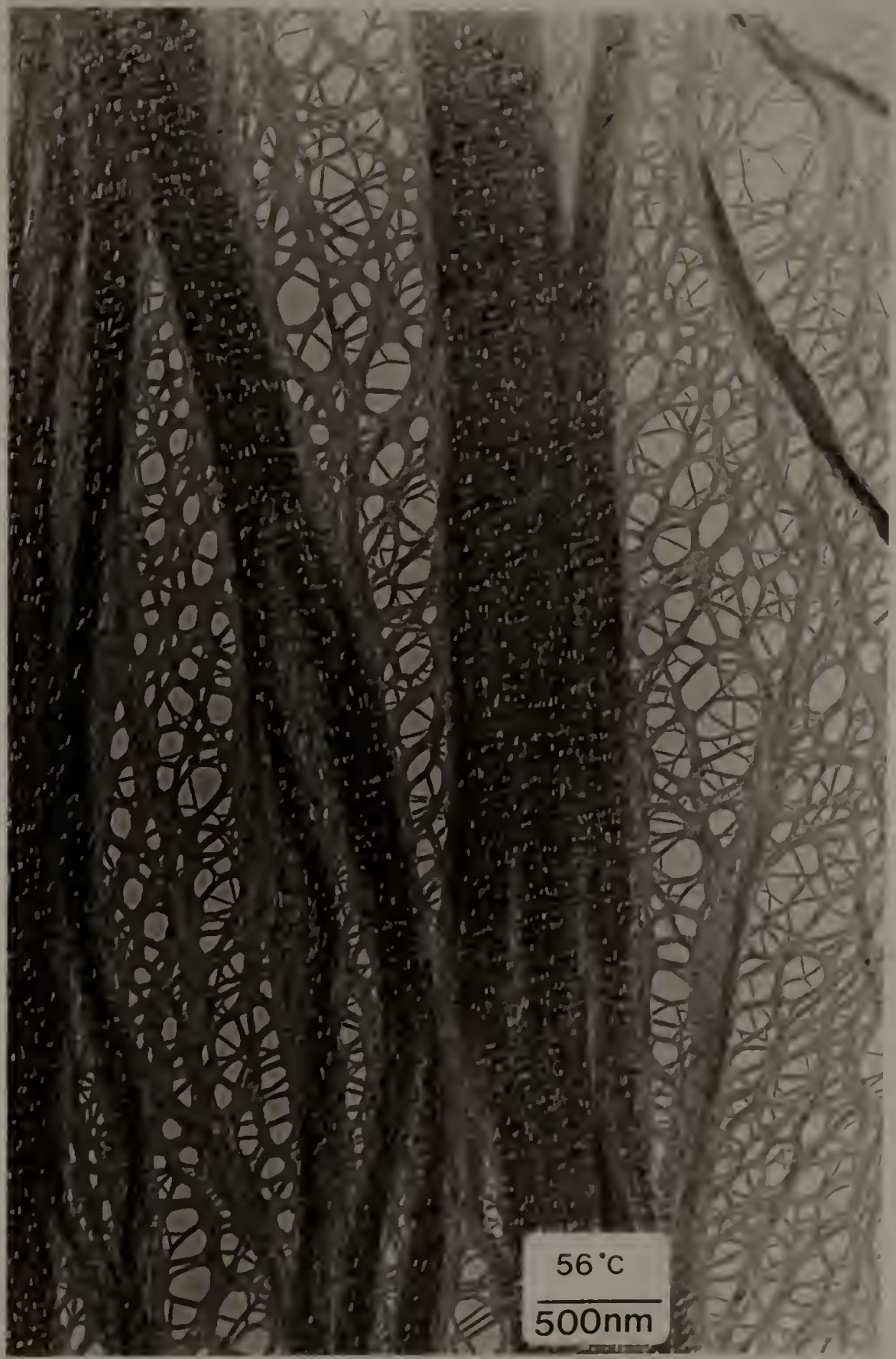
56 °C
500nm

Figure 7.10

Brightfield micrograph with inset electron diffraction pattern of as-drawn HDPE taken at 122 °C showing a loss of lamellar character and crystallinity. Chain axis vertical.


122°C
200nm

Discussion

Deformation of polyethylene can be considered to be a flow process in which entanglements and crystallites serve as constraints to chain motion. The effect of these constraints varies with temperature and stress level. For example, the yield stress of polyethylene decreases strongly with increasing temperature (Young, 1981; Meinel and Peterlin, 1971; Smith et al., 1981a).

The increase in chain mobility and crystalline phase ductility with increasing temperature will be used in the following description to account for the differences in deformation morphologies exhibited at 56, 93, and 129 °C and previously at 25 °C (Chapter 5). A comparison of the morphologies shown with those observed in Chapter 6 for SSE/PD ultrahigh modulus PE will be used to determine the processing temperature range required to achieve optimum mechanical properties. Furthermore, the deformation processes which occurred during SSE/PD will be inferred from those seen here.

The utility of TEM (especially using the darkfield mode) in detailing the transformation of morphology with draw will be emphasized in the following development. As indicated in Chapter 5, Gibson et al., (1978) used indirect methods to ascertain the presence of crystalline bridges between lamellae. Specifically, wide angle x-ray scattering (WAXS) measurements yielded a weight average crystal thickness (parallel to the chain direction) which exceeded the average long period value obtained by small angle x-ray scattering (SAXS). Assuming uniform

deformation throughout the sample, this implied that crystalline bridges had formed, spanning the amorphous layers of what was essentially a modification of the microfibrillar model of Peterlin (Fig. 5.1).

However, the observations made here suggest that the continuous crystalline phase is comprised of long fibrillar crystals of essentially uniform diameter rather than a series arrangement of wide lamellae and narrow crystalline bridges. In fact, TEM observations indicated that the assumption in the above model of uniform deformation was inappropriate for HDPE deformed at high temperatures. As shown in Fig. 7.3, HDPE elongated at 93 and 129 °C deformed very nonuniformly along the elongation direction, achieving high strains in crazed regions while leaving the original lamellar morphology relatively intact in uncrazed regions. Since the microfibrils were nonperiodic along the chain direction, only the lamellar stacks would give rise to SAXS long period peaks. SAXS long period measurements would thus indicate an erroneously low degree of deformation. In contrast, both microfibrils and lamellae would contribute to WAXS crystal thickness measurements. Protofibrils in particular would give rise to a large average crystal thickness.

The studies made here paralleled another study in which bulk gel-spun fibers of UHMWPE were deformed and characterized by SAXS, WAXS, and scanning electron microscopy (SEM) (Van Hutten et al., 1985). Many details of the deformation process could not be determined in this previous study since all microscopy samples were gold coated, and diffraction contrast (and darkfield imaging) could not be employed. In addition, SAXS and WAXS gave information averaged over the bulk

material. The darkfield micrographs shown here, on the other hand, gave new insight into the decrystallization process, and enabled the undisputable identification of protofibrils and long crystalline regions in crazed material.

Van Hutten et al. (1985) detected the same microfibrillation (crazing) process as was seen here. This indicated that bulk HDPE deforms in the same way as thin films, underscoring the importance of thin film studies in the understanding of bulk deformation behavior. The UHWPE gel fibers of Van Hutten et al. were extended to a much greater maximum draw ratio than the HDPE films used here, as indicated by the fact that lamellae were entirely transformed into microfibrillated material.

It has been suggested by others that very extensive drawing can lead to undesirable mechanical properties since the resultant microfibrils are no longer "held in place" by lamellae, but rather are free to undergo extensive shear (Zachariades et al., 1980). Such shear could lead to for instance, strain-softening, which is known to occur when PE is deformed at high temperatures (Petermann et al., 1982; Smith et al., 1981a). Moreover, the tendency to undergo strain-softening increases as the entanglement density in undeformed PE decreases (Smith et al., 1981a). Apparently, strain-softening occurs when the number of interconnections between microfibrils is so low that shear between microfibrils can easily occur. At high temperatures, intermicrofibrillar tie molecules can detach from crystalline anchor points either by chain translation through the crystalline lattice (slip

and unfolding) or by chain scission. In materials of low entanglement density, it appears that the original number of interfibrillar tie molecules is low, resulting in fewer constraints to microfibrillar shear. It should be noted, however, that the lateral coalescence of microfibrils would hinder shear between microfibrils by increasing the friction between them.

Melting and Decrystallization

In Chapter 5, the possibility of a rise in temperature and subsequent melting during decrystallization was negligible, since the ambient temperature was 25 °C (equilibrium peak melting temperature being 135 °C), the elongation rate was low, and thin films were used. In the present experiments, however, the ambient temperature was higher, as was the possibility of partial melting before or during deformation. It is therefore of interest to determine whether or not thermally-induced melting accompanied deformation.

The microstructure and state of the crystalline phase of as-drawn films at elevated temperatures was determined using a microscope stage maintained at 122 °C. The resultant micrographs indicated that a significant degree of (quiescent) melting had indeed occurred. In fact, at 122 °C the HDPE as-drawn film consisted of apparently isolated crystallites. Therefore, the initial state of as-drawn films at 129 °C was not lamellar, and thus the lateral cohesion between kebabs was poor due to surface melting (Tanabe et al., 1986), melting of small crystals

(Pope and Keller, 1976) and a possible reduction in the number of tie molecules and entanglements interconnecting adjacent kebabs. This meant that stress would not be efficiently transferred between shish-kebabs at high temperatures. Instead, individual shish-kebabs would be stressed and would fibrillate apart as opposed to groups of interconnected shish-kebabs.

These findings and deductions are consistent with the thermal analysis (DSC) characterization data in Chapter 4 of as-drawn HDPE film which exhibited a (quiescent) melting range from ca. 104 to 143 °C. Partial melting (of thin crystals and at crystal surfaces) would not only decrease the cohesion between shish-kebabs, but may also have resulted in melting of defective regions within shish-kebabs to the extent that the crystalline phase continuity of the shish-kebab was destroyed. The shrinkage of shish-kebabs at temperatures below the melting temperature has been attributed to such an event (Grubb and Keller, 1978). This would reduce the reinforcement of the noncrystalline phase. Partial melting at temperatures above 104 °C does not, however, explain how crazes could propagate at 93 °C, 11 ° C below the onset of (quiescent) melting. Assuming that the amount of temperature rise during deformation was negligible (due to the slow strain rates and thinness of films) one can only conclude that craze growth and propagation did not require thermally-induced melting. Rather, crazes grew when the local stress equalled or exceeded the yield stress of the crystalline phase. As indicated above, melting did occur when films were unstressed and at high temperatures ($\geq$ 104 °C). Since

near isothermal deformation conditions were employed, it will be assumed that additional melting (due to a rise in temperature) did not accompany subsequent deformation, especially considering the fact that straining PE decreases the entropy of the disordered phase, and brings about an increase in melting point (Flory, 1947). In fact, the crystal shear processes which were seen by darkfield TEM indicated unambiguously that the deformation microstructure resulted from yielding rather than melting at elevated temperatures and subsequent recrystallization.

The Alpha Transition of Polyethylene

High temperatures reduce the yield stress of the crystalline phase, and cause it to deform in a visco-elastic manner. This is in contrast to deformation at lower temperatures where crystals behave more like rigid bodies until very high stresses are reached. The temperature at which PE crystals change from rigid bodies (which transfer stress) to visco-elastic ones (which alleviate stress through flow processes) when subjected to a cyclic low strain (less than 1 %) is known as the alpha transition. As indicated in Chapter 4, the mechanisms associated with the alpha loss are believed to involve shear between and within mosaic blocks. In the present study, grain boundary motion in the form of shear between mosaic blocks (the α_1 loss) was directly imaged in darkfield micrographs. In addition, the processes which led to long crystal formation involved a significant degree of intracrystalline

shear and chain slip, and can be associated with the more energetic α_2 process.

The alpha transition temperature increases with increasing strain rate (Kajiyama et al., 1973). That is, the crystalline phase yield stress of PE is both temperature and strain rate dependent. The alpha loss peak for the HDPE used here was located at 73 °C for a strain rate of 1 hz. (See Chapter 4 for details.) Only one loss peak was resolved. This value corresponds only to a very low stress level. In the present thin film deformation studies, the films were highly strained and therefore became highly stressed. As such, the processes associated with the alpha losses occurred at temperatures below the alpha transition temperature, albeit at much higher stress levels.

Both the α_1 and α_2 processes commenced upon yielding. Kebabs sheared apart (α_1) and fed into shish crystals (α_2) at the craze interface, in a way reminescent of craze growth in amorphous, glassy polystyrene (PS). PS craze fibrils elongate predominantly by drawing from the bulk as opposed as undergoing draw-down (creep) of the fibril (Lauterwasser and Kramer, 1979; Kramer, 1983). This surface drawing process results in a variation of draw ratio throughout the PS craze, the tip and "midrib" regions of the craze experiencing the least amount of surface drawing and therefore displaying the highest draw ratio. In the present study, no such draw ratio variations, as revealed by the preferential formation of long crystals in a given region of the craze, was detected. This indicated that a "midrib" region of high strain was not present. In fact, the most highly-drawn microfibrils (identified as

containing the lowest amount of chain folded blocks) seemed to be randomly placed throughout crazes.

While microfibrils elongated via decrystallization and surface drawing at craze interfaces, kebab remnants already within the interiors of the crazes underwent further shear. In this way, microfibrils also experienced draw-down (Figs. 7.4 and 7.6). Draw-down did not occur to the extent that microfibrils broke. However, it occurred nonuniformly within crazes, as indicated by the diversity in size and number of chain-folded crystal remnants among neighboring microfibrils. Draw-down effectively increased the draw ratio of microfibrils by decreasing remnant size and therefore the population of chain folds. This led to strain-induced crystallization and protofibril formation.

Generally, the crystalline phase shear processes imaged during kebab decrystallization were highly localized within the crystal. In other words, the crystallites appeared to shear into smaller crystalline remnants, individual remnants remaining essentially intact. Only the interfaces between the crystal remnants experienced deformation. This type of shear has been termed block shear (Adams et al., 1986). In contrast, diamond-shaped kebabs were occasionally seen. The transformation of a square kebab into a diamond-shaped crystal indicated that shear occurred between several planes within the kebab, rather than between only two planes. This type of shear has been termed fine shear. It has been suggested that both types of crystal shear occur by a dislocation mechanism, whereby the crystalline order of the crystal remnants remains intact during deformation (Petermann and Gleiter,

1973b). Alternatively, it is possible that the diamond shape arose from nonisothermal crystallization conditions (Bashir et al., 1984). However, since diamond-shaped kebabs were not seen in as-drawn films, this is considered unlikely.

Noncrystalline phase chain reorganization during deformation was constrained by entanglements, crystallites, and by the Van der Waals forces which existed between chains (which were particularly high in crystals). The decrease in lateral cohesion between crystallites and crystalline chains at high temperatures facilitated chain reorganization via flow processes. Due to the low yield stress, enhanced chain mobility, and poor cohesion between shish-kebabs at high temperature, HDPE crazed when stressed. The high degree of chain extension and alignment which was brought about in crazed regions led to extensive strain-induced crystallization.

At low deformation temperatures (25 and 56 °C), crazes nucleated but did not propagate, due to the higher yield stress and greater reinforcing capabilities of the crystalline phase. Instead, cavities coalesced between bundles of shish-kebabs and resulted in heterogeneous fibrillation. Although the stress levels which arose in fibrils resulted in some decrystallization, the resultant strain was not sufficient to bring about appreciable strain-induced crystallization. This may have derived in part from the fact that elongation was much more uniform (along the chain direction) at these low temperatures than in microfibrillated material, resulting in low levels of local strain.

The value of the detailed information obtainable only by microscopy was clearly shown in the preceeding discussion. For instance, TEM revealed that the high draw ratios achieved at high temperature was a result of the much greater ductility of the crystalline phase. In particular, TEM indicated that HDPE elongates very nonuniformly when deformed at temperatures above the alpha transition. Indeed, the high degree of noncrystalline chain extension in areas of high local strain gave rise to extensive crystalline regions. This suggests that a continuous crystalline phase and ultrahigh modulus polyethylene can be produced by drawing at temperatures above the alpha transition, where the draw stress is low enough for chains to extend with a minimum of chain scission. This concurs with previous studies of bulk-drawn PE (Perkins and Porter, 1977).

Continuous Crystal Formation

The objective of the present study was to mimic and better understand those processes giving rise to ultrahigh modulus PE. A comparison of the microstructures observed here with those of ultrahigh modulus SSE/PD bulk samples seen in Chapter 6 indicated that this was achieved. In both cases, the highly drawn materials were very crystalline and were comprised of long fibrillar crystalline regions. In fact, protofibrils of equivalent structure formed by both processes. Moreover, microfibrils laterally coalesced in the thin films much as

protofibrils did in SSE/PD material. This further supported the continuous crystalline phase model comprised of laterally coalesced protofibrils, introduced in Chapter 6. The well-known increase in tensile modulus with draw can be attributed to an increase in noncrystalline phase extension and extensive strain-induced crystallization. Darkfield microscopy of thin films allowed the details of the decrystallization and (re)crystallization processes accompanying SSE/PD to be observed.

One might query how a crazing process can be used to mimic the solid state extrusion/post-drawing process, since extrusion is done under hydrostatic pressure, which would undoubtedly hinder the dilational requirements of crazing. It must be recalled that post-drawing accounted for the vast majority of the total draw, solid state extrusion being used only up to a draw ratio of six. The post-drawing process involved uniaxial tension, without application of hydrostatic pressure, and therefore crazing may well be responsible for the high degree of chain extension and strain-induced crystallization observed in Chapter 6.

Crystal Thickness versus Deformation Temperature

Certain small angle x-ray scattering studies have indicated that the long period of bulk-deformed HDPE reflects only the deformation temperature and not the crystallization conditions of the original undeformed material (Cornelluissen and Peterlin, 1967; Peterlin and

Sakaoku, 1967; Peterlin, 1972). Reductions in long period were at first explained in terms of thermally-induced melting (arising from frictional losses during deformation) and subsequent recrystallization at the ambient temperature (Peterlin and Sakuoku, 1967; Peterlin, 1967). Changes in long period were assumed to reflect analogous changes in crystal thickness. Further analysis revealed, however, that the temperature rise accompanying deformation in these materials was insufficient to bring about melting. Instead, reductions in long period were attributed to the presence of a negative lateral pressure during tensile deformation (Peterlin, 1972), in which the melting point was reduced with negative pressure in accordance with the Clausius-Clapeyron equation (refer to Chapter 5). Meanwhile, it was shown by electron microscopy that deformed thin films and single crystals retained their original crystallite thickness throughout deformation (Ingram, 1967; Peterlin, 1971; Peterlin, 1972). This last finding most likely reflects the relatively low strains achieved.

The dependence of crystal thickness and long period (the sum of the thicknesses of the crystalline and noncrystalline layers) on deformation temperature can be explained in terms of decrystallization and strain-induced crystallization processes. The relative amounts of decrystallization and recrystallization which occur during deformation are temperature dependent. A reduction in the average crystal thickness following room temperature deformation can be explained in terms of defect generation within mosaic blocks, and the absence of significant strain-induced crystallization and annealing. The change in SAXS long

period would depend on the extent of deformation (and noncrystalline phase elongation), and the degree of periodicity in deformed lamellar stacks. A substantial amount of deformation could lead to a reduction in long period through defect generation within crystals. At high temperatures, both decrystallization and strain-induced crystallization as well as annealing occur. SAXS measurements (corresponding to the relatively undeformed lamellar stacks) would indicate an increase in average long period due to the thermally-induced melting of small crystals (Pope and Keller, 1976) and annealing, while an increase in average crystal thickness would result from decrystallization followed by strain-induced crystallization in crazed regions and annealing as well. Therefore, deformation at high temperature would result in an increase in crystal thickness and long period, while deformation at low temperature would result in a decrease in crystal thickness and possibly long period, in agreement with the previously cited SAXS and WAXS data. Note that at no point was it necessary to invoke a temperature rise and melting to explain these observations. It is proposed that the "negative lateral pressure" mechanism of crystal destruction propounded by Peterlin (1972) and earlier by Hookway (1957), a very general way to the decrystallization processes which were shown here.

Conclusions

Darkfield mode TEM provided a window through which the details of the conversion of chain-folded to chain-extended crystals and the

processes leading to the formation of a continuous crystalline phase could be seen. The advantages of directly imaging the deformation morphology versus obtaining indirect (averaged) x-ray scattering data was illustrated. Specifically, the two extreme structural models for the formation of a continuous crystalline phase are both consistent with previously published scattering data. Observation by TEM, however, indicated that neither of the extremes: microfibrils containing periodically alternating chain-folded lamellae and amorphous phases, with chain-extended crystalline bridges spanning the amorphous phase; nor an extensive chain-extended crystal containing defects, were accurate representations of the microstructure of ultradrawn polyethylene. Instead, the crystalline phase consisted of laterally coalesced protofibrils as discussed in Chapter 6, the formation and structure of which is summarized in the following.

Thin, highly oriented, single crystal-like textured, shish-kebab morphology films of HDPE were uniaxially elongated at 56, 93, and 129 °C in the same manner as was used previously at 25 °C. At low temperatures (25 and 56 °C) the material elongated uniformly whereas nonuniform elongation was found at high temperatures (93 and 129 °C). In fact, in the latter case the HDPE film consisted of highly extended material in crazed regions and relatively undeformed lamellar material in uncrazed regions. The crazing process involved the decrystallization and elongation of shish-kebabs, each shish-kebab giving rise to a craze microfibril. Kebabs fed into microfibrils in a way reminescent of surface drawing in polystyrene crazes (Lauterwasser and Kramer, 1979).

Once within a craze, the chain-folded crystals underwent further draw-down (creep) and strain-induced crystallization, forming long crystalline microfibrils, termed protofibrils, of almost uniform diameter ($\leqslant$ 7 nm), except where occasional remnants of chain folded crystals resided (Fig. 6.5). In fact, crystalline regions as long as 3 microns formed by strain-induced crystallization of the noncrystalline chains interconnecting these remnants. The resultant craze microstructure is shown schematically in Fig. 7.3. The similarity between this microstructure and that obtained in Chapter 6 for ultradrawn fibers as well as elsewhere for bulk gel-drawn PE (Van Hutten et al., 1985) indicated that the morphology seen in these thin film studies is a good representation of that which forms in the bulk.

A comparison of the morphologies of thin films and HDPE drawn at 129 °C, and SSE/PD PE indicated that the tensile drawing of thin films at temperatures above the alpha transition can be used to better understand the formation of a continuous crystalline phase. Both thin film and SSE/PD PE deformed by the same decrystallization and stain-induced crystallization mechanisms, and led to an increase in crystallinity as well as the formation and lateral coalescence of protofibrils. Indeed, the structure of protofibrils seen in both cases was virtually identical. In addition to lateral coalescence, microfibrils in crazed regions of thin films retained lateral interconnections by means of tie fibrils. The similarity of microstructure between SSE/PD and crazed regions implied that such lateral interconnections exist between protofibrils in ultrahigh modulus

materials as well. Due to the propensity of ultradrawn PE to fibrillate, it is unlikely that these interconnections are very strong.

The decrystallization process which occurred in thin films at high temperatures was equivalent to that outlined for deformation at 25 °C in Chapter 5 (Fig. 5.10), although it no doubt occurred at lower stress levels. Darkfield micrographs (Figs. 7.4 - 7.7) enabled the detailed visualization of <001> crystal shear and defect generation within crystals, as well as the final conversion of chain-folded crystals to much longer more chain-extended crystals. Both block shear and fine shear of the crystalline phase was observed.

The main difference between deformation at high and low temperatures was attributed to the lower yield stress and enhanced chain mobility at high temperatures. Although partial thermally-induced melting had occurred at 122 °C, as indicated by viewing as-drawn films at this temperature, it was shown that even material which was not partially melted (e.g. at 93 °C) crazed as long as it was above the alpha transition temperature. The alpha transition took place at 73 °C, 1 hz for isotropic HDPE, cooled from 180 °C at room temperature. At low temperatures (25 and 56 °C), no long crystals were detected, implying that little strain-induced crystallization occurred. The absence of crazed regions and long crystals at temperatures below the alpha transition was due to the high yield stress of the crystalline phase and the resultant arrest of craze propagation by shish-kebabs. The reduction in average crystal thickness of polyethylene with deformation was explained in terms of near isothermal decrystallization (in the

absence of strain-induced crystallization). This indicated that such a reduction in average crystal thickness can be interpretted without invoking a rise in temperature (and associated melting and recrystallization). Likewise, the increase in average crystal thickness with deformation at high temperatures was explained in terms of decrystallization, annealing, and strain-induced crystallization.

C H A P T E R VIII

THE DEFORMATION BEHAVIOR OF ORIENTED LINEAR LOW DENSITY POLYETHYLENE FILMS

Abstract

Thin, single crystal-like textured, shish-kebab morphology films of drawn linear low density polyethylene (LLDPE) were deformed in the same manner as outlined in Chapter 5, and directly viewed by transmission electron microscopy (TEM). All of these materials were branched essentially randomly along the backbone chain and had branch contents as high as 2.4 mole %. Characterization data in Chapter 4 indicated a reduction in the mechanical stability of the crystalline phase with increasing branch content. TEM investigations done here indicated that LLDPE film deformed by the same mechanisms as observed for high density polyethylene (HDPE) in Chapter 5. In all cases, chain-folded crystals decreased in size via decrystallization, a process which was previously shown to involve <001> crystal shear, chain slip, and the generation of internal defects within crystals (Fig. 5.10). The reduction of yield stress with increased branching resulted in a less fibrillar and more webbed deformation microstructure in LLDPE than found for HDPE. In all cases, deformation led to the formation of a network in which crystallites acted as crosslink points, the number density of crosslinks increasing with branch content. Network formation occurred

much more uniformly in highly branched LLDPE, whereas the network structure in HDPE consisted of a hierarchy of fibril sizes. This suggested that shish-kebabs gave much more reinforcement to films in the latter case.

Introduction

The use of LLDPE has become more and more widespread ever since the discovery of Ziegler-Natta catalysts in the mid-1950's. In fact, it has been stated that if the low pressure process of making polyethylene had been discovered prior to the high pressure process, no LDPE plants would exist today. This is clearly supported by the replacement of LDPE by LLDPE in many product markets (e.g. utility bags, food storage bags, etc.). Although much research has been directed towards understanding the physical and mechanical properties of LLDPE (Capaccio and Ward, 1984; Wunderlich, 1973 a and e; Sequela and Rietsch, 1986a and b; Alamo et al., 1984; Mandelkern, 1985; Krigas et al., 1985; Martuscelli, 1975; Cady, 1987), many fundamental questions remain unresolved. Specifically, recent studies have dealt with the nature of the crystal/amorphous interface, the inclusion (or exclusion) of branches in crystals, and the fractionation of chains during crystallization according to branch content and distribution. Much work has also gone into controlling branching characteristics, so that one can "choose" the branching and subsequent mechanical and physical properties.

Many of the materials characterized in Chapter 4 were deformed at room temperature and observed by TEM in order that the effects of branch content and length on deformation behavior could be studied. The use of gel-drawn films with a high degree of chain orientation enabled elongational forces to be applied along a single crystallographic direction throughout the entire sample, thus simplifying interpretation of the deformation process. These studies are deemed particularly pertinent to the understanding of deformation behavior in materials made by industrial processes such as extrusion, film blowing or ultradrawing, which impart a high degree of chain orientation to the final product.

Experimental

A full description of the materials and film preparation techniques used in this study, as well as thermal, mechanical and morphological characterization of as-drawn films can be found in Chapter 4. A partial summary of characterization data is given in tables 4.1 and 4.2.

The microscopy techniques used here have been outlined in Chapter 5. In fact, the room temperature deformation microstructure of HDPE in Chapter 5 will be used as a basis of comparison in the present investigation. As with HDPE, LLDPE films were elongated uniaxially along the chain direction at a nominal rate of 5×10^4 mm/s. Hindered film contraction resulted in the development of a biaxial planar stress field. The local strain in films was very inhomogeneous and could not

be related to the nominal strain. A few of the films viewed were shadowed with gold (after elongation) at a glancing angle to enhance contrast between adjacent kebab crystals.

Results

All LLDPE samples deformed by the same mechanisms as did HDPE. Upon elongation, the amorphous phase extended and cavited. Cavities coalesced along the chain direction, and the material fibrillated into bunches of shish-kebabs. At low strains, the shish-kebabs themselves elongated without any noticeable destruction of kebabs. It is believed that the stressed shish-kebabs first elongated at defective regions, and subsequent elongation occurred when a critical stress had been reached, by drawing kebabs into shish crystals. Once kebabs were totally incorporated into the shish crystals, draw-down (creep) occurred. The decrystallization process by which crystallites were transformed into a more chain-extended form (via chain slip, crystal shear, and defect generation) was as discussed in Chapter 5.

A comparison of the deformation morphologies of HDPE and LLDPE indicated that the networks which formed in LLDPE strongly resembled those of HDPE (Figs. 8.1 - 8.3). Crystallites served as crosslink points in these networks (Fig. 8.2b) as would be expected for films made from a gel precursor state. Close scrutiny of Fig. 8.1b revealed that the tips of cavitated regions in LLDPE were spanned by a thin continuous film. This was not observed in the HDPE counterpart (Fig. 8.1a).

Figure 8.1

Brightfield micrographs of polyethylene elongated parallel to the chain axis at 25 °C of A) HDPE (Marlex), and B) LLDPE (Dowlex, 0.3 mole % hexyl branches). Arrows identify remnants of a continuous film spanning cavity tips. Chain axis vertical.

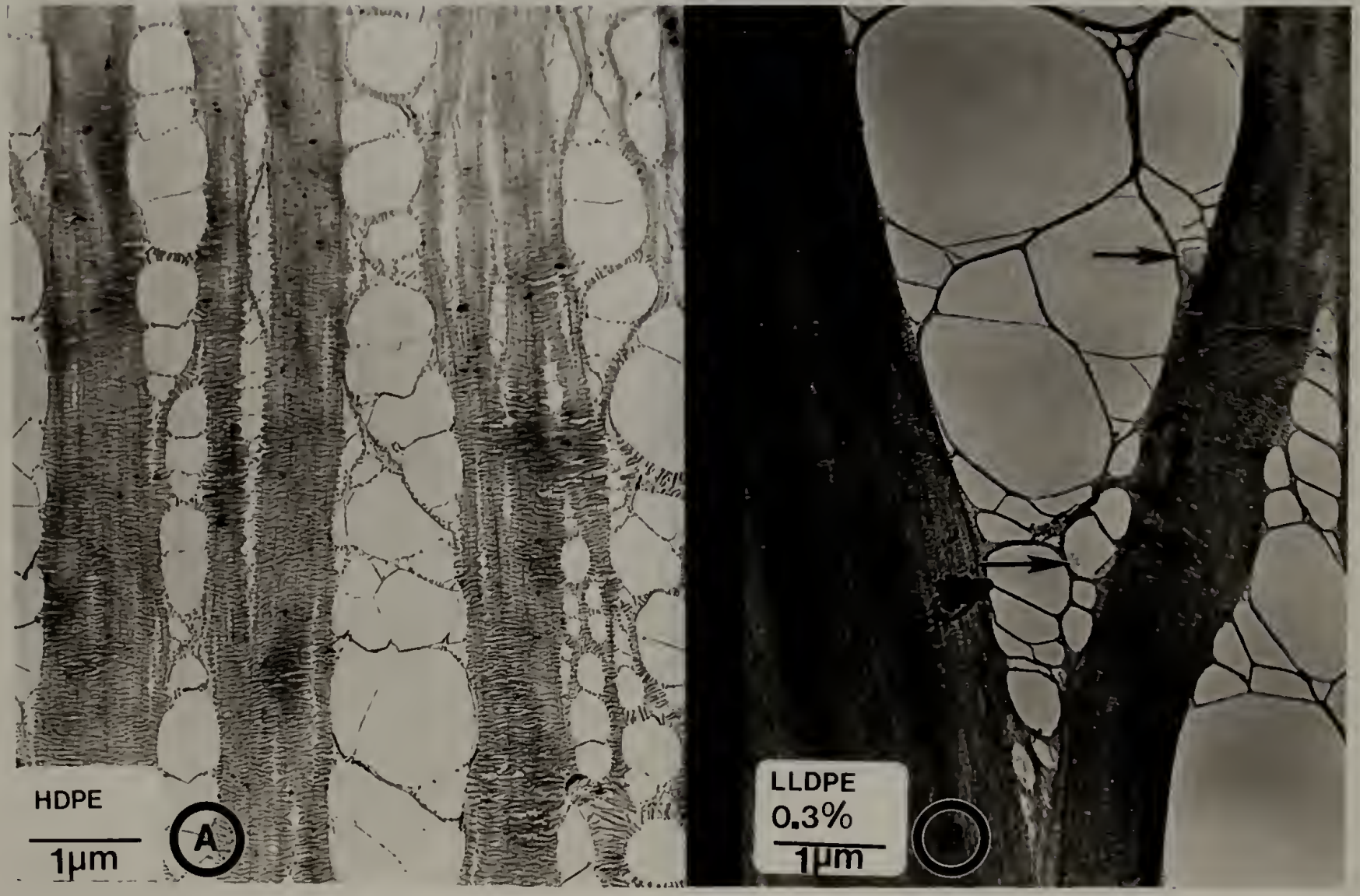
HDPE
1μm
A
LLDPE
0.3%
1μm

Figure 8.2

Brightfield micrographs of polyethylene elongated at 25 °C parallel to the chain axis of A) LLDPE (NTX-017, 1.23 mole % butyl branches), chain axis vertical, and B) LLDPE (NTX-018, 2.29 mole % butyl branches) displaying network structure with crystalline crosslinks.

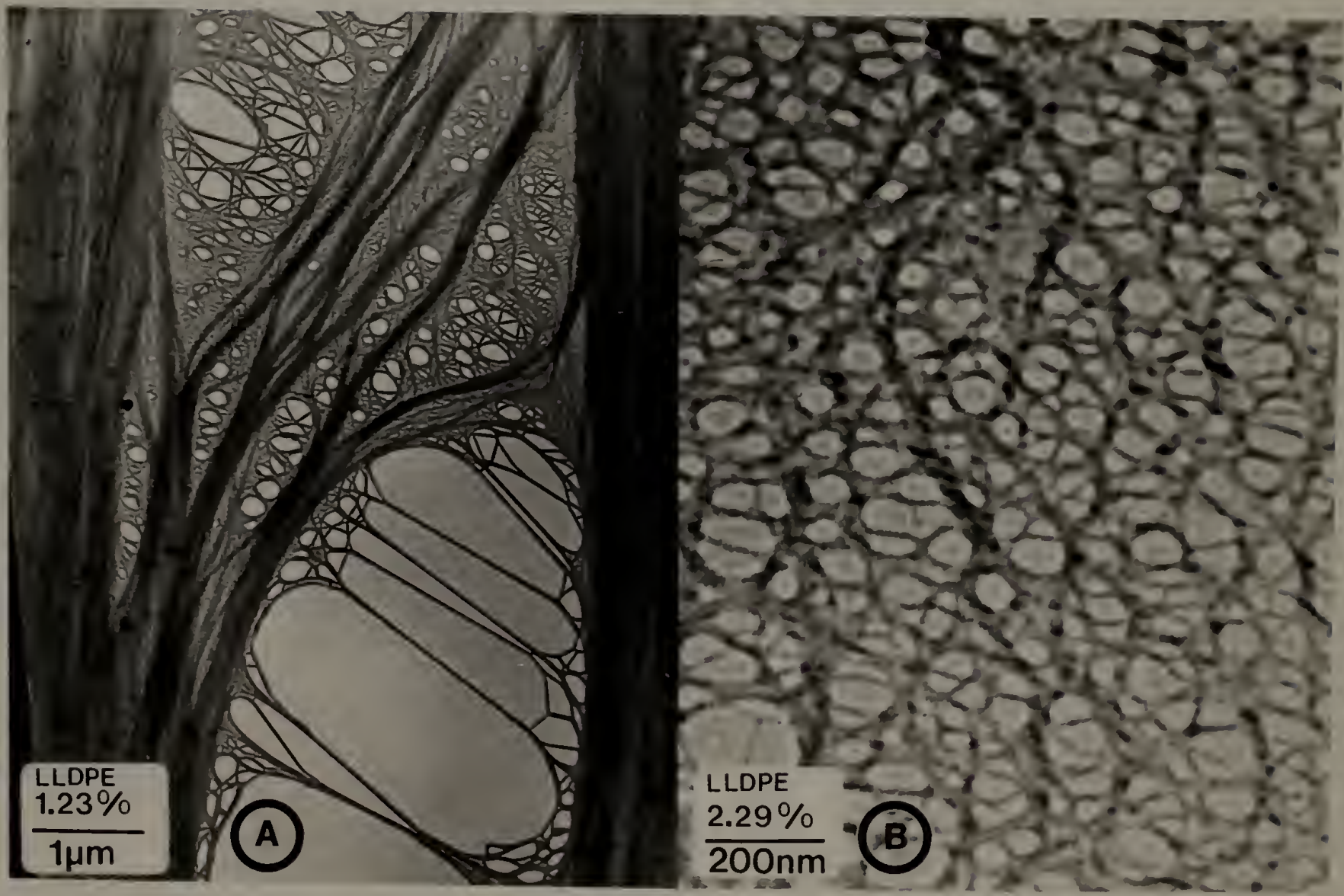
LLDPE
1.23%
1µm
A
LLDPE
2.29%
200nm
B

Figure 8.3

Brightfield micrographs of polyetheylene elongated perpendicular to the chain axis at 25 °C and gold decorated. Note the comparable morphologies of A) HDPE (Marlex) and B) LLDPE (RC-4, 2.36 mole % butyl branches) as well as the more fibrous nature of HDPE.

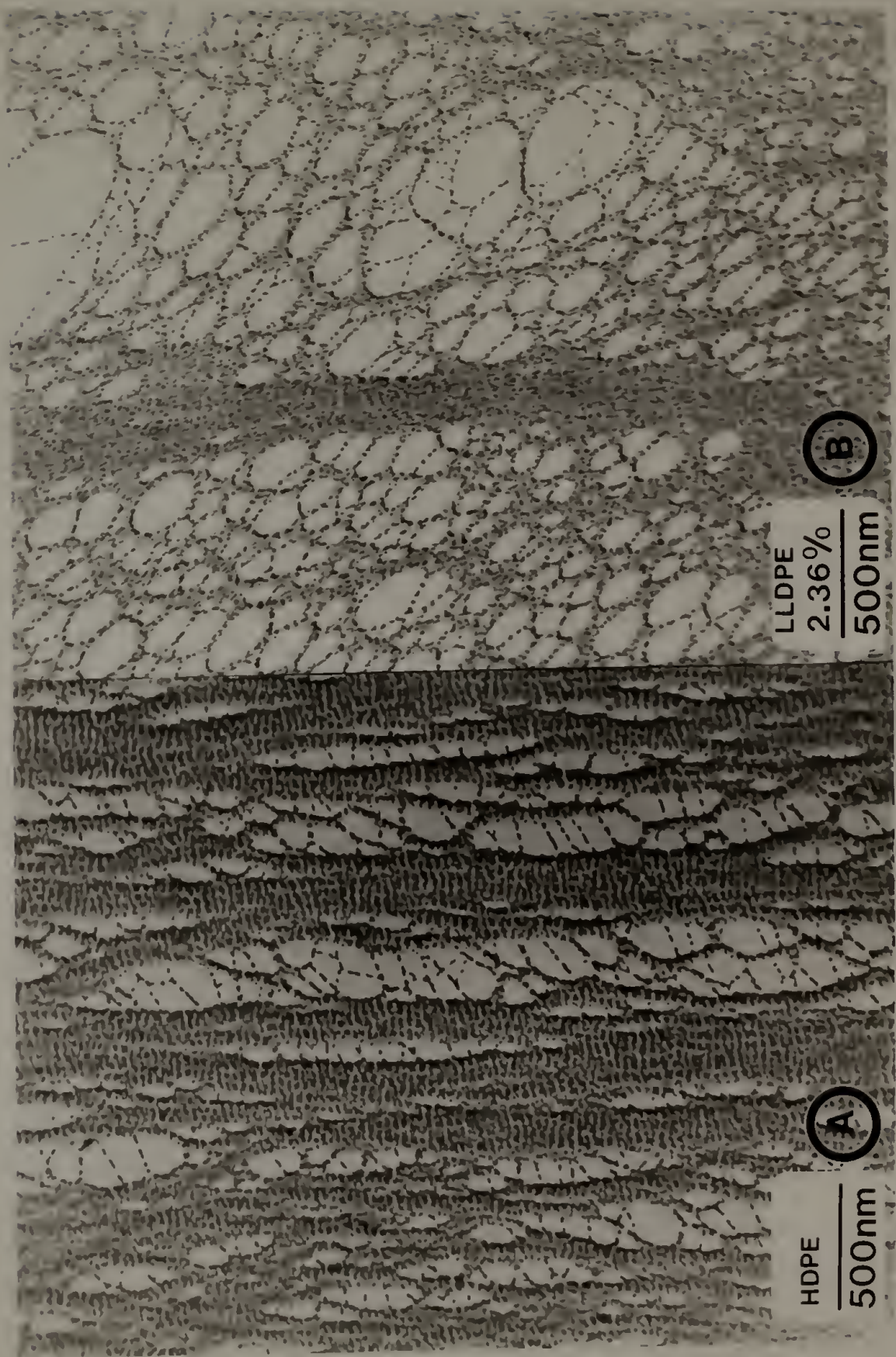
HDPE
500nm
A
LLDPE
2.36%
500nm
B

Indeed, at lower strains, distinct film thinning could be seen in all of the LLDPE samples (Fig. 8.4b). Such striations were also occasionally, though much less frequently seen in HDPE (Fig. 8.4a). In addition, the transition from uncavitated to cavitated material appeared to be much more gradual in LLDPE than in HDPE (Fig. 8.2a). It appeared that flow processes in LLDPE during deformation reduced the concentration of stress at cavity tips, and were responsible for the more webbed and less fibrillar microstructure in LLDPE (Figs. 8.2b and 8.3 a and b).

Discussion

The main concern of this study was to first, determine whether or not LLDPE and HDPE deform by the same mechanisms, and second, determine how a reduction in the modulus and crystalline phase yield stress (i.e. an increase in ductility) due to smaller average crystallite size, poorer crystal perfection, and lower crystallinity, affected deformation behavior and microstructure. The ductility of a material can be modified in many ways. For instance, brittle behavior increases (ductility decreases) when the material is deformed at low temperature (Young, 1981), when the draw ratio of the material is increased (Hallam et al., 1986), or if the sample width (Sandiford and Willbourn, 1960) or thickness (Carpinteri et al., 1986) is increased (due to alteration of the stress state). In order to understand the effect of branching on ductility, one must know how the morphology of as-drawn LLDPE affects

Figure 8.4

Brightfield micrographs of polyethylene elongated parallel to the chain axis at 25 °C of A) HDPE (Marlex) and B) LLDPE (NTX-018, 2.29 mole % butyl branches). Note the occurrence of film thinning prior to fibrillation. Chain axis vertical.


HDPE
500nm
B
LLDPE
2.29%
500nm

chain mobility. With this in mind, the characterization of as-drawn film will be reviewed.

The main factor responsible for morphological differences between the LLDPE and HDPE samples used here was branch content. As branch content increased, both crystal size (width and thickness) and perfection were reduced, resulting in crystal lattice expansion (Bunn, 1960; Wunderlich, 1973a; Walter and Reding, 1956; Holdsworth and Keller, 1969; Perez et al., 1987). This reduced the magnitude of Van der Waals attraction between adjacent crystal planes, and facilitated crystal shear much as it would be facilitated by an increase in temperature. Such a reduction in the mechanical stability of the crystalline phase with branching was supported by the fact that the alpha transition temperature decreased with increasing branch content, indicating greater chain mobility within the crystalline phase of highly branched LLDPE. The reduction in crystalline phase stability would be accompanied by a reduction in yield stress.

Popli and Mandelkern (1987) have correlated a decrease in yield stress with a decrease in average crystal thickness as well as crystallinity. In addition, yield stress is also influenced by the concentration of stress at crystal surfaces. For instance, an increase of yield stress with noncrystalline phase orientation has been attributed to the extension of tie molecules with draw (Linder and Samuels, 1985). It is believed that the greater the number of taut tie molecules along a crystal surface, the lower the load borne by each one, and the lower the stress concentration at the crystal surface.

Brightfield images indicated that LLDPE deformed more uniformly than HDPE, and that the cavitation process in LLDPE was preceeded by an observable and distinct stage of film thinning. Both of these processes are consistent with enhancement of flow (reduced yield stress) with branching. In HDPE, on the other hand, stress builds up during deformation, resulting in yielding at flaws before the material as a whole has reached the yield stress. The more fibrillar nature of HDPE versus highly branched LLDPE (Figs. 8.2 and 8.3B) suggested that the shish-kebabs in HDPE were either more numerous or less defective than those in LLDPE and therefore reinforced the material better. It is possible that the incorporation of branches in shish-kebabs, or the reduction in shish-kebab length due to branching, greatly reduced their reinforcement capabilities. The domination of deformation by flaws in the amorphous phase between shish-kebabs in HDPE led to inhomogeneous deformation as well as larger cavity sizes and the absence of films spanning cavity tips. In LLDPE, deformation occurred at a lower stress level. The large amount of flow which occurred during deformation gave cavities a more "blunted" appearance than found in HDPE. In addition, flow processes mitigated the stress-concentrating effects of flaws, making LLDPE films less susceptible to flaws, and therefore more extendable.

The differences in network topology between LLDPE and HDPE may have reflected the smaller crystallite size and higher crystallite number density found in LLDPE. For instance, if these films are approximated by networks held together by cubic crystal blocks, and

typical values of crystallinity and average crystal thickness of LLDPE film are taken to be 50% and 10 nm, respectively, while those of HDPE are 75% and 27 nm, respectively, then the average number of crystals per unit volume in LLDPE is thirteen times greater than that of HDPE. When these crystallites are viewed as crosslinks, the higher number density of crosslinks in LLDPE would result in a finer network with smaller cavities than found in HDPE.

Conclusions

From the preceeding observations, it was evident that gel-drawn films of LLDPE (up to 2.4 mole % ethyl- to hexyl- branches) deformed by the same mechanisms as those of HDPE. Upon deformation, the noncrystalline phase elongated and then cavitated. These cavities then coalesced between shish-kebabs, and the material fibrillated. As branch concentration increased, the fibrillar appearance gave way to more of a network-like appearance. This is believed to be due to the dentrimental effects of branching on shish-kebab length and perfection. Once the yield stress was reached, decrystallization occurred via crystal shear and chain slip (and possibly crystal defect generation as well).

The dependence of mechanical properties on branching was attributed to the effect of branching on crystalline phase stability. Crystal size, perfection, and crystallinity were reduced with increasing branch content. Branching is known to result in crystal lattice expansion and a reduction in yield stress as well as modulus, leading to

enhanced chain mobility. The uniformity of deformation microstructure and high extendability of LLDPE (versus HDPE) was attributed to a decrease in yield stress and an increase in flow phenomena during deformation. Specifically, the susceptibility of LLDPE to flaws was mitigated by a low flow stress, which prevented stress build-up. In addition, the network-like rather than fibrillar appearance of deformed highly branched LLDPE was attributed to the greater number of crystalline crosslink points in LLDPE as well as the probable high number of defects within shish-kebabs.

C H A P T E R IX

SUMMARY

Transmission electron microscopy was used to observe in detail the uniaxial deformation of oriented polyethylene and the formation of an extensive crystalline phase in both bulk and thin films. Bulk films of ultrahigh molecular weight polyethylene were received which had been deformed at elevated temperatures by solid state extrusion followed by post-drawing (SSE/PD) to draw ratios up to 250. Most importantly, the ultradrawn (draw ratio $\geq$ 97) samples exhibited tensile moduli exceeding 175 GPa and strengths exceeding 3 GPa. The thin films were made using the technique of Petermann and Gohil (1979) by gel drawing HDPE as well as LLDPE at temperatures slightly below their peak melting endotherm temperature. The room temperature (25 °C) deformation behavior of the thin films was then characterized. Moreover, the deformation behavior of HDPE films at temperatures as high as 129 °C was observed. The resultant deformation morphologies were then compared with each other and those of the SSE/PD samples.

Generally, differences in deformation microstructure were related to the effect of deformation temperature and branch content on ductility with respect to that of HDPE at room temperature. Crystalline phase ductility was high at high temperatures due to reduced crystal thickness, and lattice expansion, facilitating dislocation formation and motion. Likewise, ductility in LLDPE increased with branch content due

to the incorporation of branch defects into the crystal lattice (causing lattice expansion), as well as by a reduction in crystal thickness. Crystal size and crystallinity were reduced at high temperatures by crystal surface melting and melting of small crystals and were reduced with increasing branch content due to the interruption of crystallization by branch defects.

The effects of high temperature and branching on crystalline phase ductility paralleled one another in many ways. Depending on deformation temperature and branch content, however, these effects manifested themselves to different degrees. In the present case, high temperature (129 °C) had a much more marked effect on deformation microstructure than branch content (up to 2.4 mole percent). In fact, LLDPE fibrillated in a manner similar to HDPE deformed below the alpha transition, although slight differences in microstructure reflected the lower yield stress of LLDPE. On the other hand, thin films of HDPE deformed at temperatures exceeding the alpha transition temperature crazed, each shish-kebab giving rise to a craze fibril.

To fully understand why deformation microstructure was so strongly affected by temperature, one must understand how chain mobility in the noncrystalline phase is coupled to that in the crystalline phase. The constraints imposed on chain slippage by entanglements and the crystalline phase are greatly reduced at high temperatures. Above the alpha transition, chain slippage through crystallites and the resultant enhancement of mobility within the amorphous phase, coupled with chain extension due to the application of stress, resulted in strain-induced

crystallization. This indicated that although chain mobility was high at e.g. 129 °C, it was not so high as to bring about chain relaxation (and loss of an extended conformation) prior to strain-induced crystallization. Had temperatures well above the melting range been used, much more chain relaxation would have occurred prior to crystallization.

Substantial strain-induced crystallization occurred in thin HDPE film which was deformed at temperatures above the alpha transition temperature, being particularly evident in crazed regions. This suggested that polyethylene should be drawn at temperatures above the alpha transition temperature if a continuous (sample-spanning) crystalline phase is to form. Observations of ultradrawn bulk films using darkfield TEM substantiated this. Extensive (3 micron) crystalline regions were present. Indeed, since darkfield TEM gives only a lower bound of crystal size, it is likely that such crystalline regions were much larger and may even have formed a sample-spanning cluster, as suggested by the ultrahigh tensile modulus of these films.

Protofibrils constituted the fundamental structural units of the extensive crystalline regions found in ultradrawn SSE/PD films. Equivalent protofibrils were found in the HDPE films which had been deformed at 129 °C. Each protofibril was $\leq$ 10 nm wide and up to several hundred nanometers long. Within the protofibril, crystalline blocks were arranged in series, each block being typically 8 nm thick (along the chain direction). The fact that adjacent blocks within a protofibril were simultaneously diffracting indicated that they were

interconnected by crystalline bridges. Moreover, adjacent protofibrils laterally coalesced and diffracted simultaneously. This suggested that crystal/crystal junction points existed between the protofibrils. Such lateral interconnections between protofibrils would enable a sample-spanning crystalline phase to form even if individual protofibrils themselves were not sample-spanning.

The protofibril microstructure resembled that which has been proposed for shish-kebabs (Fig. 5.2) except here the shish core is almost as wide as the kebabs and the kebabs have both fold and fringed micellar top surfaces. In this model, the shish core consists of a series of fringed micelles which have fused together, and which contain occasional defects (Grubb and Keller, 1978). Indeed, there is reason to believe that protofibrils constitute a highly deformed state of shish-kebabs, and that the same processes which gave rise to shish-kebabs (from chain-folded crystals) were also operative during protofibril formation. For instance, shish crystals were present after single crystals were SSE to a draw ratio of 6, as was made evident by the simultaneous diffraction of lamellae (only a few mosaic blocks wide) within a stack. Thus, shish-kebabs can be considered to be precursors of protofibrils.

Protofibrils formed from single crystal mats by the processes of decrystallization and strain-induced crystallization. The effects of decrystallization, the mechanically-induced reorganization of the crystalline phase, were shown in SSE/PD materials (draw ratios from 6 to 250) as well as in thin films deformed at 25, 56, 93, and 129 °C. The

decrystallization process was discussed in detail in both Chapters 5 and 7, and is shown schematically in Fig. 5.10. It occurred via <001> crystal shear as well as chain slip and unfolding and defect generation within the interiors of crystals, such that lamellae gave rise to mosaic blocks of reduced width and thickness without undergoing thermally-induced melting and recrystallization. Darkfield micrographs taken of material deformed at 129 °C gave particularly detailed information on the decrystallization which preceeded the surface drawing of kebabs into craze fibrils (Figs. 7.4 - 7.6). The conversion of lamellae into mosaic blocks and the drawing of mosaic blocks into protofibrils was also well depicted in darkfield micrographs of SSE/PD polyethylene. By a draw ratio of 42, protofibrils were observed to coexist with lamellae, and by a draw ratio of 250 no lamellae were left at all, providing a good explanation for the well known disappearance of SAXS long period peaks in ultradrawn PE. Strain-induced crystallization resulted in the formation of crystalline bridges between lamellae and eventually between the mosaic block remnants in protofibrils, resulting in an increase in the crystallinity and crystalline phase continuity along the chain direction.

To summarize, darkfield TEM morphological observations of bulk ultrahigh tensile modulus films of polyethylene suggested that such films contain a sample-spanning crystalline phase. Deformation studies on thin, oriented HDPE film further indicated that such a phase is most likely to form in polyethylene drawn above the alpha transition temperature. Moreover, microstructures which arose in both highly drawn

thin and bulk films suggested that the continuous crystalline phase is comprised of protofibrils which coalesce and attain crystalline phase continuity via lateral crystal/crystal junction points. Such protofibrils resemble shish-kebabs with very small kebabs and are believed to arise from shish-kebabs through decrystallization and strain-induced (re)crystallization processes.

REFERENCES

Adams, W.W., Briber, R.M., Sherman, E.S., Porter, R.S., and Thomas, E.L. (1985), "Microstructure of High Modulus Solid State Extruded Polyethylene: 2. X-Ray Scattering Studies of 12, 24, and 36X Extrusion Draw Ratio", Polymer, 26, 17.

Adams, W.W., Yang, D., and Thomas, E.L. (1986), "Direct Visualization of Microstructural Deformation Processes in Polyethylene", J. Materials Sci., 21, 2239.

Alamo, R., Domszy, R.C., and Mandelkern, L. (1984), "Thermodynamic and Structural Properties of Copolymers of Ethylene", J. Phys. Chem., 88, 6587.

Andrews, E.H. (1964), "Crystalline Morphology in Thin Films of Natural Rubber II. Crystallization Under Strain", Proceedings of the Royal Soc. (London): Series A, 277, 562.

Barham, P.J., Hill, M.J., and Keller, A. (1980) "Gelation and Production of Surface Grown Polyethylene Fibers", Colloid and Polymer Sci., 258, 899.

Barham, P.J. (1982), "Gelation and the Production of Stiff Polyethylene Fibers", Polymer, 23, 1112.

Bashir, Z., Odell, J.A., Keller, A. (1984), "High Modulus Filaments of Polyethylene with Lamellar Structure by Melt Processing: the Role of the High Molecular Weight Component", J. Materials Sci., 19, 3713.

Bashir, Z., Odell, J.A., Keller, A. (1986), "Stiff and Strong Polyethylene With Shish Kebab Morphology By Continuous Melt Extrusion", J. Materials Sci., 21, 3993.

Bassett, D.C. (1981), Principles of Polymer Morphology, Cambridge Univ. Press, New York.

Beresford, D.R. and Bevan, H. (1963), "The Effect of Tension on 6-6 Nylon", Polymer, 5(5), 247.

Berney, C.V., Cohen, R.E., and Bates, F.S. (1982), "Sphere Sizes in Diblock Copolymers: Discrepancy Between Electron Microscopy and Small-Angle Scattering Results", Polymer, 23, 1222.

Bevis, M. and Crellin, E.B. (1971) "The Geometry of Twinning and Phase Transformations in Crystalline Polyethylene", Polymer, 12, 666.

Bowden, P.B., and Young, R.J. (1974), "Review. Deformation Mechanisms in Crystalline Polymers", J. Materials Sci., 9, 2034.

Bunn, C.W. (1960), "The Structure of Polyethylene", Polythene, Renfrew, A., and Morgan, P., Eds., Interscience Publishers, New York, Ch.5.

Burfield, D.R., and Kashiwa, N. (1985), "DSC Studies of Linear Low Density Polyethylene. Insights into the Disrupting Effect of Different Comonomers and the Minimum Fold Chain Length of the Polyethylene Lamellae", Makromolekulare Chemie, 186, 2657.

Cady, L.D. (1987), "LLDPE Properties Tied to Branch Distribution", Plastics Eng., January, 25.

Cannon, C.G. (1982), "Orientation Processes in the Drawing of Dry Gel Films of Polyethylene and Polypropylene", Polymer, 23, 1123.

Cannon, S.L., McKenna, G.B., and Statton, W.O. (1976), "Hard Elastic Fibers (A Review of a Novel State for Crystalline Polymers)", J. Polymer Sci., Macromolecular Reviews, 11D, 209.

Capaccio, G., Crompton T.A., and Ward, I.M. (1976), "The Drawing Behavior of Linear Polyethylene. I. Rate of Drawing as a Function of Polymer Molecular Weight and Initial Thermal Treatment", J. Polymer Sci., Physics Edn., 14, 1641.

Capaccio, G., Gibson, A.G., Ward, I.M. (1979), "Drawing and Hydrostatic Extrusion of Ultra-High Modulus Polymers", Ultra-High Modulus Polymers, A. Ciferri and I.M. Ward, eds., Applied Science Publ., London, 1.

Capaccio, G., and Ward, I.M. (1984), "The Drawing Behavior of Polyethylene Copolymers", J. Polymer Sci., Physics Edn., 22, 475.

Carpinteri, A., Marega, C., Savadori, A. (1986), "Size Effects and Ductile-Brittle Transition of Polypropylene", J. Materials Sci., 21, 4173.

Cayrol, B. and Petermann, J. (1974), "Elastic Hard Fibers", J. Polymer Sci., Physics Edn., 12, 2169.

Cembrola, R.J., and Stein, R.S. (1980), "Crystal Orientation Relaxation Studies of Polyethylene", J. Polymer Sci., Physics Edn., 18, 1065.

Chanzy, H.D., Smith, P., Revol, J.-F., Manley, R. St. J. (1987), "High Resolution Electron Microscopy of Ultradrawn Gels of High Molecular Weight Polyethylene", Polymer Comm. 28, 133.

Chuah, H.H., De Micheli, R., and Porter, R.S. (1983), "Density Changes on Drawing by Solid State Extrusion of High-Density Polyethylene", J. Polymer Sci., Letters, 21, 791.

Chuah, H.H. and Porter, R.S. (1984), "Solid-State Extrusion of Chain-Extended Polyethylene", J. Polymer Sci., Physics Edn., 22, 1353.

Chuah, Hoe Hin, Lin, J.S., Porter, Roger S. (1986), "On Deformation of Polyethylene: The Question of Melting and Recrystallization", Macromolecules, 19(11), 2732.

Ciferri, A. and Ward, I.M., eds., (1979), Ultra-High Modulus Polymers, Applied Science Publishers, London.

Clark, E.S., and Scott, L.S. (1974), "Superdrawn Crystalline Polymers: A New Class of High-Strength Fiber", Polymer Eng. and Sci., 14, 682.

Corneluissen, R., Peterlin, A. (1967), "The Influence of Temperature on the Plastic Deformation of Polyethylene", Makromolekulare Chemie, 105, 193.

Decandia, F., Vittoria, V., and Peterlin, A. (1985), "Time Dependence of Mechanical and Transport Properties", J. Polymer Sci., Physics, 23, 1217.

Dhawan, F., Chanbey, D.R., Yadav, Y.S., Jain, P.C., and Nanda, V.S. (1980), "Effect of Solid State Extrusion on Melting Behavior and Morphology of HDPE", Polymer J., 12(7), 411.

Domszy, R.C., Alamo, R., Edwards, C.O., and Mandelkern, L. (1986), "Thermoreversible Gelation and Crystallization of Homopolymers and Copolymers", Macromolecules, 19, 310.

D'Ouville, E.L. (1960), "Manufacturing Processes: Standard Oil Co. (Indiana) Polymerization", Polythene, 2nd edn., A. Renfrew and P. Morgan, Eds., Interscience Publishers, New York, pg. 35.

Duckett, R.A. (1983), "Polymer Microstructure and Deformation Processes", International Metals Rev., 28(3), 158.

Ehrlich, P., and Mortimer, G.A. (1970), "Fundamentals of the Free-Radical Polymerization of Ethylene", Adv. Polymer Science, 7, 386.

Fava, R.A. (1971), "Polyethylene Crystals", J. Polymer Sci., Macromolecular Reviews, 5D, 1.

Fawcett, E.W. and Gibson, R.O. (1934), "The Influence of Pressure on a Number of Organic Reactions in the Liquid Phase", Chemical Society, London, Journal: Part 1, 386.

Fischer, E.W., and Goddar, H. (1969), "Elektronenmikroskipische Untersuchungen an Verstrecktem Polyathylen", J. Polymer Sci., 16C, 4405.

Flory, P.J. (1947), "Thermodynamics of Crystallization in High Polymers. I. Crystallization Induced by Stretching", J. Chem. Physics, 15, 397.

Flory, P.J. (1949), "Thermodynamics of Crystallization in High Polymers. IV. A Theory of Crystalline States and Fusion in Polymers, Copolymers and Their Mixtures with Diluents", J. Chem. Physics, 17(3), 223.

Flory, P.J. (1962), "On the Morphology of the Crystalline State in Polymers", J. American Chemical Soc., 84, 2857.

Flory, P.J., and Yoon, D.Y. (1978), "Molecular Morphology in Semicrystalline Polymers", Nature, 272, 226.

Flory, P.J., Yoon, D.Y., and Dill, K.A. (1984), "The Interphase in Lamellar Semicrystalline Polymers", Macromolecules, 17, 862.

Freedman, A.M., Bassett, D.C., Vaughan, A.S., and Olley, R.H. (1986), "On Quantitative Permanganic Etching", Polymer, 27, 1163.

Friedrich, K. (1983), "Crazes and Shear Bands in Semi-Crystalline Thermoplastics, Advances in Polymer Science, 52/53, Springer-Verlag, New York, H.H. Kausch, ed., 225.

Frye, C.J., Ward, I.M., Dobb, M.G., and Johnson, D.J. (1979), "Direct Measurements of Crystallite Size Distribution in Ultra-High Modulus Polyethylene Fibers", Polymer, 20, 1310.

Furuhata, K., Yokokawa, T., Seoul, C., and Miyasaka, K. (1986), "Drawing of Ultrahigh-Molecular-Weight Polyethylene Single-Crystal Mats: The Crystallinity", J. Polymer Sci., Physics Edn., 24, 59.

Furumiya, A., Akana, Y., Ushida, Y., Masuda, T., and Nakajima, A. (1985), "Relationship Between Molecular Characteristics and Physical Properties of Linear Low Density Polyethylene", Pure and Appl. Chem., 57(6), 823.

Geil, P.H. (1963), Polymer Single Crystals, Interscience Publishers, New York.

Gent, A.N. and Jeong, J. (1986), "Plastic Deformation of Crystalline Polymers", Polymer Engineering and Science, 26(4), 285.

Gibson, A.G., Ward, I.M., Cole, B.N., and Parsons, B. (1974), "Hydrostatic Extrusion of Linear Polyethylene", J. Materials Sci., 9, 1193.

Gibson, A.G., Davies, G.R., and Ward, I.M. (1978), "Dynamic Mechanical Behavior and Longitudinal Crystal Thickness Measurements on Ultra-High Modulus Linear Polyethyloene: A Quantitative Model for the Elastic Modulus", Polymer, 19, 683.

Glauert, A.M., (1972 - 1981), Practical Methods in Electron Microscopy, Elsevier, North Holland, Inc., New York, 1 - 9.

Grubb, D.T., Keller, A., and Groves, G.W. (1972), "Origin of Contrast Effects in the Electron Microscopy of Polymers. Part 1: Polyethylene Single Crystals", J. Materials Sci., 7(2), 131.

Grubb, D., and Keller, A. (1972), "Origin of Contrast Effects in the Electron Microscopy of Polymers. Part 2: Polyethylene Spherulites", J. Materials Sci., 7(7), 822.

Grubb, D. (1974), "Review. Radiation Damage and Electron Microscopy of Organic Polymers", J. Materials Sci., 9, 1715.

Grubb, D.T., and Keller, A. (1978), "Thermal Contraction and Extension In Fibrous Crystals of Polyethylene", Colloid and Polymer Sci., 256, 218.

Grubb, D.T. (1982), "Electron Microscopy of Crystalline Polymers", Developments in Crystalline Polymers -- I., D.C. Bassett, Ed., Applied Science Publishers, Englewood, New Jersey, Ch. 1.

Hallam, M.A., Cansfield, D.L.M., Ward, I.M., Pollard, G. (1986), "A Study of the Effect of Molecular Weight on the Tensile Strength of Ultra-High Modulus Polyethylene", J. Materials Sci., 21, 4199.

Halpin, J.C., and Kardos, J.L. (1972), "Moduli of Crystalline Polymers Employing Composite Theory", J. Appl. Physics, 43(5), 2235.

Hay, I.L., and Keller, A. (1966), "A Study on Orientation Effects in Polyethylene in the Light of Crystalline Texture", J. Materials Sci., 1, 41.

Heidenreich, H.D. (1964), Fundamentals of Transmission Electron Microscopy, Interscience, John Wiley & Sons, New York.

Heise, B., Kilian, H.-G., and Wulff, W. (1980), "Deformation and Microstructure in Uniaxially Stretched Polyethylene", Progress in Colloid and Polymer Sci., 67, 143.

Hess, K., Kiessig, H. (1943), "The Fine Structure of Polyamide Fibers", Naturwissenschaften, 31, 171.

Hoffman, J.D. (1979), "On the Formation of Polymer Fibrils by Flow-Induced Crystallization", Polymer, 20, 1071.

Hoffman, J.D., Williams, G., and Passaglia, E. (1966), "Analysis of the α, β, and γ Relaxations in Polychlorotrifluoroethylene and Polyethylene: Dialectric and Mechanical Properties", J. Polymer Sci., Polymer Symp., 14C, 173.

Hogan, J.P. and Banks, R.L. (Phillips Petroleum Company) (1958), "Polymers and Production Thereof", U.S. Patent Office Official Gazette, 728, 173, U.S. Patent # 2,825,721.

Holdsworth, P.J., Keller, A. (1969), "Investigation of the Structure of Ethylene-Propylene and Ethylene-Butene Copolymer Crystals Using Fuming Nitric Acid. Part III. The Effects of Nitric Acid on the Physical Properties of Single Crystal Mats of Ethylene Copolymers", Makromolekulare Chemie, 125, 94.

Holmes, D.R., Palmer, R.P. (1958), "The Orientation of the Crystalline and Amorphous Regions in Polyethylene Film", J. Polymer Sci., 31, 345.

Hookway, D.C. (1957), "The Cold Drawing of Nylon 6.6", Proceedings of the Textile Institute and Fiber Society Conference, September, 1957, Boston, Massachusetts, 292.

Hosemann, R., Cackovic, H., and Wilke, W. (1967), "Die Sogenannten Einkristalle in Hochpolymeren", Naturwissenschaften, 54, 278.

Hsieh, E.T., and Randall, J.C. (1982a), "Monomer Sequence Distributions in Ethylene-1-Hexene Copolymers", Macromolecules, 15, 1402.

Hsieh, E.T, and Randall, J.C. (1982b), "Ethylene-1-Butene Copolymers: Comonomer Sequence Distribution", Macromolecules, 15, 353.

Ingram, P. (1967), "Electron Diffraction and Microscopy of Deformed Polymer Crystals. IV. The Effect of Original Crystal Thickness on Fibril Structure", Makromolekulare Chemie, 108, 281.

Irvine, P.A., and Smith, P. (1986), "Development of the Axial Young's Modulus With Draw Ratio of Flexible-Chain Polymers", Macromolecules, 19, 240.

Isaacson, M.S. (1977), "Specimen Damage in the Electron Microscope", Principles and Techniques of Electron Microscopy, 7, M.A. Hayat, Ed., Van Nostrand Reinhold Co., New York.

Ito, M., Kanamoto, M., Tanaka, K., and Porter, R.S. (1981), "Pulsed NMR Studies of Crystalline-State Extrusion of High-Density Polyethylene", Macromolecules, 14, 1779.

Juska, T. and Harrison, I.R. (1982), "A Proposed Plastic Deformation Mechanism for Semicrystalline Polymers", Polymer Eng. Rev., 2, 13.

Kajiyama, T., Okada, T., Sakoda, A., and Takayanagi, M. (1973), "Analysis of the α-Relaxation Process of Bulk Crystallized Polyethylene Based on That of a Single Crystal Mat", J. Macromolecular Sci., Physics, B7(3), 583.

Kanamoto, T., Sherman, E.S., and Porter, R.S. (1979), "Extrusion of Polyethylene Single Crystals", Polymer J., 11, 497.

Kanamoto, T. Fujimatsu, S., Tsuruta, A., Tanaka, K., and Porter, R.S. (1981), "X-Ray Diffraction Study of Solid State Extrusion of Melt-Crystallized High Density Polyethylene", Reports on Progress in Polymer Physics, Japan, 24, 185.

Kanamoto, T., Tsuruta, A., Tanaka, K., Takeda, M., and Porter, R.S. (1983a), "On Ultra-High Tensile Modulus by Drawing Single Crystal Mats of High Molecular Weight Polyethylene", Polymer J., 15(4), 327.

Kanamoto, T., Tsuruta, A., Tanaka, K., Takeda, M., and Porter, R.S. (1983b), "Drawing of Ultra-High Molecular Weight Polyethylene from Single Crystal Morphology", Reports on Progress in Polymer Physics, Japan, 26, 347.

Kanamoto, T., Ito, M., Ogura, K., Tanaka, K., and Porter, R.S. (1984), "Deformation Profiles: Effect on the Properties of High Density Polyethylene Drawn by Solid State Extrusion", ACS Symposium Series #260, Polymers For Fibers and Elastomers, J.C. Arthur, Jr., Ed.

Kanig, G. (1973), "Ein Neues Kontrastierverfahren fur die Elektronenmikroskipische Untersuchung von Polyathylen", Kolloid Z.Z. Polymere, 251, 782.

Kanig, G. (1975), "Neue Elektronenmikroskipische Untersuchungen uber die Morphologie von Polyathylenen", Colloid and Polymer Sci., 57, 176.

Katti, S.S. and Schultz, J.M. (1982), "The Microstructure of Injection-Molded Semicrystalline Polymers: A Review., Polymer Eng. and Sci., 22, 1001.

Kausch, H.H. and Devries, K.L. (1975), "Molecular Aspects of High Polymer Fracture as Investigated by ESR-Technique", International J. of Fracture, 11(5), 727.

Keith, H.D., Padden, F.J., Jr., and Vadimsky, R.G. (1966), "Intercrystalline Links in Polyethylene Crystallized From the Melt", J. Polymer Sci., Physics Edn., 4, 267.

Keith, H.D., Padden, F.J., Jr., and Vadimsky, R.G. (1971), "Intercrystalline Links: Critical Evaluation", J. Appl. Physics, 42(12), 4585.

Keller, A. (1968), "Polymer Crystals", Reports on Progress in Physics, 31(II), 623.

Keller, A. (1979), "Routes to High Modulus by Ultra-Orientation of Flexible Molecules", Ultra-High Modulus Polymers, A. Ciferri and I.M. Ward, Eds., Applies Science Publishers, Essex, England, Ch. 11.

Keller, A. (1982), "Radiation Effects and Crystallinity in Polyethylene and Paraffins", Developments in Crystalline Polymers -- I, Bassett, D.C., Ed., Applied Science Publishers, Englewood, New Jersey, Ch. 2.

Kramer, E.J. (1983), "Microscopic and Molecular Fundamentals of Crazing", Advances in Polymer Science, 52/53, Springer-Verlag, New York, H.H. Kausch, ed., 1.

Krigas, T.M., Carella, J.M., Struglinski, M.J., Christ, B., and Graessley, W.W. (1985), "Model Copolymers of Ethylene With Butene-1 Made by Hydrogenation of Polybutadiene: Chemical Composition and Selected Physical Properties", J. Polymer Sci., Physics Edn. 23, 509.

Krueger, D., and Yeh, G.S.Y. (1972), "Morphology of Polyethylene Microfibrils and "Shish Kebabs"", J. Macromolecular Sci., B6, 431.

Lauterwasser, B.D. and Kramer, E.J. (1979), "Microscopic Mechanisms and Mechanics of Craze Growth and Fracture", Philosophical Mag. A: 39, 469.

Linder, B.E., and Samuels, R.J. (1985), "Prediction of Axial and Off-Axis Yield Behavior of Isotactic Polypropylene Film from Structural State Parameters", Polymer Eng. and Sci., 25(14), 875.

Maddams, W.F., and Preedy, J.E. (1978), "X-Ray Diffraction Orientation Studies on Blown Polyethylene Films. II. Measurements on Films from a Commecial Blowing Unit", J. Appl. Polymer Sci., 22, 2721.

Mandelkern, L. (1964), Crystallization of Polymers, McGraw Hill, New York, a) Ch.8.

Mandelkern, L. (1976), "Structure and Properties of Polymer Crystals Formed in Dilute Solution", Annual Review of Materials Science, 6, 119.

Mandelkern, L. (1985), "The Relation Between Structure and Properties of Crystalline Polymers", Polymer J., 17, 337.

Martuscelli, E.J. (1975), "A Review of the Properties of Polymer Single Crystals with Defects Within the Macromolecular Chain", J. Macromol. Sci., Physics Edn., B11(1), 1.

Meinel, G., and Peterlin, A. (1971), "Plastic Deformation of Polyethylene II. Change of Mechanical Properties During Drawing", J. Polymer Sci., Part A2, 9, 67.

Miles, M., Petermann, J., and Gleiter, H. (1976), "Structure and Deformation of Polyethylene Hard Elastic Fibers", J. Macromol. Sci., B12(4), 523.

Morton, M., and Fetters, L.J. (1975), "Anionic Polymerization of Vinyl Monomers", Rubber Chem. Technol. 48, 359.

Nagasawa, T. and Shimomura, Y. (1974), "Mechanism of Formation of Shish Kebab Structure", J. Polymer Sci., Physics Edn., 12, 2291.

Natta, G. (1956), "Stereospezifische Katalysen und Isotaktische Polymere", Angewandte Chemie, 68, 393.

Nowlin, T.E. (1985), "Low Pressure Manufacture of Polyethylene", Prog. Polymer Sci., 11, 29.

Olley, R.H., Hodge, A.M., and Bassett, D.C. (1979), "A Permanganic Etchant for Polyolefins", J. Polymer Sci., Physics Edn., 17, 627.

Palmer, R.P. and Cobbold, A.J. (1964), "The Texture of Melt Crystallized Polyethylene as Revealed by Selective Oxidation", Makromolekulare Chemie, 74, 174.

Patel, G.N. (1980), "Chemical Methods in Polymer Physics", Methods in Experimental Physics, 16B, Academic Press, Inc., New York, 237.

Patridge, R.H. (1970), "Excitation Energy Transfer in Alkanes I. Exciton Model", J. Chem. Physics, 52, 2485.

Paulos, J.P., and Thomas, E.L. (1980), "Effect of Postdrawing on the Permeability of Gases in Blown Polyethylene Film", J. of Appl. Polymer Sci., 25, 15.

Pennings, A. (1977), "Bundle-Like Nucleation and Longitudinal Growth of Fibrillar Polymer Crystals From Flowing Solutions", J. Polymer Sci., Polymer Symp. 59, 55.

Pennings, A. and Meihuizen (1979), "Polyethylene Fibers with Ultra-High Modulus and Strength Produced by Flow-Controlled Crystallization", Ultra-High Modulus Polymers, A. Ciferri and I.M. Ward, Eds., Applied Science Publishers, Essex, England, Ch. 3.

Perez, E., Van der Hart, D.L., Crist, Buckley, Jr., Howard, P.R. (1987), "Morphological Partitioning of Ethyl Branches in Polyethylene by ^{13}C Nuclear Magnetic Resonance", Macromolecules, 20(1), 78.

Perkins, W., and Porter, R.S. (1977), "Review: Solid State Deformation of Polyethylene and Nylon and its Effects on Their Structure and Morphology", J. Materials Sci., 12, 2355.

Peterlin, A., Ingram, P., Kiho, H. (1965), "Electron Diffraction and Microscopy of Deformed Polymer Crystals, II. Fibers", Makromolekulare Chemie, 86, 294.

Peterlin, A. (1967), "Folded Chain Concept of Fiber Structure", Kolloid Z.Z. Polymere, 216 - 217, 129.

Peterlin, A., and Sakaoku, K. (1967), "Surface Replicas of Drawn Polyethylene III. The Morphology of Drawing with Neck Formation", J. Appl. Physics, 38(11), 4152.

Peterlin, A. (1971), "Molecular Model of Drawing Polyethylene and Polypropylene", J. Materials Sci., 6, 490.

Peterlin, A. (1972), "Plastic Deformation of Unoriented Crystalline Polymers Under Tensile Load", Advances in Polymer Science and Engineering, K.D. Pae, D.R. Morrow, Y. Chen, eds., Plenum Press, New York, pg. 1.

Peterlin, A. (1976), "Crystallization From a Strained Melt or Solution", Polymer Eng. and Sci., 16, 126.

Peterlin, A. (1977), "Drawing and Annealing of Fibrous Material", J. Appl. Physics, 48(10), 4099.

Peterlin, A. (1978), "Annealing of Drawn Polymers", Polymer Eng. and Sci., 18(6), 488.

Peterlin, A. (1979), "Elastic Modulus and Strength of Fibrous Material", Polymer Eng. and Sci., 19, 118.

Petermann, J. and Gleiter, H. (1973a), "Observations of Radiation Damage Effects In Paraffin and Polyethylene Crystals", Kolloid Z.Z. Polymere, 251, 850.

Petermann, J., and Gleiter, H. (1973b), "Plastic Deformation of Polyethylene Crystals by Dislocation Motion", J. Materials Sci., 8, 673.

Petermann, J., and Gohil, R.M. (1979), "A New Method for the Preparation of High Modulus Thermoplastic Films", J. Materials Sci., 14, 2260.

Petermann, J., Gohil, R.M., Massud, M., and Goritz, D. (1982), "Plastic Deformation of Linear Polyethylene Containing Row Structures", J. Materials Sci., 17, 100.

Phillips, P.J., and Philpot, R.J. (1986), "Direct Evidence for Melting During Drawing of Polyethylene", Polymer Comm., 27(10), 307.

Pope, D.P. and Keller, A. (1976), "Temperature-Induced Reversible Changes In Long Spacing in Oriented Polyethylene", J. Polymer Sci., Physics Edn., 14, 821.

Popli, R. and Mandelkern, L. (1987), "Influence of Structural and Morphological Factors on the Mechanical Properties of Polyethylenes", J. Polymer Sci., Physics Edn., 25, 441.

Porter, R.S. (1971), "The Concept of Continuous Crystals", American Chemical Society Polymer Preprints, 12(2), 39.

Porter, R.S. and Casale, A. (1985), "Recent Studies of Polymer Reactions Caused by Stress", Polymer Eng. and Sci., 25(3), 129.

Postema, A.R., Hoogsteen, W., Pennings, A.J. (1987), "Crazing in Ultra-High Molecular Weight Gel-Fibers", Polymer Comm., 28(5), 148.

Prevorsek, D.C., Harget, P.J., Sharma, R.K., and Reimscheussel, J. (1973), "Nylon 6 Fibers: Changes in Structure Between Moderate and High Draw Ratios", J. Macromolecular Sci., Physics, B8, 127.

Rachapudy, H., Smith, G.G., Raju, V.R., and Graessley, W.W. (1979), "Properties of Amorphous and Crystallizable Hydrocarbon Polymers. III. Studies of the Hydrogenation of Polybutadiene", J. Polymer Sci., Physics Edn., 17, 1211.

Randall, J.C. (1977), Polymer Sequence Determination: A ^{13}C Method, New York, Academic Press.

Reimer, L. (1984), Transmission Electron Microscopy, Springer Verlag, New York.

Reck, E.M., Schenk, H., and Wilke, W. (1985), "Investigation of the Deformation and Relaxation of Various Polyethylenes by X-ray Diffraction", Progress in Colloid and Polymer Sci., 71, 154.

Renfrew, A., and Morgan, P., Eds., (1960) Polythene, 2nd edn., Interscience Publishers, Inc., New York.

Sadler, D.M. and Keller, A. (1977), "Neutron Scattering Studies on the Molecular Trajectory in Polyethylene Crystallized from Solution and Melt", Macromolecules, 10, 1128.

Sakurada, I., Ito, T., Nakamai, K. (1966), "Elastic Moduli of the Crystal Lattices of Polymers", J. Polymer Sci., C15, 75.

Samuels, R.J. (1985), "Polymer Structure: The Key to Process-Property Control", Polymer Eng. and Sci., 25(14), 864.

Sanchez Cuesta, M., Martinez Salazar, J., Balta Calleja, F.J. (1987), "X-Ray Diffraction Study of Lattice Distortions in Branched Polyethylene Rapidly Quenched From the Melt", Polymer Bulletin, 17(1), 23.

Sandiford, D.J.H., and Willbourn, A.H. (1960), "General Mechanical Properties", Polythene, 2nd edn., A. Refrew and P. Morgan, Eds., Interscience Publishing Co., New York, ch. 8.

Santee, E.R., Jr., Chang, R., and Morton, M. (1973a), "300 MHz Proton NMR of Polybutadiene Measurement of Cis-Trans Isomeric Content", J. Polymer Sci., Letters, 11, 449.

Santee, E.R., Jr., Mochel, V.D., and Morton, M. (1973b), "Proton NMR of Polybutadiene at 300 MHz: Cis-1,4-Trans-1,4 Linkages", J. Polymer Sci., Letters, 11, 453.

Schelten, J., Ballard, D.G.H., Wignall, G.D., Longman, G.W., and Schmatz, W. (1976), "Small-Angle Neutron Scattering Studies of Molten and Crystalline Polyethylene", Polymer, 17, 751.

Schultz, J.M. (1984), "Microstructural Aspects of Failure in Semicrystalline Polymers", Polymer Eng. and Sci., 24(10), 770.

Seguela, R., and Rietsch, F. (1986a), "Tensile Drawing Behavior of Ethylene/Alpha-Olefin Copolymers: Influence of the Co-Unit Concentration", Polymer, 27, 703.

Seguela, R., and Rietsch, F., (1986b), "Tensile Drawing Behavior of a Linear Low-Density Polyethylene: Changes in Physical and Mechanical Properties", Polymer, 27, 532.

Seto, T., Hara, T., Tanaka, K. (1968), "Phase Transformation and Deformation Processes in Oriented Polyethylene", Japanese J. Appl. Physics, 7(1), 31.

Seymour, R.S. and Cheng, T. (1986), Eds., History of Polyolefins, Kluwer Academic Publishers, Hingham, Massachusetts.

Sherman, E.S., Porter, R.S., and Thomas, E.L. (1982), "Microstructure of High Modulus Solid State Extruded Polyethylene: I. Electron Microscopy Studies of 12, 24, and 35 Extrusion Draw Ratio", Polymer, 23, 1069.

Shimanouchi, T., Asahina, M., Enomoto, S. (1962), "Elastic Moduli of Oriented Polymers I. The Simple Helix, Polyethylene, Polytetrafluoroethylene, and a General Formula", J. Polymer Sci., 59, 93.

Smith, P., and Lemstra, P.J. (1980), "Ultradrawing of High-Molecular-Weight Polyethylene Cast From Solution", Colloid and Polymer Sci., 258(7), 891; "Ultra High Strength Polyethylene Filaments by Solution Spinning/Drawing", J. Materials Sci., 15, 505.

Smith, P., Lemstra, P.J., and Booij, H.C. (1981a), "Ultradrawing of High-Molecular-Weight Polyethylene Cast From Solution. II. Influence of Initial Polymer Concentration.", J. Polymer Sci., Physics Edn., 19, 877.

Smith, P., Lemstra, P.J., Pijpers, J.P.L., and Kiel, A.M. (1981b), "Ultradrawing of High-Molecular-Weight Polyethylene Cast From Solution. III. Morphology and Structure.", Colloid and Polymer Sci., 259(11), 1070.

Smith, P.J., Boudet, A., and Chanzy, H. (1985), "The Structure of Ultradrawn High Molecular Weight Polyethylene Revealed by Electron Microscopy at 100 and 1500 kV", J. Materials Sci., Letters, 4, 13.

Sprague, B.S. (1973), "Relationship of Structure and Morphology to Properties of "Hard" Elastic Fibers and Films", J. Macromolecular Sci., Physics, B8(1-2), 157.

Springer, H., Hengse, A., Hoehne, J., Schich, A., Hinrichsen, G. (1986), "Investigation on Crystallization and Melting Behavior of Linear Low Density Polyethylene (LLDPE)", Prog. Colloid and Polymer Sci., 72, 101.

Staudinger, H. (1932), Die Hochmolelcuren Organischen Verbindungen, Springer, Berlin.

Stein, R.S. (1973), "Rheo-optical and Dialectric Studies of the α-Loss Region of Low Density Polyethylene", J. Macromolecular Sci., Physics, B8(1), 29.

Sumita, M., Miyasaka, K., Ishikawa, K. (1977), "The Effect of Drawing on the Melting Point and Heat of Fusion of Polyethylene", J. Polymer Sci., Physics Edn., 15, 837.

Swallowe, G.M., Field, J.E., Horn, L.A. (1986), "Measurements of Transient High Temperatures During the Deformation of Polymers", J. Materials Sci., 21, 4089.

Swan, P.R. (1962), "Polyethylene Unit Cell Variations with Temperature", J. Polymer Sci., 56, 403.

Takayanagi, M., Imada, K., and Kajiyama, T. (1966), "Mechanical Properties and Fine Structure of Drawn Polymers", J. Polymer Sci., Polymer Symp., 15C, 263.

Takayanagi, M., and Kajiyama, T. (1973), "Structural Factors in Deformation of Crystalline Polymers", J. Macromolecular Sci., Physics, B8(1), 1.

Tanabe, Y., Strobl, G.R., and Fischer, E.W. (1986), "Surface Melting in Melt-Crystallized Linear Polyethylene", Polymer, 27(8), 1147.

Tanaka, A., Chang, E.P., Delf, B., Kimura, I., and Stein, R.S. (1973), "Rheo-Optical Studies of the Nature of the Alpha-Loss Mechanism of Polyethylene", J. Polymer Sci., Physics Edn., 11, 1891.

Thomas, E.L. (1986), "Electron Microscopy", Encyclopedia of Polymer Science and Engingeering, 5, 2nd edn., John Wiley & Sons, New York.

Tsuruta, A., Kanamoto, M., Tanaka, K., and Porter, R.S. (1985), "Estimation of Crystalline Tie Molecules in Ultradrawn Polyethylene Extrudates", J. Polymer Sci., Physics Edn., 23, 429.

Turner-Jones, A. (1962), "The Triclinic Crystal Form of Polymethylenes and Polyethylenes", J. Polymer Sci., 62, S53.

Ueda, H., Karasz, F.E., Farris, R.J. (1986), "Characterization of Mixtures of Linear Polyethylenes of Ultrahigh and Moderate Molecular Weights", Polymer Eng. and Sci., 26(21), 1483.

Van Hutten, P.F., Koning, C.E., and Pennings, A.J. (1984), "The Deformation Behavior of Polyethylene Shish-Kebabs Produced by Stirring-Induced Crystallization", Colloid and Polymer Sci., 262, 521, and references therein.

Van Hutten, P.F., Koning, C.E., and Pennings, A.J. (1985), "Plastic Deformation of Ultrahigh Molecular Weight Polyethylene", J. Materials Sci., 20(5), 1556.

Vile, J., Hendra, J., Willis, H.A., Cudby, M.E.A., and Bunn, A. (1984), "Chain Branching in High Pressure Polymerized Polyethylene: 2.", Polymer 25, 1173.

Voight-Martin, I.G., Alamo, R., Mandelkern, L. (1986), "A Quantitative Electron Microscopy Study of the Crystalline Structure of Ethylene Copolymers", J. Polymer Sci., Physics Edn., 24, 1283.

Walter, E.R., Reding, F.P. (1956), "Variations of Unit Cell Dimensions in Polyethylene", J. Polymer Sci., 21, 561.

Wang, J., Harrison, I.R. (1980), "Crystallite Size and Lamellar Thickness by X-Ray Methods", Methods of Experimental Physics, 16B, 128.

Ward, I.M. (1983), Mechanical Properties of Solid Polymers, 2nd edition, Wiley, New York, pg. 270.

Ward, I.M. (1984), "The Role of Molecular Networks and Thermally Activated Processes in the Deformation Behavior of Polymers", Polymer Eng. and Sci., 24(10), 724.

Watt,I.M. (1985), The Principles and Practices of Electron Microscopy, Cambridge University Press, New York.

Wunderlich, B. (1973), Macromolecular Physics, volumes 1, 2, and 3, Academic Press, New York, a) vol. 1, pp. 153-157;
b) vol. 1, p. 405;
c) vol. 3, chapter 8;
d) vol. 3, chapter 9.
e) vol. 3, chapter 10.
f) vol. 1, chapter 4.

Yang, D., and Thomas, E.L. (1984), "An Electron Microscopy and X-Ray Diffraction Study of the Microstructure of Melt-Drawn Polyethylene Films", J. Materials Sci., 19, 2098.

Yeh, G.S.Y. (1976a), "Strain-Induced Crystallization II. Subsequent Fibrillar-to-Lamellar Transformation", Polymer Eng. and Sci., 16(3), 145.

Yeh, G.S.Y. (1976b), "Strain-Induced Crystallization I. Limiting Extents of Strain-Induced Nuclei", Polymer Eng. and Sci., 16(3), 138.

Young, R.J. (1981), Introduction to Polymers, Chapman and Hall, New York, ch. 5.

Zachariades, A.E., Mead, W.T., and Porter, R.S. (1980), "Recent Developments in Ultraorientation of Polyethylene by Solid State Extrusion", Chemical Reviews, 80, 351.

Zachariades, A.E. and Porter, R.S. (1981), "New Developments in Solid-State Extrusion", J. Macromolecular Sci., Physics, B19(3), 377.

Zachmann, H.G. (1967), "The Entropy of Crystallized Solids Composed of Long Chain Molecules", Statistical Mechanics: Foundations and Applications, Proc. of I.U.P.A.C. Meeting, Copenhagen, 1966, Thor A. Bak, ed., W.A. Benjamin, Inc., New York, pg. 237.

Ziegler, K., Holzkamp, E., Breil, H., and Martin, H. (1955), "Das Mulheimer Normaldruck-Polyathylen-Verfahren", Angewandte Chemie, 67, 541.

Zwijnenburg, A. and Pennings, A.J. (1976), "Longitudinal Growth of Polymer Crystals From Flowing Solution. III. Polyethylene Crystals in Couette Flow", Colloid and Polymer Sci., 254, 868.